LULEÅ UNIVERSITY OF TECHNOLOGY

2002:28

DOCTORAL THESIS

Industry Applications of Multivariable Control

Wolfgang Birk

Department of Computer Science and Electical Engineering
Division of Automatic Control

2002:28 • ISSN: 1402 - 1544 • ISRN: LTU - DT - - 02/28 - - SE

DOCTORAL THESIS

Industry Applications of Multivariable Control

Wolfgang Birk

Control Engineering Group
Department of Computer Science and Electrical Engineering
Luleå University of Technology
SE-971 87 Luleå, Sweden

Dissertation
for the degree of Doctor of Philosophy (Ph.D.) in the subject area of *Automatic Control*, which with the due permission of the Faculty Board at Luleå University of Technology, will be defended in public, in room D770 in the D-building at Luleå University of Technology on Friday the 27th of September 2002, at 9:00 am.

Akademisk avhandling
för avläggande av teknologie doktorsexamen inom ämnesområdet *Reglerteknik*, som med vederbörligt tillstånd Tekniska Fakultetsnämnden vid Luleå tekniska universitet, kommer att offentligen försvaras, i sal D770 i D-huset vid Luleå tekniska universitet, fredagen den 27:e september 2002, kl. 9:00.

Supervisor / Handledare
Professor Alexander Medvedev, Luleå University of Technology, Luleå, Sweden.

Faculty Opponent / Fakultetsopponent
Professor Björn Wittenmark, Lund University of Technology, Lund, Sweden.

Examination Committee / Betygsnämnd
Professor Svante Gunnarsson, Linköping Institute of Technology, Linköping, Sweden
Docent Kurt-Erik Häggblom, Åbo Akademi University, Åbo, Finland.
Docent Elling W. Jacobsen, Royal Institute of Technology, Stockholm, Sweden.

2002:28 • ISSN: 1402 - 1544 • ISRN: LTU - DT - - 02/28 - - SE

DOCTORAL THESIS

Industry Applications of Multivariable Control

by

Wolfgang Birk

Control Engineering Group
Department of Computer Science and Electrical Engineering
Luleå University of Technology
SE-971 87 Luleå, Sweden

August 2002

Supervisor
Professor Alexander Medvedev,
Luleå University of Technology,
Luleå, Sweden.

2002:28 • ISSN: 1402 - 1544 • ISRN: LTU - DT - - 02/28 - - SE

Published 2002
Printed in Sweden by University Printing Office, Luleå

To Ulrika

All truth passes through three stages. First, it is ridiculed. Second, it is violently opposed. Third, it is accepted as being self-evident.

Arthur Schopenhauer
(1788 - 1860)

Abstract

In the face of environmental regulations, optimization of industrial processes becomes necessary. This doctoral thesis summarizes the results of three application-driven projects in automatic control that were aimed at process optimization in the steel industry. The objective of the projects was to apply advanced control strategies to two important processes in steel making, namely pulverized coal injection (PCI) in blast furnaces and LD converters. Firstly, an LQ multivariable controller with gas leakage detection system for PCI vessels is designed and analyzed. Secondly, a foam level control system for the LD converter process using an audio signal for measurement is designed. Thirdly, it is attempted to create a single line flow control system for PCI using a video camera. In the latter two cases the conservative approach of inferring unmeasurable physical quantities from the audio and video sources is used.

Moreover, all the designs are tested through implementation or experiments at the industrial plant. The control and gas leakage detection system ended up as a full-scale industrial implementation, whereas the projects comprising audio and video information is still at an experimental stage.

Work with implementation and experiments pays off in experiences and further insights in the application of control theory, and reveals weaknesses and gaps in the existing theory. Thus, application-driven projects lead to practical solutions and at the same time pose new theoretical challenges. Consequently, this chain of events is favorable to both practitioners and theoreticians, and in turn stimulates the collaboration of industry and academia. Unfortunately, in many research projects this sequence is reversed which complicates technology transfer into industry.

As a spin-off effect from the multivariable control project of the PCI process two topics are addressed anew. In the problem of measurement/actuator pairs assignment for decentralized control, the geometrical background of Gramian-based interaction measures is clarified. It is shown that weighted Gramian-based interaction measures can be effectively used for control structure design. In control structure improvement of multivariable control systems, it is shown that improvement potentials can be deduced from coarse models of the closed-loop system. Finally, in the projects comprising audio and video signals in control applications, it is concluded that the theory is rather undeveloped and that these sources should be treated as a multivariable system.

Contents

Preface

In writing this thesis, the author's aim has been to summarize research work that has been conducted between 1997 and 2002 at the Control Engineering Group at Luleå University of Technology in Sweden, under the supervision of Professor Alexander Medvedev.

The presented results are from three application-driven projects that are aimed at process optimization in the steel industry. Two processes in steel making are considered, pulverized coal injection in blast furnaces and LD converters. The application of existing control theory gave insights that motivated research in the area of control structure design.

Funding was provided by Norrbottens Research Council, Swedish National Board for Industrial and Technical Development (NUTEK) and the Swedish Research Council (TFR). Cooperating partners were the Division for Process Metallurgy at the Royal Institute of Technology in Stockholm, Embedded Internet System Laboratory at Luleå University of Technology, SSAB Tunnplåt AB in Luleå and SSAB Oxelösund AB.

Acknowledgements

When I first came to Luleå as an exchange student in 1994, I intended to stay half a year, then return to Germany in order to finish my studies and immediately after that start working in the industry. But as soon as I got exposed to the life in northern Sweden, the people, the culture and the university, these plans gradually changed and I am very grateful for that. Because, life is much more inspiring now!

There are two things that had, and still have, a large effect on me. First, there are all the good friends that I have made during my time here. Second, there are all the excellent opportunities that the *Department of Computer Science and Electrical Engineering* and especially the *Control Engineering Group* have offered me. It is therefore, that this thesis has come into being.

Certainly, there are some people that I want to mention in particular. First of all, my supervisor, Prof. Alexander Medvedev who with his ideas, insight and vast amount of knowledge, encouraged and guided me through my PhD studies. His friendship means a lot to me and I hope that we will have further contact and collaboration in the future.

Then, I would like to thank some close friends at the department. Andreas Johansson was always a great co-worker and a sounding board for me. I hope we can continue with that in the future. With Michael Bask I had many great ideological and political discussions, as well as his allowance for me to siege his apartment for one year. Johan Karlsson was a really fantastic opponent in all the relaxing billiard games we had and I am always glad to get his invaluable opinion. Thank you all! You really kept me going here!

Of course, I want to express my gratitude to the members of the *Control Engineering Group* at Luleå University of Technology, who created a pleasant and creative environment, where I really could feel at home. Far too often, I seem to have mixed up the corridor at work with my home.

During my work in the research projects I was fortunate and grateful to meet many people from both industry and university who contributed largely to the success of the projects by believing in our ideas, giving a helping hand or working with us. Especially I am indebted to Robert Johansson and Bert Paavola from SSAB

Tunnplåt Luleå, Daniel Widlund from SSAB Oxelösund AB, Professor Pär Jönsson and Ioannis Arvanitidis from the Division of Process Metallurgy at the Royal Institute of Technology and Olov Marklund from Embedded Internet Systems Laboratory at Luleå University of Technology.

And from the bottom of my heart, I want to express my deepest gratitude to my family and to my fiancée Ulrika. Without their love, belief and endless support, I could not have come this far. You are always in my thoughts!

Luleå, August 2002
Wolfgang Birk

Introduction

Energy efficiency is becoming more important in the industry over the coming years due to governmental regulations regarding greenhouse gas emissions. In a study by the *European Commission* [11] it is indicated that an emissions reduction of 12% for the industry sector should be met by the year 2010.

Consequently, industrial processes need to be optimized for energy efficiency, beside the usual objectives, which are quality and cost efficiency. The application of advanced control strategies in industry becomes thus more important. In this thesis, the use of multivariable control techniques and estimation methods in some processes in the steel industry are studied.

Since multivariable control is a vast area of research, the parts related to this work are briefly reviewed. Moreover, it is shown how audio and video information can be used in control applications and that these information sources have a multivariable character. The connection to the industry applications is then established and the beneficial use of multivariable control is pinpointed.

1 Multivariable control

The theory of multivariable systems has been studied since the 1960's and is therefore well documented in the literature. In [52], [32] and [16] many aspects of analysis and synthesis of controllers are highlighted and references to important publications in the area are given.

The following day-life example gives a motivation for the use of multivariable control techniques and introduces some properties that have to be dealt with in multivariable systems, *i.e.* interaction.

1.1 Motivational example

A simple example from road traffic is a crossing of two roads, see Fig. 1. Since there are four traffic flows entering and exiting this crossing, the system has multiple inputs

and multiple outputs. Hence, such a road crossing is a multivariable system.

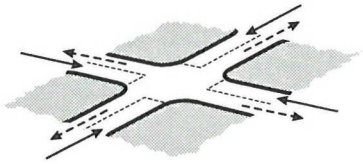

Fig. 1: Road crossing. Entering traffic (solid), Exiting traffic (dashed).

The functionality of the crossing is usually ensured by traffic rules, traffic lights or traffic signs. One could say, that these constitute a controller. The main tasks for this controller are to provide traffic safety and a smooth traffic flow.

The simplest way to operate a crossing is to introduce a rule for the *right of way* and assign it to each entering traffic flow. Obviously, this is a scalar approach for controlling the traffic, as each flow is controlled individually and the other traffic flows are handled as disturbances. From personal experience it is known that this works well for calm crossings, but leads to traffic congestion for busy crossing or to possible accidents if flows meet in the crossing at the same time. And certainly, without considerable rationality of the drivers such crossings would not work at all.

The reason for the performance limitation is interaction, namely the individual control loops interact as a certain action of a driver leads to a counteraction by another driver. Without a sophisticated controller the performance can not be improved.

A more advanced scheme to operate a crossing is to put up traffic signs or traffic lights. Usually, some traffic flows get higher priorities than other traffic flows. Thus, these rules apply to several traffic flows at the same time and are multivariable control approaches. Again from personal experience it is known that the traffic usually flows more safely and smoother even if the crossing is busy. Additionally, the performance depends less on the rationality of the drivers. Moreover, the obtained improvements are not based on constructive changes of the crossing but on changes of the control strategy.

Certainly, there are fundamental limitations for the improvements. These limitations then depend on the construction of the crossing and cannot be circumvented by control strategies. Thus, it is important to identify fundamental limitations.

It can be concluded that multivariable control is favorable and even simple modifications of the control structure can lead to large performance improvements. There is of course a trade-off, improved performance comes with higher costs of design and/or operation, *i.e.* more knowledge is needed to design or maintain the control algorithms.

1.2 Multivariable systems

In this thesis linear time invariant systems are considered. Some notation is introduced here and the aspects related to the thesis are presented. For more detailed information on multivariable systems, the interested reader is referred to [48, 26, 52, 32, 16].

The output of a linear multivariable system with m inputs, p outputs and zero initial condition is given as the convolution of an input signal with its impulse response function matrix

$$y(t) = \int_{t_1}^{t_2} g(t-\tau)u(\tau)d\tau \tag{1}$$

where $y(t) \in \mathcal{L}_2^p[t_1, t_2]$ and $u(t) \in \mathcal{L}_2^m[t_1, t_2]$. The impulse response function has to be bounded and thus $g(t) \in \mathcal{L}_1^{p\times m}[t_1, t_2]$. The restriction to the time interval $[t_1, t_2]$ makes it possible to consider unstable multivariable systems as long as $g(t)$ is bounded in the interval. For stable systems the interval can be set to $(-\infty, \infty)$ or $[0, \infty)$. When the latter interval is used, initial conditions can be considered.

Often in linear systems analysis the impulse response function $g(t)$ is expressed in terms of a state space realization, which is a set of linear differential equations

$$\dot{x}(t) = Ax(t) + Bu(t) \tag{2a}$$
$$y(t) = Cx(t) + Du(t) \tag{2b}$$
$$x(0) = 0 \tag{2c}$$

where $A \in \mathbb{R}^{n\times n}$, $B \in \mathbb{R}^{n\times m}$, $C \in \mathbb{R}^{p\times n}$ and $D \in \mathbb{R}^{p\times m}$.

The frequency domain representation of (1) can be obtained by applying the Laplace transform and is given by

$$Y(s) = G(s)U(s) \tag{3}$$

where s denotes the Laplace variable and $Y(s)$, $U(s)$ denote the Laplace transform of $y(t)$ and $u(t)$, respectively. $G(s)$ is referred to as the transfer function matrix, which is the Laplace transform of the impulse response function $g(t)$.

Of course, there are more representations, *e.g.* the matrix fraction description, but they are not used in the thesis and are thus omitted here. Briefly, the matrix fraction description is a factorization of the transfer function matrix (3). More information can be found in [16] and [32].

The different representations are connected with each other. Clearly, the state space representation (2) is simply the differential equation which has the impulse response matrix (1). The transfer function matrix representation can be derived from (2) by applying the Laplace transform and then solving the equation system for $Y(s)$ which yields

$$G(s) \triangleq C(sI - A)^{-1}B + D \tag{4}$$

where I denotes the identity matrix of appropriate size. For the sake of simplicity, the Laplace operator is dropped in the sequel.

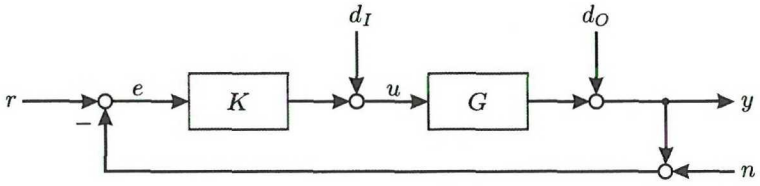

Fig. 2: Multivariable feedback system

When a controller $K(s)$ is applied to the multivariable system $G(s)$ with negative output feedback, then the complementary sensitivity transfer matrix T and the sensitivity transfer matrix S of the closed loop system are defined as

$$T = (I + GK)^{-1} GK \tag{5}$$

$$S = I - T = (I + GK)^{-1} \tag{6}$$

Both T and S are transfer matrices in the closed loop system depicted in Fig. 2 and reflect the relative sensitivity of the closed loop system to changes in G. The following relationships can be easily verified

$$Y = TR - TN + SGD_I + SD_O \tag{7a}$$

$$E = SR - SN - SGD_I - SD_O \tag{7b}$$

$$U = KSR - KSN - KSGD_I - KSD_O \tag{7c}$$

where the uppercase notation is used for the Laplace transform of the corresponding signals.

Clearly, important properties of the closed loop system can be derived from the sensitivity function matrices, *e.g.* stability, performance and robustness. There, the analysis of the singular values of the sensitivity functions plays a key role.

The main differences between scalar and multivariable systems are the presence of *interaction* and *directionality* in the latter. Moreover, proper scaling of the process model is very important, as the application of some analysis tools yield different results for different scalings, *e.g.* see [52].

1.2.1 Interaction

Although the term *interaction* is frequently used, its meaning is rarely defined, leaving the reader to his own personal interpretations. It is generally known, that the cause for interaction in multivariable control systems is the coupling of process variables, which is exhibited in non-zero off-diagonal elements in the process transfer function matrix G. Still, a more clear definition for interaction is needed.

Suppose, a process is run in closed-loop and the closed-loop system consists of two subsystems A and B, as depicted in Fig. 3. Then two cases have to be considered:

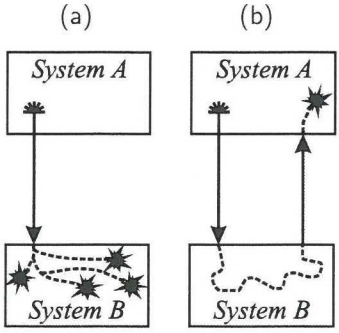

Fig. 3: Effects of interaction in multivariable systems

1. There is a path from A to B, see Fig. 3a.
   Then A acts as a disturbance on B, but not vice versa. Usually, B can be designed so that the effect of A is attenuated, [36].

2. There exists a loop from A via B back to A, see Fig. 3b.
   Then the dynamics of A are altered, which can have an effect on the stability of the closed loop system. This effect can first be studied after A and B are designed, which complicates controller synthesis.

Therefore, it is necessary to examine a closed-loop system for paths and loops between sub-systems. During controller design process couplings are often neglected in order to simplify the design task. These neglected couplings can then be used to determine the path and loops in a multivariable control system. Thereby, one achieves a decomposition of the closed-loop control system. In [60, 61], this type of decomposition is discussed for two-by-two systems with decentralized control. In this thesis, a generalization to arbitrary control structures and system sizes is given. It can be concluded that the controller has to be considered or at least assumptions on the performance of the closed-loop system are needed in order to draw correct conclusions on interaction.

Contrary to the above approach where interaction is quantified from a closed-loop perspective, the prediction of interaction from an open-loop perspective has already been dealt with in [3]. There, the *relative gain array* (RGA) has been introduced

$$RGA(G) = G(0) \times G^{-T}(0) \tag{8}$$

where $\times$ is the Schur or Hadamard product of two matrices and $-T$ denotes the matrix inverse transpose.

The RGA is dimensionless and independent of any scaling of G, namely the multiplication from left and right by diagonal matrix. Moreover, values close to one indicate no interaction and large interaction, otherwise. In order for the RGA to be applicable, the performance of the closed-loop system needs to achieve zero steady state control

error and each of the p feedback loops has to have a scalar controller, *i.e.* the control structure has to be diagonal. Certainly, this imposes restrictions on the reliability of the measure.

The RGA has been introduced as a static gain measure, but it has been shown in [25], that the RGA can be extended to a frequency dependent tool

$$\Lambda(G) = G(j\omega) \times G(j\omega)^{-H} \tag{9}$$

where H denotes the complex conjugate transpose and $\Lambda(G) = RGA(G)$ at $\omega = 0$.

Clearly, both RGA and Λ can only be derived for square process, namely $p = m$. According to [52], the inverse can be replaced by the pseudo-inverse, see [53], in order to overcome this problem

$$\Lambda(G) = G(j\omega) \times (G(j\omega)^{\dagger})^{H} \tag{10}$$

A similar interaction measure for 2×2 systems is the *Rijnsdorp Interaction Measure* which has been suggested in [46]

$$\kappa(s) = \frac{G_{12}(s)G_{21}(s)}{G_{11}(s)G_{22}(s)} \tag{11}$$

In [18] it is then shown that the measure is related to the RGA via the non-linear map

$$RGA(G) = \frac{1}{1 - \kappa(0)} \tag{12}$$

Recently, it has been shown that the *Rijnsdorp Interaction Measure* can be restated for arbitrary systems in [61]. There the measure is denoted relative interaction array (RIA) and can be defined in terms of the frequency dependent RGA

$$\phi_{ij} = \frac{1}{\lambda_{ij}} - 1 \tag{13}$$

where λ_{ij} are the elements in Λ and ϕ_{ij} are the elements in the RIA. For the RIA the same prerequisites as for the RGA are needed. The advantage of the RIA is the description of the interaction as a transfer function and that no interaction is associated with zero.

The main disadvantage of both the RGA and the RIA is the restriction to one controller structure and the performance requirement. An elimination of the restrictions is yield by the μ interaction measure, [18]. When a diagonal or block-diagonal controller is considered, then the design is based on the associated diagonal or block-diagonal part of the process transfer function matrix, namely

$$K(s) = \text{diag}(K_1(s), \ldots, K_p(s)) \tag{14}$$

$$\hat{G}(s) = \text{diag}(G_{11}(s), \ldots, G_{pp}(s)) \tag{15}$$

Now, the relative error of the design model transfer function matrix $\hat{G}(s)$ and the process transfer function matrix $G(s)$ can be defined as

$$\epsilon(s) = (G(s) - \hat{G}(s))\hat{G}^{-1}(s) \tag{16}$$

Then it is suggested to use $\mu^{-1}(\epsilon(s))$ as an interaction measure, where μ is the structured singular value, [10]. If the design system is stable, then the interaction measure also gives an upper bound for the largest singular value with an arbitrary controller $K(s)$ as

$$\bar{\sigma}\left(\hat{G}(s)K(s)(I + \hat{G}(s)K(s))^{-1}\right) < \mu^{-1}(\epsilon(s)) \tag{17}$$

Additionally, a stability condition for a chosen control structure can be stated based on ϵ.

It can be concluded that there are interaction measures that either compute the interaction in a closed-loop system or predict the interaction from the process transfer function matrix in combination with requirements on the controller. Hence, control system designs can be evaluated in terms of their interaction properties.

1.2.2 Directionality

Multivariable system can be described by dint of matrices and vectors. Since directions are important properties in vector and matrix analysis, these are likewise useful in the analysis of multivariable systems. It can be seen from the derivation of the gain of the multivariable system, that the gain not only depends on frequency but also on the direction of the input signal, *e.g.* see [52, 32].

Consequently, the Bode magnitude of the elements in G is not sufficient to characterize the gain of a multivariable system. Instead, the singular values provide the necessary information. The singular values of G can be derived via the singular value decomposition (SVD) of the frequency response of G at an arbitrary frequency ω_a

$$G(j\omega_a) = U\Sigma V^H \tag{18}$$

where $U \in \mathbb{C}^{p\times p}$, $V \in \mathbb{C}^{m\times m}$ and $\Sigma \in \mathbb{R}^{p\times m}$. Σ is a diagonal matrix with $l = \min(p, m)$ singular values on the diagonal, which are ordered as follows

$$\overline{\sigma} = \sigma_1 \geq \sigma_2 \geq \cdots \geq \sigma_l = \underline{\sigma} \geq 0$$

The column vectors of the unitary matrices U and V constitute the output and input directions, respectively. Each singular value is associated with one output and input direction. Clearly, the singular values and directions are a function over frequency. For more information on directions and the analysis of matrices, the interested reader is referred to [22].

In the analysis of multivariable systems the maximum singular value $\overline{\sigma}(G)$ can be interpreted similarly to Bode's magnitude of scalar systems. It has to be noted that,

contrary to the magnitude of scalar systems, the singular values are not analytic. In addition, the minimum singular value $\underline{\sigma}(G)$ is important in respect to input saturation and its relation to $\overline{\sigma}(G)$ concerns sensitivity analysis, see *e.g.* [37, 58].

When the directionality of a process is analyzed, the condition number can be used as quantification. One way to define the condition number is as follows

$$\gamma(G) \triangleq \frac{\overline{\sigma}(G)}{\underline{\sigma}(G)} \tag{19}$$

A large value of the condition number connotes a large difference between $\underline{\sigma}(G)$ and $\overline{\sigma}(G)$, which indicates that directions in signals have large impact on the gain of the multivariable system. Process models that have large condition numbers are called *ill-conditioned*, which can indicate that the process is difficult to control.

Since the condition number depends on the scaling of a multivariable process, it can be suggested that the minimized condition number should be considered if the scaling is uncertain

$$\gamma^*(G) = \min_{D_1, D_2} \gamma(D_1 G D_2) \tag{20}$$

where D_1 and D_2 are diagonal real and positive matrices.

In [52] and [4] it is shown that the RGA (9) and the minimized condition number (20) can also be used to evaluate the sensitivity of the closed-loop system to model uncertainty. Indications for the sensitivity can already be obtained from the analysis of the process model.

1.3 Controller Synthesis

The synthesis of controllers for multivariable systems has been studied for many years, and a wide variety of techniques are available, see *e.g.* [48], [26], [32], [17], [42] and [59]. Usually, the synthesis of a controller for a multivariable process can be divided into two phases, the selection of the control structure and the design of the controller.

1.3.1 Control Structure Design

The selection of the control structure is a crucial step in the synthesis of multivariable controllers. Although no specific assumptions are made on the control law, the structure of the controller poses restrictions on achievable performance and even stability of the closed loop system.

The aim of *control structure design* is to determine a control structure with minimal topological complexity, *i.e.* minimal number of non-zero elements in controller transfer function matrix K, that can fulfill the desired performance specifications. Moreover, the decision is solely based on a model of the process in question. First attempts are reported in [12] and later an overview of the area is given in [38, 39, 40]. It has also

been seen that stability, interaction and control structure are closely connected, see [44] and [18].

Suppose, the multivariable transfer function matrix G is of size $p \times m$, then a full multivariable controller K has the size $m \times p$. This is also the control structure of maximal topological complexity. Now, the task of *control structure design* is to find a set of sub-systems in K that reduce the topological complexity and potentially yield the desired performance of the closed-loop system. These sub-systems can be either scalar or multivariable controllers.

1.3.2 Decentralized Control

The control structure of minimal topological complexity is the decentralized control structure, *i.e.* K is diagonal and all controllers are scalar. It can only be applied to square processes, namely $p = m$. When this control structure is chosen, then m measurement/actuator pairs have to be selected, which is one combination out of $m!$ possible combinations. Consequently, criteria are needed to make the selection of the pairs.

The interaction measures RGA and RIA give estimates for the interaction in multivariable control systems where decentralized control is applied and have been effectively used for the selection of measurement/actuator pairs, *e.g.* see [43], [61], [49] and [28]. The pairs are selected by minimizing the overall distance of the RGA or RIA pairs to one or zero, respectively.

The exclusive usage of the RGA or RIA can sometimes yield unstable selection of pairs in some cases. A discussion of this can be found in [52]. As the *Niederlinski index* [44] or the *μ-interaction measure* [18] give a stability condition for decentralized controllers, the above criteria should take these into account. A criterion that considers the RIA and *μ-interaction measure* is discussed in [14].

Recently, a selection criterion based on the Hankel singular values (HSV) has been suggested [6]. There, a participation matrix is computed that consists of the normalized sum of the HSV of each scalar sub-system of G

$$\Psi_{ij} = \frac{\text{trace}(\Gamma_{cj}\Gamma_{oi})}{\text{trace}(\Gamma_c\Gamma_o)} \tag{21}$$

where Γ_c and Γ_o are the controllability and observability gramian of G, respectively. Γ_{cj} denotes the controllability gramian of G for input j alone and Γ_{oi} denotes the observability gramian of G for output i alone. The pairs that yield the overall largest value are then selected for decentralized control.

A modification of (21) that only makes use of the largest HSV, namely the Hankel norm is suggested in [57]. The new measure is denoted *Hankel interaction index array*

and is defined as

$$[\Sigma]_{ij} = \frac{||G_{ij}(s)||_H}{\sum_{q,r} ||G_{qr}(s)||_H} \tag{22}$$

where $||\bullet||_H$ denotes the Hankel norm. Again, the pairs that yield the overall largest value are selected. Common for both measures is the consideration of both controllability and observability of the sub-system in the criteria. Thus, the aim is to use pairs that have considerable impact on the behavior of the process.

Certainly, there are more selection criteria available for decentralized controllers, *e.g.* closed-loop disturbance gains, performance relative gain array and partial relative gains, but are omitted here. A discussion of those can be found in [52] and [20].

After a selection of the measurement/actuator pairs is made, then m scalar controllers are designed independently. For the controller synthesis, all scalar techniques are admissible.

1.3.3 Centralized Control

When more complex controller structures are admitted, then the combinatorial complexity of the structure selection problem increases. Instead of selecting pairs, arbitrary blocks can be selected. The choice of blocks becomes necessary, when a distinction of pairs is not possible from the above criteria.

A generalization of the RGA to the use of block diagonal structures is derived in [33]. There the concept of block relative gains (BRG) is introduced. The principal idea is to select a block diagonal structure and derive a measure in a similar manner as the RGA. The BRG for an $n \times n$ size block is then given as

$$\Lambda_B^l = G_B \left[G^{-1}\right]_B \tag{23a}$$

$$\Lambda_B^r = \left[G^{-1}\right]_B G_B \tag{23b}$$

where the index B denotes the block. If the analyzed block is not a scalar sub-system, then the left BRG Λ_B^l and right BRG Λ_B^r are not identical.

The analysis is then conducted by first considering small blocks and then advancing to larger blocks. For each selection the BRG is computed and evaluated. There, blocks that have left BRGs with diagonal elements and eigenvalues close to one are considered for control. The right BRGs are only secondarily analyzed due to their physical insignificance. It is suggested that the decision process is iterative and that control structures are screened out.

Alternatively, in [31] screening tools for arbitrary control structures based on the structured singular value theory are suggested. The approach is based on the analysis of achievable robust performance and is complicated in terms of the definition of

the robust performance objectives. Additionally, the approach is computationally intensive due to the necessary optimizations.

Compared to that the use of the gramian-based approach [6] is simple. There, the computation of the participation matrix can be generalized to the use of multivariable sub-systems. Then (21) can be restated so that the controllability and observability gramians of a multivariable sub-system are used instead. The decision for a control structure is then made according to the overall largest value.

Contrary to the RGA, the three tools can evaluate a fully centralized controller. Moreover, a fully centralized controller yields the best values for BRG and gramian-based tool. Consequently, design and implementation effort of the fully centralized controller has to be considered during the selection.

When a fully or partially centralized control structure is chosen, then the controller can be synthesized in several ways

- Direct multivariable controller design
- Decoupling and subsequent scalar controller design
- Sequential loop closing design

For the direct multivariable controller design many techniques are available: $\mathcal{H}_2$, $\mathcal{H}_\infty$ and μ synthesis, only to mention some. Clearly, the choice of the design technique depends on the available models and on the environment in which the controller is used. Therefore, it would be prejudiced to give any technique a competitive edge. A further discussion of the design techniques is omitted here and the interested reader is referred to the literature, *e.g.* see [52, 32, 17, 9, 13, 16, 48].

Design via decoupling is performed in two steps. First, a dynamic system is designed which compensates for couplings between process variables. Second, the process with the decoupling system behaves as a collection of scalar processes for which scalar controllers are designed. Thereby, the multivariable control problem is reduced to several scalar control problems. The usage of these decoupling networks is often unreliable due to its sensitivity to parameter uncertainties in the process model or due to approximations in the decoupling network. Moreover, the implementation of inverse-based decoupling networks is often difficult due to non-causal dynamics. A more detailed discussion of the subject can be found in [52, 32]. Still, when decoupling is possible, then the subsequent controller design is straightforward.

As well in the case of sequential loop closing a two-step approach is chosen. However, the multivariable system needs to be square. In the first step the closing sequence is determined and then in the second, one controller is designed at a time considering the dynamics of the already closed loops. Moreover, this technique can be used in combination with a pairs selection tool. The controllers are then designed with scalar techniques. A drawback of this method is its dependency on the loop closing order, which has to be maintained in order to guarantee stability, see [32].

2 Audio and video in control applications

During the last decade the computational power of processors has increased tremendously, enabling the handling of complex tasks in short times. Audio and video information is long been considered incongruous with real-time control applications due to long processing times. Indeed, audio and video create new application areas for closed-loop control, as new physical contiguities become accessible.

In addition to that, audio and video differ from usual measurement devices as they deliver signals that reflect several physical contiguities, *e.g.* a video signal can reflect the position of several objects in space. Moreover, the output signal can be multidimensional, *e.g.* a video signal is a matrix of pixels. Thus, the sensor should be interpreted as a multivariable system and should be treated accordingly.

Unfortunately, the direct usage of these types of information sources is rare in control engineering and the theory is rather undeveloped. Consequently, in applications where audio or video is used as sensors, a secondary scalar measurement is inferred from the audio or video information. Usually, the secondary measurement is obtained by means of feature extraction, *e.g.* image analysis. The dynamics of the feature extraction is then ignored in the subsequent design and analysis of the closed-loop system. The application of audio and video in closed-loop control is now shortly reviewed.

2.1 Audio

Audio information from a process can be obtained in two different ways. Firstly, a specially designed audio signal is emitted and the resulting echo is then received and processed. In that way an active measurement procedure is employed, as the process is affected by the signal. This methodology is often used in ultrasonic measuring applications.

Secondly, only the audio emissions of the process are recorded and processed, which is a passive measuring technique. Usually a better knowledge of the process is needed in order to characterize the audio features that are emitted by the process. Moreover, the process is not affected by the sensing method, and thus is non-intrusive. In this thesis the latter method is used.

Some examples for inferential control and monitoring schemes are discussed in [5, 24, 23, 56]. In all cases physical contiguities are inferred from spectral characteristics of the audio signal. Consequently, spectral decomposition of the short time windowed signal is used to extract features that are correlated with the contiguities. A similar approach is employed in the thesis.

Applying time/frequency analysis to the audio signal splits the scalar signal into a vector signal. Thereby, the measurement device becomes a multivariable system with a large number of outputs. A model for this system could then be used to design efficient measurement devices. Unfortunately, the theory of such multivariable

systems is poorly developed, which makes the modelling a complicated task.

2.2 Video

Similar to measurement with audio, active and passive methods utilizing video can be designed. Again, only the passive methods are considered here.

The video signal is a two-dimensional image that consists of a large number of pixels and varies over time. Each pixel can be interpreted as a sensor signal, but since the observed contiguity might move over the image array, the pixels are not independent signals in relation to the contiguity. When a camera records an object, then a 3D object is mapped into a 2D image. Thereby, a contiguity can become unobservable, which motivates the need for models. Consequently, the design task for an inferential measurement device based on video is more complicated than for audio.

In the area of robotics, video is widely used, *e.g.* for guidance, object recognition or obstacle avoidance. On the contrary, the usage in closed-loop control application is rather rare but some examples can be found. In [21] a review of existing measurement techniques for particulate processes is given. Most important, there it is shown that the application of video has great potential and can be very beneficial. The use of video in control applications is also reported in [27, 19, 45, 47, 30].

Additionally, the calibration of video based measurement device is more involved than for audio, due to the dependency on the *line of sight*. Moreover, when a video-based system is interpreted as a multivariable system, the number of outputs is increasing tremendously, *i.e.* cameras with more than one million pixels are not costly anymore.

2.3 Challenges

When secondary measurements are inferred from audio or video, then non-linear dynamics are often introduced into the process, which may lead to unobservability or unexpected performance of the closed loop system, see [41, 15]. Consequently, models for measurement devices comprising audio or video are needed. Thereby, the analysis and design of closed-loop system is facilitated. But due to the complexity of the modelling task, new tools are needed that simplify the handling of large numbers of inputs and outputs. These tools should first select a model structure of minimal topological complexity, which can represent the process dynamics significant for closed-loop control. Clearly, there are similarities to control structure design and it should therefore be investigated how these ideas or tools are applicable.

The calibration of audio and video is usually complicated due to the dependency on the environment, *i.e.* signal to noise ratio can vary over time. In applications of video the recorded image is affected by external light sources and by obstacles in the line of sight. In the case of audio, the noise level can vary and additional sound sources may appear unintentionally. Such occurrences can be interpreted as disturbances or

uncertainties. Hence, a control system that uses audio or video has to be insensitive to such events.

Beside the complicating factors and problems that may arise, audio and video have several advantages. Firstly, equipment costs can be reduced, when off-the-shelf hardware can be used instead of special measurement equipment. Secondly, maintenance and replacement is possible without interruption of plant operation, as the audio and video are non-intrusive. Certainly, the control system needs to be able to handle hardware replacement. Thirdly, multiple contiguities can be observed with one device.

3 Industry applications

The integration of multivariable control with industry applications is necessary in order to reduce the gap between theory and practice. Thereby, the industry can benefit from advanced control strategies and at the same time the scientific community can profit from application experience and newly emerged ideas. In other words, both parts can benefit from more interweavement.

3.1 Performance enhancement and advanced control

The application of advanced control techniques often leads to new possibilities in plant operation. For example, the operation of gas pipelines can be improved by means of multivariable control [55, 1], releasing plant operators from tedious set-point adjustments. Moreover, advanced control creates the possibility to optimize plant performance which in turn yields higher profits, [54, 2].

The popularity of scalar control loops is due to their simplicity in design, tuning and maintenance. However, there is no real proof that scalar control loops are more robust, though it seems to be a common assumption. Besides, it is clear that the achievable performance is more limited for single loops than for multivariable control structures, [8]. When multivariable control is considered, the topological complexity of a controller has to be weighted against the performance improvements.

Fundamental limitations are inherent in industrial process from construction. It is therefore necessary that these limitations are considered when performance objectives are formulated, [51]. Otherwise, unattainable performance specifications might be the result. There, multivariable design techniques are necessary tools for both determination of performance specifications and design of an appropriate controller.

The application of advanced control strategies also reveals other insufficiencies in a process as variations of process variables are reduced. In turn, further optimization of software and hardware becomes possible. Another advantage is a prolonged life-cycle of the plant, since advanced control leads to a better utilization of the plant capacity.

Thereby, costly investments in new hardware can be deferred.

3.2 Necessity of industrial tests

Many research projects are conducted to be successful in a laboratory setup. For research in areas where new manufacturing methods, products or techniques are developed, this is understandable. But if the goal of a project is to optimize processes, improve product quality or reduce costs, the target should be successful industrial tests. There are of course several reasons.

First of all, laboratory setups often comprise simplifications of an industrial process, especially non-linearities and couplings to other processes are removed. Additionally, there are less disturbances and noise. Thus, conclusions on performance improvements are not reliable until they are validated through tests at the real process.

Secondly, implementation issues are rarely considered during research, which can lead to difficulties when results are transferred to the real process. When advanced controllers are tested or permanently installed, the plant control system needs to be able to support them. However, frameworks for the implementation of multivariable controllers in programmable logic controllers (PLC) are still rare. Thus, the transition from laboratory setups to the industry plant becomes a complicated task.

When industrial tests are performed they have to be endorsed by the organization of the industry. It is necessary to have the support on all parts of the hierarchy, *i.e.* plant operators, maintenance, engineering and management. Otherwise, tests rarely succeed if come to pass at all. Thus, even promising results might not be considered for industrial implementation.

Besides, and from personal experience of the author, the design of advanced control strategies is the smallest part when a full-scale industrial application is pursued. When an advanced controller is considered for permanent installation, then the spent efforts for industrial tests pay back in smoother upgrade from present control to the new control strategy.

3.3 Innovation and economical benefits

Industry management assimilates innovation if the economical benefits of the innovation can be pinpointed. Otherwise, innovations are not immediately accepted.

Assessing economical benefits is not an easy task. As industrial processes are complex, control performance improvements do not need to be reflected in the resulting product. Hence, economical benefits are hard to prove and recently more attention has been paid to the economical evaluation of control projects, see *e.g.* [7, 34, 35, 29]. The main idea is to set up a rigid framework which enables the analysis of both performance improvements and economical benefits. It is argued that a level of statistical

significance is required in order to demonstrate an economical profit.

It can be concluded that economical benefits due to performance improvements can only be ensured after long-term industrial tests.

4 Concluding remarks

It is clear from the presentation that multivariable control strategies have a great potential and are needed in the industry. It has also been pointed out, that there are obstacles that still have to be overcome so that multivariable control becomes more accessible for engineers.

In this thesis, the considered industry applications are taken from the steel industry, pulverized coal injection in blast furnaces and LD-converters. The latter is only dealt with as an experimental setup. In the projects, the industry has always been involved, which facilitated the transition from design via experiments and tests to permanent installation of multivariable controllers. Both sides, industry and university, have profited from the close collaboration.

Additionally, new ideas have emerged during these projects, which partially have not yet taken physical form. Clearly, the use of multivariable techniques is developing, *i.e.* interaction analysis in combination with control structure design. Recent publications [50, 57] show that interaction analysis is an active area of research and that the assessment of interaction from process data is an important issue. When interaction measures can be estimated from process data, then on-line control structure design becomes possible.

Moreover, control structure design could facilitate the integration of audio and video in control applications, since selection of reduced multivariable system structures could be based on the evaluation of interaction measures. This is certainly an area of interest for future research.

5 Bibliography

[1] Richard Bailey and Chuck Holcomb, *Application update - HMI, SCADA reduces pipeline monitoring and costs*, Control Engineering (2001), 22.

[2] Hilmar Bischof, Thomas Pelster, Tim Morrison, Klaus Rößler, and Michael Sugars, *Advanced control improves - german aromatics operation*, Oil & Gas Journal (2000), 68–71.

[3] E.H. Bristol, *On a new measure of interaction for multivariable process control*, IEEE Transactions on Automatic Control **11** (1966), 133–134.

[4] Jie Chen, James S. Freudenberg, and Carl N. Nett, *The role of the condition number and the relative gain array in robustness analysis*, Automatica **30** (1994), no. 6, 1029–1035.

[5] G. Chryssolouris, P. Sheng, and F. von Alvensleben, *Process control of laser grooving using acoustic sensing*, Journal of Engineering for Industry, Transactions of the ASME **113** (1991), no. 3, 268–275.

[6] Arthur Conley and Mario E. Salgado, *Gramian based interaction measure*, Proc. of the 2000 Conference on Decision and Control, Sydney, 2000.

[7] I.K. Craig and R.G.D. Henning, *Evaluation of advanced industrial control projects: A framework for determining economic benefits*, Control Engineering Practice **8** (2000), 769–780.

[8] Hong Cui and Elling W. Jacobsen, *Performance limitations in decentralized control*, Journal of Process Control **12** (2002), 485–494.

[9] Richard C. Dorf and Robert H. Bishop, *Modern control systems*, Addison-Wesley, 1998.

[10] John Doyle, *Analysis of feedback systems with structured uncertainties*, Proc. IEE-D **129** (1982), no. 6, 242–250.

[11] Environment Directorates-General, *Economic evaluation of sectoral emission reduction objectives for climate change*, Study, European Commission, http://europa.eu.int/comm/environment/, October 2001.

[12] A.S. Foss, *Critique of chemical process control theory*, AIChE Journal **19** (1973), 209–214.

[13] Gene F. Franklin, J. David Powell, and Abbas Emami-Naeini, *Feedback control of dynamic systems*, third ed., Addison-Wesley, 1994.

[14] E. Gagnon, A. Desbiens, and A. Pomerleau, *Selection of pairing and constrained robust decentralized PI controllers*, Proc. of American Control Conference, San Diego, USA, June 1999.

[15] Guillermo D. González and Rafael Odgers, *Issues in the design of control loops using soft-sensors*, Proc. of IFAC 13th Triennial World Congress, San Francisco, USA, 1996, pp. 499–504.

[16] Graham C. Goodwin, Stefan F. Graebe, and Mario E. Salgado, *Control system design*, Prentice Hall, 2000.

[17] Michael Green and David J. N. Limebeer, *Linear robust control*, Englewood Cliffs : Prentice Hall, 1995.

[18] Pierre Grosdidier and Manfred Morari, *The μ interaction measure*, Ind. Eng. Chem Res. **26** (1987), 1193–1202.

[19] M. Guarini, J. Cacares, A. Guesalaga, A. Cipriano, J. Olmendo, and H. Lorenzo, *Sensor for assessing the quality of the mineral flotation process*, Proc. of 1994 IEEE International Symposium on Industrial Electronics, Santiago, Chile, May 1994.

[20] Kurt E. Häggblom, *Control structure selection via relative gains of partially controlled systems.*, Proc. of the European Control Conference, Brussels, Belgium, 1997.

[21] Camiel Heffels, Reinhard Polke, Matthias Raedle, Bernd Sachweh, Michael Schaefer, and Norbert Scholz, *Control of particulate processes by optical measurement techniques*, Particle & Particle Systems Characterization **15** (1998), no. 5, 211–218.

[22] Roger A. Horn and Charles R. Johnson, *Topics in matrix analysis*, Cambridge University Press, 1991.

[23] R. Hou, A. Hunt, and R.A. Williams, *Acoustic monitoring of hydrocyclone performance*, Minerals Engineering **11** (1998), no. 11, 1047–1059.

[24] ———, *Acoustic monitoring of pipeline flows: Particulate slurries.*, Powder Technology **106** (1999), no. 1, 30–36.

[25] M. Hovd and S. Skogestad, *Simple frequency-dependent tools for control systems analysis, structure selection and design*, Automatica **28** (1992), no. 5, 989–996.

[26] Y.S. Hung and A.G.J. MacFarlane, *Multivariable feedback: a quasiclassical approach*, Lecture Notes in Control and Inform. Sci., vol. 40, Springer-Verlag, Berlin, 1982.

[27] A.P. Kjaer, P.E. Wellstead, and W.P. Heath, *On-line sensing of paper machine wet-end: dry-line detector.*, IEEE Transactions on Control Systems Technology **5** (1997), no. 6, 571–585.

[28] I.K. Kookos and A.I. Lygeros, *An algorithmic method for control structure selection based on the RGA and RIA interaction measures*, Trans IChemE **76, Part A** (1998), 458–464.

[29] P. Lant and M. Steffen, *Benchmarking for process control: Should I invest in improved process control?*, Water Science and Technology **37** (1998), no. 12, 49–54.

[30] John Erik Larsson, Thomas Gustafsson, and Stefan Ronnback, *Paper machine dry line positioning system*, Proc. of 1998 Conf. on Control Systems: Information Tools to Match the Evolving Operator Role, Sept 1-3, Porvoo, FIN, September 1998.

[31] Jay H. Lee, Richard D. Braatz, Manfred Morari, and Andrew Packard, *Screening tools for robust control structure selection*, Automatica **31** (1995), no. 2, 229–235.

[32] J.M. Maciejowski, *Multivariable feedback design*, Addison-Wesley, 1989.

[33] Vasilios Manousiouthakis, Robert Savage, and Yaman Arkun, *Synthesis of decentralized process control structures using the concept of block relative gain*, AIChE Journal **32** (1986), no. 6, 991–1003.

[34] T.E. Marlin, J.D. Perkins, G.W. Barton, and M.L. Brisk, *Advanced process control applications*, Tech. report, NC: Instrumentation Society of America, Research Triangle park, 1987.

[35] ———, *Benefits from process control: Results of a joint industry-university study*, Journal of Process Control **1** (1991), 57–83.

[36] A. Medvedev and G. Hillerström, *An external model control system*, Control Theory Adv. Tech. **10** (1995), no. 4, part 4, 1643–1665.

[37] Manfred Morari, *Design of resilient processing plants III - A framework for the assessment of dynamic resilience*, Chemical Engineering Science **38** (1983), 1881–1891.

[38] Manfred Morari, Yaman Arkun, and George Stephanopoulos, *Studies in the synthesis of control structures for chemical processes. I. Formulation of the problem. process decomposition and the classification of the control schemes.*, AIChE J. **26** (1980), no. 2, 220–232.

[39] Manfred Morari and George Stephanopoulos, *Studies in the synthesis of control structures for chemical processes. II. Structural aspects and the synthesis of alternative feasible control schemes*, AIChE J. **26** (1980), no. 2, 232–246.

[40] ———, *Studies in the synthesis of control structures for chemical processes. III. Optimal selection of secondary measurements within the framework of state estimation.*, AIChE J. **26** (1980), no. 2, 247–260.

[41] Manfred Morari and George Stephanopoulus, *Minimizing unobservability in inferential control schemes*, International Journal of Control **31** (1980), no. 2, 367–377.

[42] Manfred Morari and Evanghelos Zafiriou, *Robust process control*, Englewood Cliffs : Prentice Hall, 1989.

[43] Carl Nett, *Decentralized control system design for a variable-cycle gas turbine engine*, Proc. of the 28th IEEE Conference on Decision and Control (Tampa, USA), vol. 2, 1989, p. 1301.

[44] A. Niederlinski, *A heuristic approach to the design of linear multivariable interacting control systems*, Automatica **7** (1971), 691–701.

[45] Carl R. Petrus, *Integration of imaging pyrometry into the wampum plant automation project*, Proc. of 1997 39th IEEE/PCA Cement Industry Technical Conference, Hershey, PA, USA., April 1997.

[46] J.E. Rijnsdorp, *Interaction on two-variable control systems for distillation columns*, Automatica **1** (1965), no. 1, 15–28.

[47] G. Robertson, J. Olson, P. Allen, B. Chan, and R. Seth, *Measurement of fiber length, coarseness and shape with the fiber quality analyzer*, Process Control News **20** (2000), no. 1.

[48] Howard Harry Rosenbrock, *Computer-aided control system design*, London : Academic Press, 1974.

[49] Henning Schmidt and Elling W. Jacobsen, *Control structure design of an offshore separator train*, Report, S3-Automatic Control, Royal Institute of Technology, SE-10044 Stockholm, 2002, IR-S3-REG-0203.

[50] C.T. Seppala, T.J. Harris, and D.W. Bacon, *Time series methods for dynamic analysis of multiple controlled variables*, Journal of Process Control **12** (2002), 257–276.

[51] María M. Seron, Julio H. Braslavsky, and Graham C. Goodwin, *Fundamental limitations in filtering and control*, Springer-Verlag, 1997.

[52] S. Skogestad and I. Postlethwaite, *Multivariable feedback control - analysis and design*, John Wiley & Sons, 1996.

[53] Gilbert Strang, *Linear algebra and its applications*, third ed., Harcourt, Inc., 1988.

[54] Vance J. VanDoren, *Optimizatin means higher profits*, Control Engineering (1999), 56–60.

[55] Ganesh Venkataramanan, Ujjal Basu, Peter Linden, and E. Philip Ferber, *Smoother amd more economic operation of gas pipelines*, IEEE Transactions on Industry Applications **36** (2000), no. 5, 1430–1434.

[56] T. Wessa, S. Kueppers, M. Rapp, and J. Reibel, *Validation of an industrial analytical sensor procedure realized with a SAW-based sensor system.*, Sensors and Actuators, B: Chemical **70** (2000), no. 1-3, 203–213.

[57] Björn Wittenmark and Mario E. Salgado, *Hankel-norm based interaction measure for input-output pairing*, Proc. of the 2002 IFAC World Congress, Barcelona, 2002.

[58] C.C. Yu and W. Luyben, *Design of multiloop SISO controllers in multivariable processes.*, Industrial and Engineering Chemistry Process Design and Development **25** (1986), 498–503.

[59] Kemin Zhou, *Robust and optimal control*, Prentice Hall, 1996.

[60] Zhong-Xiang Zhu, *Loop decomposition and dynamic interaction analysis of decentralized control systems*, Chemical Eningeering Science **51** (1996), no. 12, 3325–3335.

[61] ———, *Variable pairing selection based on individual and overall interaction measures*, Ind. Eng. Chem. Res. **35** (1996), no. 1, 4091–4099.

Contribution

During the period from 1997 to 2002, the author has been in involved in several research projects conducted at the *Control Engineering Group* at *Luleå University of Technology*.

In the following sections the connection between the projects and the included papers is clarified. Additionally, the contribution of the author to the research projects is shortly summarized. Finally, a list of further publications is given.

1 Control of pulverized coal injection

Control of pulverized coal injection was part of the project *Reliable Process Control* which was conducted by the Center for Process and System Automation (ProSA), at Luleå University of Technology. The project was financed by grants from Norrbottens Research Council. The following included papers reflect the contribution of the author

Paper 1: Wolfgang Birk and Alexander Medvedev. "Pressure and flow control of a pulverized coal injection vessel". *IEEE Transactions on Control Systems Technology*, 8(6):919–929, November 2000.

Paper 2: Wolfgang Birk and Alexander Medvedev. "Sensitivity analysis of an LQ optimal multivariable controller for a fine coal injection vessel". *IEEE Transactions on Industry Applications*, 36(3):871–876, May/June 2000.

Paper 3: Wolfgang Birk, Andreas Johansson, Robert Johansson, and Alexander Medvedev. "Implementation and industrial experiences of advanced control and monitoring in coal injection". *Control Engineering Practice*, 8(3):327–335, 2000.

The objective of the project was to show that the operation of a pulverized coal injection (PCI) plant can be made more reliable and safe by means of advanced control in combination with fault detection.

For this end, a linear quadratic multivariable controller was designed, analyzed and implemented. The design and first experiments are described in Paper 1, which

was then followed by a sensitivity analysis of the control strategy, see Paper 2. The multivariable controller was also compared with a decentralized PI controller. Finally, the multivariable controller is implemented in the PLC system of PCI plant together with a gas leakage detection system, which is designed by Andreas Johansson.

The implementation and industrial experiences of the model-based control and gas-leakage detection system in a coal injection plant are then reported in Paper 3.

2 Interaction and Control Structures

During the work with the latter project ideas concerning interaction and control structures in multivariable control systems emerged. The results are still unpublished but account for a large part of the authors contribution and thus, are included. The following papers reflect this contribution

Paper 4: Wolfgang Birk and Alexander Medvedev. "A Note on Gramian-Based Interaction Measures". Submitted to *European Control Conference ECC2003, 1-4 September, University of Cambridge, UK*, August 2002.

Paper 5: Wolfgang Birk and Alexander Medvedev. "Improving Control Structures in Multivariable Control Systems". Submitted to *Journal of Process Control*, August 2002.

Interaction in multivariable control system from an open-loop perspective has been studied widely for several decades. Still, little attention has been payed to the assessment of interaction in the closed loop system, namely considering the controller.

In Paper 4, the assignment of measurement/actuator pairs for decentralized control using gramian-based interaction measures is discussed. A geometrical interpretation of gramian-based measures is given and a generalization to weighted gramians is introduced. Clearly, the assignment is done from an open-loop perspective, where the controller remains unspecified, and needs a model for the process. Consequently, a decentralized controller structure is found and can be applied to the process.

In Paper 5 it is then suggested that an applied decentralized control structure should be evaluated from a closed-loop perspective. First, a dynamic quantification of interaction in a closed loop system is derived and secondly, the structural mismatch of a decentralized control scheme is quantified in terms of transfer function matrices. An evaluation of these transfer function matrices can be used for control structure improvements.

Hence, the tools described in these papers can be used to design, evaluate and improve controllers for multivariable systems. In both papers the coal injection process is considered as application example.

3 Audio Information in Control

In cooperation with the Division for Process Metallurgy at the *Royal Institute of Technology* in Stockholm the behavior of dynamic foaming in the LD converter is studied. The following included paper reflects the contribution of the author

Paper 6: Wolfgang Birk, Ioannis Arvanitidis, Pär Jönsson, and Alexander Medvedev. "Foam level control in a water model of the LD converter process". *Control Engineering Practice*, in print, 2002.

The aim of the project was to show that foam level in an LD converter can be estimated from audio information and that control of the foam level using the motion of the oxygen lance is possible.

The experimental setup consisting of a water model, that simulates the dynamic behavior of foaming in an LD converter, is created. A foam level estimation methodology from a microphone signal and its automatic calibration is designed. Based on a mathematical model of the dynamic behavior from lance motion to estimated foam level, a controller for foam level stabilisation is designed and applied in the water model. It is concluded that the foam level can be controlled using a microphone as measurement device and lance motion as actuator.

4 Video Information in Control

In cooperation with *Embedded Internet System Laboratory* at *Luleå University of Technology* the usage of video information in control is studied and is part of the project *Visualization of process properties.* The project is financed within the framework of the NUTEK Program *Complex technical systems.* The following paper reflects the contribution of the author

Paper 7: Wolfgang Birk, Olov Marklund, and Alexander Medvedev. "Video monitoring of pulverized coal injection in the blast furnace". *IEEE Transactions on Industrial Applications*, 38(2):571–576, 2002.

In the process industry many contiguities are often unmeasurable due to the environment, *i.e.* high temperatures, dust, high pressure. Thus, only non-intrusive measurement devices are applicable in these cases. Here, the instantaneous coal flow into a blast furnace is not directly measurable.

Therefore, image analysis of video information is used as a means to estimate the instantaneous coal flow. Using the inferred measurement the coal flow should then be stabilized. Initial experiments at the blast furnace no 3 of SSAB Tunnplåt AB Luleå, Sweden, are performed and first hand results on modelling and control of a single injection line are given.

5 Further Publications

Several publications are either too similar, *i.e.* conference papers that were with hindsight accepted for publication in journals, or the contribution of the author to them is too sparse to motivate an inclusion in the thesis. For the sake of completeness, these publications are listed below

1. Wolfgang Birk and Alexander Medvedev. "Pressure and flow control of a pulverized coal injection vessel". In *Proc. of the 1997 IEEE International Conference on Control Applications*, pages 127–132, 1997.

2. Andreas Johansson, Wolfgang Birk, and Alexander Medvedev. "Control and gas-leakage detection of pulverized coal injection: From design to experiment". In *Proc. of Reglermöte 1998, Lund, Sweden, 1998*, 1998.

3. Wolfgang Birk, Andreas Johansson, and Alexander Medvedev. "Control and gas leakage detection in a fine coal injection plant: Design and experiments". In *Proc. of 9th IFAC Symposium on Automation in Mining, Mineral and Metal Processes*, pages 271–276, 1998.

4. Andreas Johansson, Wolfgang Birk, and Alexander Medvedev. "Model-based gas leakage detection and isolation in a pressurized system via Laguerre spectrum analysis". In *Proc. of the 1998 IEEE International Conference on Control Applications*, pages 212–216, 1998.

5. Wolfgang Birk, Andreas Johansson, and Alexander Medvedev. "Model-based control for a fine coal injection plant". *IEEE Control Systems Magazine*, 19(1):33–43, February 1999.

6. Wolfgang Birk and Alexander Medvedev. "Sensitivity analysis of an LQ optimal multivariable controller for a fine coal injection vessel. In *Proc. of the IEEE Industry Applications Society 34th Annual Meeting*, 1999.

7. Wolfgang Birk and Alexander Medvedev. "Towards dynamic control of foaming". In *Proc. of the 1st Annual Symposium on Computer Science and Electrical Engineering, Luleå, Sweden, May 2000*, 2000.

8. Olov Marklund, Wolfgang Birk, and Alexander Medvedev. "Video monitoring of pulverized coal injection in the blast furnace". In *Proc. of Reglermöte 2000, Uppsala, Sweden, 2000*, 2000.

9. Wolfgang Birk, Ioannis Arvanitidis, Pär Jönsson, and Alexander Medvedev. "Physical modelling and control of dynamic foaming in an LD-converter process". In *Proc. of the IEEE Industry Applications Society 35th Annual Meeting, Sheraton Roma Hotel 8-12 October 2000 Rome Italy*, 2000.

10. Wolfgang Birk, Ioannis Arvanitidis, Pär Jönsson, and Alexander Medvedev. "Physical modelling and control of dynamic foaming in an LD-converter process". *IEEE Transactions on Industrial Applications*, 37(4):1067–1073, 2001.

11. Wolfgang Birk and Alexander Medvedev. "Foam level control in a water model of the LD converter process". In *Proc. of the 2nd Annual Symposium on Computer Science and Electrical Engineering, Luleå, Sweden, May 21-22, 2001*, 2001.

12. Wolfgang Birk, Ioannis Arvanitidis, Alexander Medvedev, and Pär Jönsson. "Foam level control in a water model of the LD converter process". In *Proc. of the 10th IFAC Symposium on Automation in Mining, Mineral and Metal Processes in Tokyo, Japan, September 4-6, 2001*, 2001.

13. Wolfgang Birk, Andreas Johansson, Alexander Medvedev, and Robert Johansson. "Model-based estimation of molten metal analysis in the LD converter: Experiments at SSAB Tunnplåt in Luleå". In *Proc. of the 2001 Annual IEEE Industry Applications Society Conference, in Chicago, USA, September 30 - October 4, 2001.*, 2001.

14. Wolfgang Birk, Olov Marklund, and Alexander Medvedev. "Video monitoring of pulverized coal injection in the blast furnace". In *Proc. of the 2001 Annual IEEE Industry Applications Society Conference, in Chicago, USA, September 30 - October 4, 2001.*, 2001.

15. Wolfgang Birk, Andreas Johansson, Alexander Medvedev, and Robert Johansson. "Model-based estimation of molten metal analysis in the LD converter: Experiments at SSAB Tunnplat in Lulea". *IEEE Transactions on Industrial Applications*, 38(2):565–570, 2002.

16. Alexander Medvedev, Andreas Johansson, Wolfgang Birk, Daniel Widlund, and Robert Johansson. "Model-based estimation of molten metal analysis in the LD converter: Experimental results". In *Proc. of IFAC World Congress, Barcelona, Spain*, 2002.

Papers

Paper 1

Pressure and Flow Control of a Pulverized Coal Injection Vessel

Published as

Wolfgang Birk and Alexander Medvedev. "Pressure and flow control of a pulverized coal injection vessel". *IEEE Transactions on Control Systems Technology*, 8(6):919–929, November 2000.

Pressure and Flow Control of a Pulverized Coal Injection Vessel

Wolfgang Birk and Alexander Medvedev
Control Engineering Group
Luleå University of Technology
S-971 87 Luleå, SWEDEN
wolfgang.birk@sm.luth.se

Abstract

This paper deals with model-based pressure and flow control of a fine coal injection vessel for the use of the blast furnace process. A control system should be in place to maintain a constant coal mass flow from the injection vessel to the blast furnace, since irregularities in the coal mass flow cause significant variations in the hot metal quality.

By means of system modeling, the structure and behavior of the coal injection vessel are analyzed. It is shown that by use of a model-based design, the control objectives can be reached and the control performance can be significantly improved compared to the PI-controllers. Alternative control strategies are discussed and compared with the conventional design. The linear quadratic gaussian (LQG) design method is used to design a MIMO controller which is validated through experiments on the coal injection plant at SSAB Tunnplåt in Luleå, Sweden.

1 Introduction and Background

Already in the early middle ages, the Chinese discovered how to reduce iron ore to iron. Ever since the process has become more and more sophisticated. Nowadays, iron is a mass product, produced in blast furnaces and later refined to steel. In order to make the process more efficient and optimized, it has become more usual to bring down the cost factors in the iron production by reducing the share of undesired by-products or the costs of energy supply.

Although coke is one of the most expensive energy carriers, it is common to use it in iron production. In Luleå, SSAB Tunnplåt reduces the production costs by partly substituting coke and using pulverized coal instead. Pulverized coal is about 40% cheaper than coke, which in fact makes it very attractive.

Since pulverized coal, in its pure form, is highly inflammable even under normal conditions, it is difficult to supply it to the process. Therefore, it is important to keep the pulverized coal isolated from the air, which can be done by using a pneumatic conveying device, where the transportation gas is nitrogen or at least has a higher rate of nitrogen compared to that of the air. The used coal injection plant is planned, designed and constructed by *BMH Claudius Peters AG* in Buxtehude, Germany.

In 1996, a research project has been started in order to make pulverized coal injection at SSAB Tunnplåt more secure and reliable. Research in the areas of fault detection, identification and control has been carried out (see [6], [9], and [2]).

Injecting coal powder in the blast furnace at a high rate of about $190kg/thm$ (ton hot metal) makes the blast furnace process very sensitive to coal flow outages, [5]. The prime concern in fine coal injection is therefore to maintain a constant coal mass flow to the blast furnace. Hence, a controller is needed to stabilize the coal mass flow.

This paper elaborates on controller design considerations and performance analysis, both theoretically and practically. The paper is structured as follows. First, the coal injection plant's structure and the injection process are described. Then, the currently used control unit is briefly analyzed followed by modelling of the injection process. The obtained model is then used for controller design in the section CONTROL STRATEGIES. There, the designed controller is compared with the currently used controller. Finally, the obtained controller is validated by means of simulation studies and practical tests, in the respective sections.

2 Coal injection plant

The coal injection plant is a highly automated plant, where incoming raw coal is stored, ground, dried and finally injected into the blast furnace. During operation, human interaction is only needed for set point adjustments.

2.1 Plant structure

Fig. 1 shows the structure of the plant, where the different sections are marked and referred to by the capital letters in the marked area. The sections A, B, C are common for the two fine coal silos. Sections D, E belong to Blast Furnace 2 and F, G to Blast Furnace 1. This article deals only with the coal injection of Blast Furnace 2. Therefore, the emphasize is placed on section E.

The raw coal handling is done in section A, where the receiving hopper is filled by trucks, delivering the raw coal from the stock. A grating on the top of the receiving hopper prevents feeding large lumps of material, in a size larger than $150mm$. The incoming raw coal is then transported by a horizontal and vertical belt conveyor system to the top of the raw coal storage bin. This storage bin has a volume of $250m^3$ and works like a buffer silo in order to equalize the raw coal feeding cycles and make coal continuously available to the mill.

The next section is the grinding plant. The mill performs several operations in one unit: grinding, drying and classifying. It works at a normal temperature between 250 and $300\,°C$. The working temperature is reached by blowing hot gas produced by the hot gas generator. The original corn size of the raw coal is reduced down to $100\mu m$,

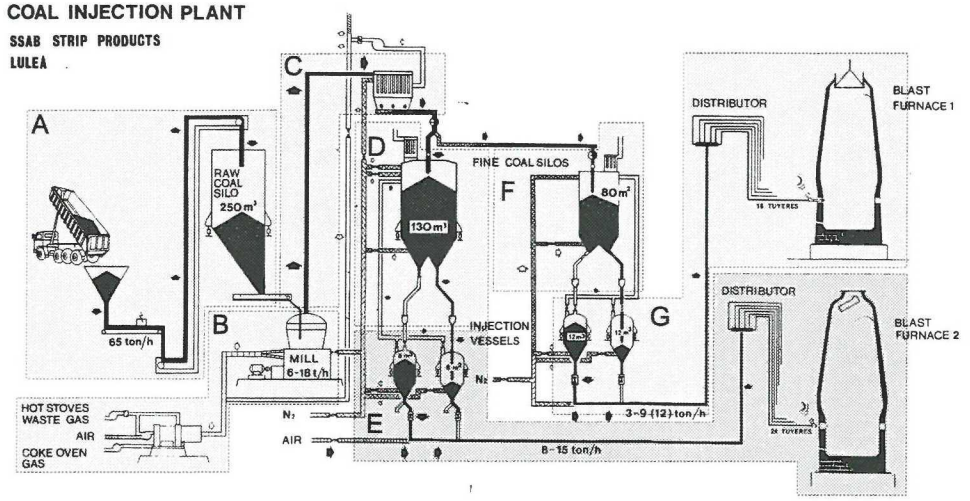

Fig. 1: Coal injection plant

and the humidity of the raw coal, which normally varies around 7%, is reduced to about 1%. The grinding capacity of the mill is controlled by the storage level in the fine coal silos.

In section C, the hot gas is blown through the mill in order to transport the classified final grinding product to the filter separator, which is placed on the top of the coal injection plant. The receiving filter separates the coal dust from the transport gas and collects the coal dust in the storage hopper from which it is discharged by a screw conveyor and a rotary airlock feeder into the fine coal silos.

There are two fine coal silos, one for each blast furnace. To each fine coal silo, two injection vessels are attached. Each one of them is built in the same way and has the same functionality. Thus, only Sections D and E are described below.

The fine coal silo collects the injectable coal powder and has a capacity of $130m^3$. It is operating under inert gas conditions which means that there is a slight overpressure of nitrogen in the silo. Since the silo is not pressure tight, a gas flow from the inside to the outside occurs, which guarantees that no air enters the fine coal silo. This gas flow is about $0.5\frac{Nm^3}{\text{min}}$. To guarantee the continuous discharge of the coal powder into the injection vessels, two outlet cones of the fine coal silo are equipped with fluidization nozzles. The two injection vessels feed the coal powder into the injection pipe where a coal distributor dispenses the coal/gas flow to 24 tuyeres, injecting the coal into the blast furnace. The injection vessels operate alternatively in order to maintain continuous injection.

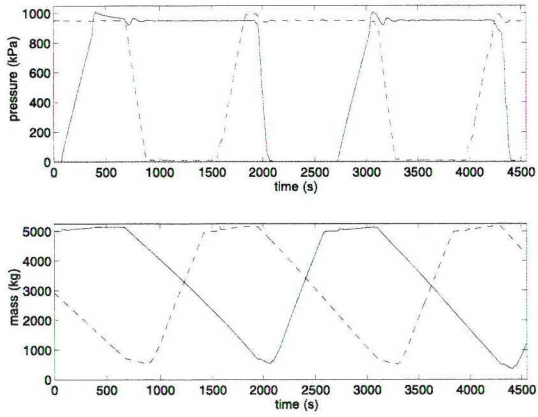

Fig. 2: Characteristic curves of vessel pressure and mass (vessel S21 - solid, vessel S22 - dashed)

Phase	Name	Description
A	Charging	The pressureless vessel is filled with coal powder
B	Pressurizing	The injection vessel is set under pressure
C	Pressure holding	Standby until the other vessel has finished injection
D	Injection	The coal powder is injected into the blast furnace
E	Ventilation	Depressurizing and ventilation of the vessel

Table 1: Process phases

2.2 Injection process

Principally, the injection process can be divided into two separate phases: a high-pressure and a low-pressure phase, where, as the names already imply, the pressure in the injection vessel is high or low, respectively. In Fig. 2, characteristic curves of vessel pressure and mass changes during a process working cycle are shown.

As already mentioned, one vessel is depressurized, charged and pressurized while the other vessel is injecting coal powder. To facilitate process identification and control, the high pressure and low pressure phases are sub-divided into more specific phases.

Fig. 3 shows one process cycle of injection vessel S21. A represents the low pressure phase and B to E belong to the high pressure phase. In Table 1, the nomenclature used in the sequel to refer to process phases is summarized.

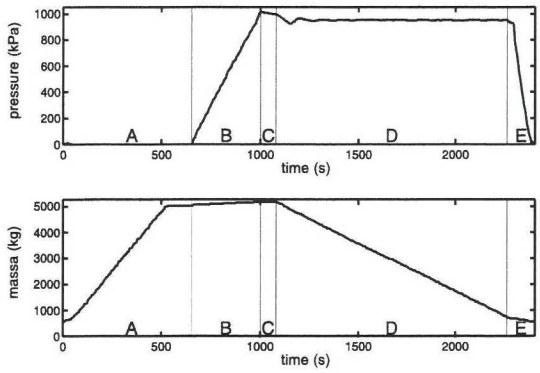

Fig. 3: Process phases of an injection vessel

After the injection vessel is filled with coal powder, the inlet valve and the ventilation valve at the top of the injection vessel are closed. At this time, the vessel has a weight of about 5 ton. When the two valves have closed, the injection vessel is pressure tight. The pressure control valve and the corresponding shut-off valve, closed during the low pressure phase, are now open. The pressure increases until it reaches the set point and the valves are shut again. As there exist leakages in the vessel body and the valves themselves are not completely tight, the pressure changes notwithstanding all valves are closed. Consequently, the pressure controller is activated and maintains the pressure around the set point value. When the other vessel has finished the injection, the vessel switches from pressure holding to injection. Then, the flow control valve opens and injection starts. Meanwhile, the other vessel flow control valve closes. During the injection phase both control valves, the pressure and the flow control valve are active. The weight of the vessel is ramping down to a minimum value while the pressure remains constant. Reaching the minimum weight, the injection vessel flow control valve closes. In the meantime, the other vessel has been charged, pressurized and stands by. If the pressure control valve and the flow control valve have closed, the ventilation valve opens and depressurizes the injection vessel. Once the pressure has dropped down to atmospheric level, the inlet valve opens and coal powder is filled in again.

3 Currently used control unit

The conventional control unit of the fine coal injection plant consists of two independent loops. One loop is for injection vessel pressure stabilization, and the other is for controlling the coal mass flow to the blast furnace. The process working cycle duration depends on the actual coal mass flow set point. Logically, a higher set point shortens the cycle time. The cycle time is normally about 40 minutes, which means

that the injection phase takes 20 minutes, approximately.

The pressure control loop is implemented by means of a PI controller, to achieve a zero steady state control error. The controller performance is exhibited in Fig. 4a. The coal mass flow controller is also a PI controller. However, since the coal mass flow is not directly measured in this particular installation, the coal mass flow is evaluated from the vessel's weighing system readings. The computations involve a differentiation, which naturally results in amplification of the measurement noise. Thus, low-pass filtering is applied and a set point compensation is employed to correct measurement errors. Installation of a flow meter would not change the situation since only one component of the two-phase flow (gas/solid) is of interest.

As seen in Fig. 4b, the mass flow controller fails to drive the control error to zero during the injection phase. A physical explanation of this fact is that the controlled pressure oscillates (see Fig. 4a), and the pressure controller changes the opening of the pressure control valve (PCV) rather fast, creating a varying nitrogen flow into the injection vessel and therefore varying coal mass discharge rate. Thus, the effected mass flow controller changes the opening of the flow control valve (FCV) in order to compensate the mass flow variations, which causes pressure variations in the injection vessels. The described interaction of the pressure and mass flow loops prevents the currently used controller from achieving flow stabilization. The shortcomings of this control strategy become even more prominent when the deviation of the mass in the injection vessel from the ideal mass trajectory is analyzed (Fig. 4c). The actual value of the mass loss can deviate as much as $150kg$ from the desired value.

To recapitulate, under the currently used control laws, the pressure p in the injection vessel is oscillatory and the coal mass flow is not held constant. In the sequel, alternative ways of controlling the injection vessels are discussed.

4 Modeling

Basically, an injection vessel is a pressurized tank process (Fig. 5). There, the following two signals are used as outputs of the model:

- Pressure p in the vessel
- Coal mass m_C, which is the integral of the coal mass flow to the blast furnace. As mentioned above, the coal mass flow cannot be reliably measured.

Natural input signals, both manipulated ones and measurable disturbances are:

- Valve opening u_N of the pressure control valve (PCV)
- Valve opening u_C of the flow control valve (FCV)

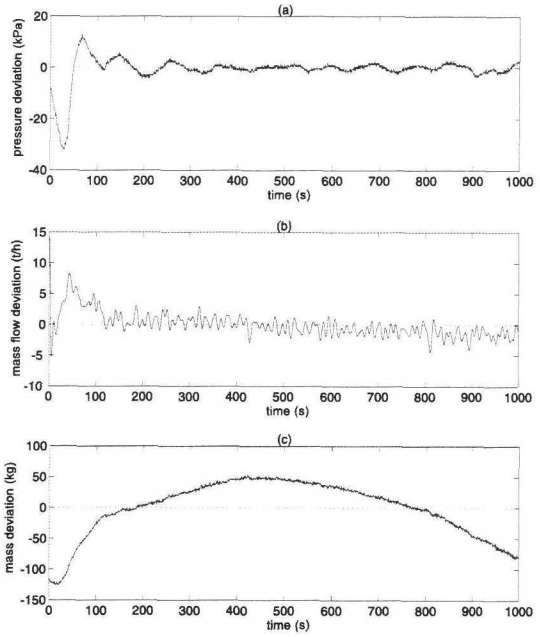

Fig. 4: Control Performance of the currently used controller

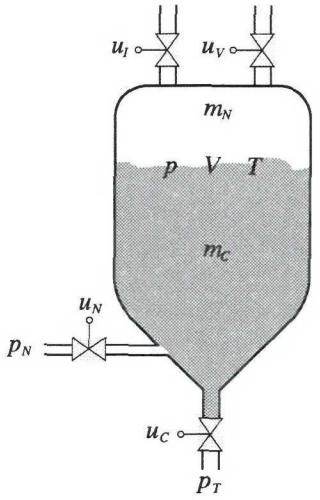

Fig. 5: Pressurized tank process

- Temperature T in the vessel
- Pressure p_N in the nitrogen net
- Pressure p_T in the transportation pipe to the blast furnace

For the sake of model simplification, some assumptions are made:

1. Variations of the pressure in the nitrogen net are small and p_N is assumed to be constant.
2. The pressure p_T at the injection point in the transportation pipe is constant.
3. Temperature variations are small.
4. No nitrogen leakage from the injection vessel during the injection phase.
5. The coal mass flow due to the weight of the coal is negligible.

A non-linear behavior of the injection vessel has been observed in [9], and a dynamic model based on the physical contiguities has been suggested. Unknown model coefficients have been derived via system identification from the measurements logged on the injection vessels. To this end, an invertible non-linear transformation on the input-output data, [9], has been utilized.

The non-linear model is used for fault detection purposes while a linear model is more suited for control purposes, since the latter only needs to represent the injection phase at a certain working point.

According to the assumptions made, two input signals can be manipulated and two output signals measured:

1. Opening of the PCV u_N
2. Opening of the FCV u_C
3. Pressure p in the injection vessel
4. Mass m of the injection vessel

These signals are used to identify and to control the process.

The non-linear model provides an approximation of the physical behaviour of the process for a wide range of working conditions and can be linearized for a particular working point (pressure) and trajectory (mass). The parameters of this linear model can as well be acquired using system identification.

Since the plant is full-time in operation and cannot be run in open-loop, the needed data for system identification has to be obtained in closed-loop. Following [12], it can be shown that the model parameters are identifiable from the closed-loop data.

Identification and validation data sets are logged on the process with a sampling time of $1s$. The identification method and its application to the coal injection plant are discussed in [6], where the subspace identification method *n4sid* is applied to the Laguerre spectra of the input/output data. There, it has been shown that *n4sid* performs better in the Laguerre domain compared to the time domain, when it is used for identification of the injection vessels. The obtained MIMO model is of order two and given by [6]:

$$x(k+1) = \underbrace{\begin{bmatrix} 0.99991 & 0.00003 \\ 0.00011 & 0.97775 \end{bmatrix}}_{\Phi} x(k) + \underbrace{\begin{bmatrix} -0.00313 & -0.03092 \\ -0.04030 & 0.02563 \end{bmatrix}}_{\Gamma} u(k) \quad (1a)$$

$$y(k) = \underbrace{\begin{bmatrix} 0.00058 & -0.04753 \\ 0.03107 & -0.00473 \end{bmatrix}}_{C} x(k) \quad (1b)$$

Since C is invertible, the similarity transformation $x(k) = C^{-1}x'(k)$ can be applied which yields

$$x'(k+1) = C\Phi C^{-1}x'(k) + C\Gamma u(k) \quad (2a)$$

$$y(k) = I_2 x'(k) \quad (2b)$$

Hence, the states of the new dynamic system coincide with the outputs.

5 Control strategies

As mentioned before, the control objective is to guarantee a constant coal mass flow from the injection vessel to the blast furnace. Though, it is desirable that the pressure is maintained constant, as high variations will propagate through the nitrogen net to other vessels. This can be achieved by pursuing different strategies. Here are two of them:

1. Two separate control loops for the pressure and the mass.
   One unit controls the vessel pressure and the other controls the coal powder mass, where the mass has to follow a pre-defined ramp. The slope of the ramp is the coal mass flow set point. For the controllers design, two SISO models for the plant have to be used.

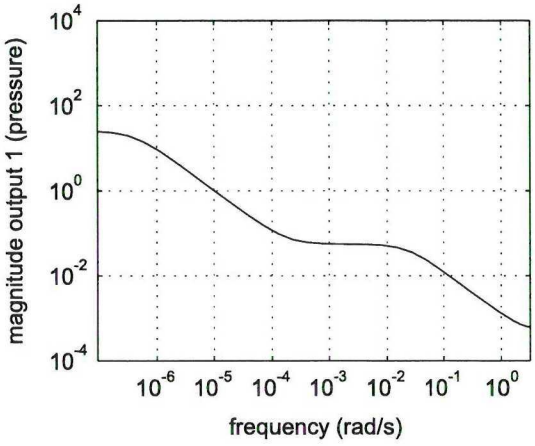

Fig. 6: Magnitude of the process coupling from the FCV to the pressure

2. A MIMO design controlling both the pressure and mass.

Strategy 1 is based on SISO models which makes the controller design and implementation easy to handle. The main disadvantage is that the couplings in the process are not taken in account. Fig. 6 depicts the coupling from the FCV to the pressure output. Obviously, this coupling is significant and cannot be neglected. The coupling from the FCV to the pressure has a high magnitude, which means that control valve movements will directly influence the pressure control loop as a rather fast time-varying disturbance. Physically, this disturbance is a gas flow from the injection vessel to the injection pipe, where the magnitude of the flow is varying in time, due to the actuator movements in the mass flow control loop.

Strategy 2 takes the couplings into consideration. Furthermore, this strategy has one more degree of freedom, as the two actuators are used together to achieve one and the same control objective. Another advantage is that the controller can eventually be tuned so that the two loops work separately. In this case, a controller similar to that of Strategy 1 is obtained, and yet the couplings in the plant are accounted for through the model. A relative disadvantage is that the design process appears to be more complicated. In addition, the MIMO controller has a centralized control structure, which can result in difficulties implementing the controller and can make the controller more vulnerable for malfunctions.

The shortcomings of the MIMO design do not wage out the advantages of this design. Therefore the SISO design will not be considered in the sequel. For performance comparison the currently used control structure, which is a design with two separate SISO loops, will be used as a reference.

An optimal design method is used to design the controller. The MIMO design is based on the so-called linear quadratic gaussian (LQG) theory, as described in [1]. It is also a major and popular design tool for multivariable linear systems (see e.g. [4], [10], and [8]).

5.1 Proportional-integral control law

Normally, assuming state feedback, a proportional-integral control law is chosen to eliminate the steady state error. However, controlling the fine coal mass, one of the closed-loop system outputs has to follow a ramp. Then, the use of a single integrator leads to a constant steady state response error. Thus, a double integration is used to drive the error in reference signal following to zero. Using the final value theorem it can be shown that even for the pressure control a double integration is needed to drive the tracking error to zero. In order to recast this control law into the framework of LQG design, the process model in (2) has to be augmented with a double integrator and can be written as

$$x'_a(k+1) = \underbrace{\begin{bmatrix} C\Phi C^{-1} & 0 & 0 \\ I_2 & I_2 & 0 \\ 0 & I_2 & I_2 \end{bmatrix}}_{\Phi_a} x'_a(k) + \underbrace{\begin{bmatrix} C\Gamma \\ 0 \\ 0 \end{bmatrix}}_{\Gamma_a} u(k) \tag{3a}$$

$$y_a(k) = \underbrace{\begin{bmatrix} I_2 & 0 & 0 \\ 0 & I_2 & 0 \\ 0 & 0 & I_2 \end{bmatrix}}_{C_a} x'_a(k) \tag{3b}$$

5.2 Kalman filter and LQ controller

Since the system is intended for continuous use, a steady-state Kalman filter is designed, in order to obtain filtered versions of the measured signals. The steady state Kalman filter seems to be sufficiently fast, as the process itself is very slow. The covariances for the Kalman filter design are adjusted according to measurement data.

In contrary, the weighting matrices for the LQ controller, that minimizes the loss function

$$J = \sum_{k=0}^{\infty} (x'_a(k)^T Q x'_a(k) + u(k)^T R u(k))$$

are designed according to the following guidelines:

- Q is chosen diagonal. All entries that are related to the pressure, its first and second integral are chosen small compared to the values related to the mass. A factor of 10 has proven to give good results. The effect is a higher degree of coal mass flow stabilization at the expense of more pressure variation.

- R is chosen diagonal. The entry related to the FCV is chosen big compared to the entry related to the PCV, yielding that the PCV is preferably used to achieve the control goals.

- The norm of R is fairly big compared to the norm of Q, what results in a quite slow response of the controller. However, this also prevents extensive valve wear, since the actuator movements become very smooth.

Using the sensitivity function, defined as the transfer matrix with the reference signals as inputs to the control errors as outputs, and the singular values of the closed-loop system, the entries in the R matrix can be fine tuned. The sensitivity function and the singular values are defined and derived in Section 5.4. An analysis has shown that the off-diagonal elements have a high influence on the couplings in the sensitivity function. In the present case, the coupling between the FCV and the pressure that has a high magnitude can be suppressed in the sensitivity function by choosing negative off-diagonal values in R.

5.3 Feedforward design

Furthermore, to reduce the controller settling time and retain a smoother set point change response, a feedforward signal from the desired coal mass flow to the valves is introduced. The design approach presented in [13, Chapter 6] is adopted.

The identified process model can be interpolated to a continuous time state space model

$$\dot{x} = A_c x + B_c u \tag{4a}$$
$$y = C_c x + D_c u \tag{4b}$$

where

$$\begin{pmatrix} A_c & B_c \\ 0 & 0 \end{pmatrix} = \frac{1}{T} \ln \begin{pmatrix} \Phi & \Gamma \\ 0 & I_2 \end{pmatrix}$$

and the matrices C_c and D_c are equal to their discrete counterparts. T denotes the sampling time. Rewriting (4) gives

$$\begin{bmatrix} \dot{x} \\ y \end{bmatrix} = \underbrace{\begin{bmatrix} A_c & B_c \\ C_c & D_c \end{bmatrix}}_{G} \begin{bmatrix} x \\ u \end{bmatrix}$$

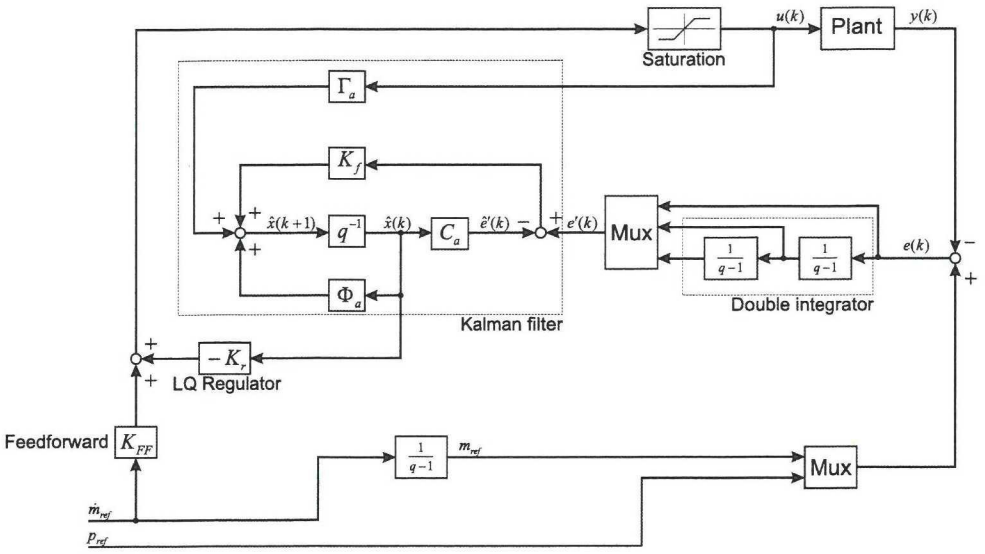

Fig. 7: Block diagram of the MIMO controller with feedforward

The block matrix G is inverted and then partitioned according to the vectors dimensions of $x, u, \dot{x}, y$ which results in

$$\begin{bmatrix} x \\ u \end{bmatrix} = \begin{bmatrix} G_{x\dot{x}}^{-1} & G_{xy}^{-1} \\ G_{u\dot{x}}^{-1} & G_{uy}^{-1} \end{bmatrix} \begin{bmatrix} \dot{x} \\ y \end{bmatrix} \tag{5}$$

Obviously the relationship $u = G_{u\dot{x}}^{-1}\dot{x}$ from (5) describes how u influences $\dot{x}$. Since in steady state

$$\dot{x} = \dot{x}_{ss} = \begin{bmatrix} 0 \\ \dot{m}_{ref} \end{bmatrix}$$

a steady state input signal u_{ss} is given by

$$u_{ss} = G_{u\dot{x}}^{-1}\dot{x}_{ss}$$

The resulting feedforward gain matrix is therefore chosen to be $G_{u\dot{x}}^{-1}$ and the feedfoward path introduced in the closed-loop structure.

In the next section, the favorable impact of the feedforward signal on the controller performance is illustrated by simulation. Fig. 7 depicts the MIMO design with additional feedforward path.

5.4 Comparison with the currently used controller

In order to compare the MIMO controller with the currently used controller, the MIMO model is used in both cases. Then, the sensitivity functions and the singular values are compared. One important result is the comparison of the bandwidth of the closed loop system with that of the currently used controller and the MIMO controller.

First, the sensitivity functions are derived. Let the closed-loop system be given by

$$\begin{aligned} x_{cl}(k+1) &= \Phi_{cl}x_{cl}(k) + \Gamma_{cl}r(k) && \text{(6a)} \\ y(k) &= C_{cl}x_{cl}(k) && \text{(6b)} \end{aligned}$$

Defining and introducing the error $e(k) = r(k) - y(k)$ in (6) results in the sensitivity function

$$\begin{aligned} x_{cl}(k+1) &= \Phi_{cl}x_{cl}(k) + \Gamma_{cl}r(k) && \text{(7a)} \\ e(k) &= -C_{cl}x_{cl}(k) + I_2 r(k) && \text{(7b)} \end{aligned}$$

(7) can also be written as a transfer matrix, which is abbreviated by

$$e(k) = \underbrace{\left[\begin{array}{c|c} \Phi_{cl} & \Gamma_{cl} \\ \hline -C_{cl} & I_2 \end{array}\right]}_{S(q)} r(k)$$

By applying the singular value decomposition to $S(q)$ the singular values $\sigma_i(S(q))$ of the sensitivity function are obtained.

Fig. 8 contains four subplots describing the dependencies in the closed loop system, where the columns are associated with the inputs and the rows with the output variable. Comparing the sensitivity function contributions of the LQG design with the corresponding entries for the currently used controller shows that the latter is a more sensitive design. It is obvious that the mass flow control loop of the currently used controller is highly sensitive to low frequency disturbances (see lower right subplot). In case of the currently used controller, the frequencies of the resonance peaks in the plots are excited in the experiments on the actual plant (see Fig. 4a).

Now, the singular values of the above sensitivity functions are compared (see Fig. 9). Depending on the input direction, the bandwidth of the currently used controller varies much more than the bandwidth of the MIMO LQG design. Obviously the

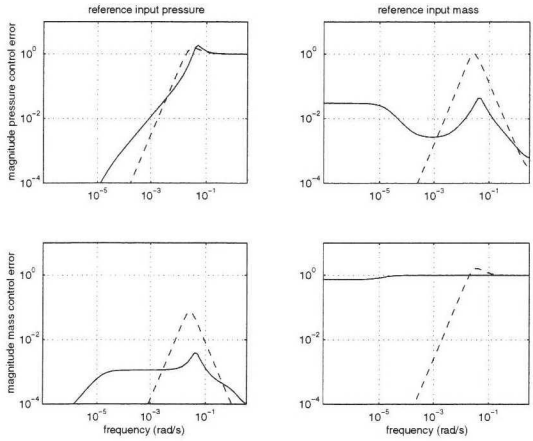

Fig. 8: Magnitudes of the input sensitivity function (currently used controller - solid, MIMO LQG - dashed).

MIMO design yields a much better and more certain bandwidth than the currently used controller does. In addition, the singular values of the sensitivity function at low frequencies have much lower magnitude than the currently used controller and therefore yields faster tracking.

A disadvantage of the MIMO LQG design is the rather high peak of the sensitivity function, a value of 2.12 can be reached. Since the plant model has two zeros outside the unit circle, a peak larger than 1 is unavoidable [11]. However, according to measured data, the frequencies around the sensitivity function peaks of the MIMO controller are not excited (see Practical Tests).

6 Simulations

In this section, the following two cases are compared to each other by means of computer simulation:

1. MIMO controller without feedforward
2. MIMO controller with feedforward

For the simulations, a rather high but realistic coal mass flow set point is chosen ($15\frac{t}{h}$), and a step in the pressure reference of about $16kPa$. In order to examine the controllers ability to work around a different working point, the nominal values of the parameters have been changed. In addition, process noise and sensor noise are simulated, but are not discussed here.

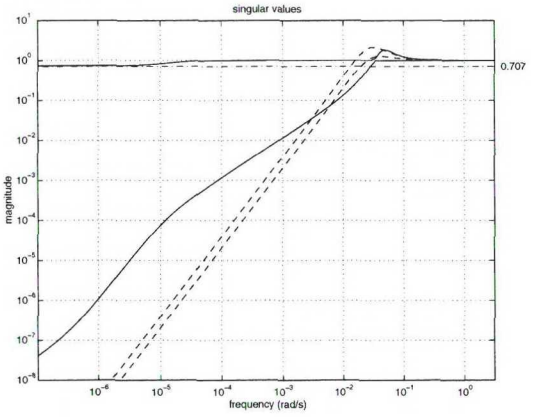

Fig. 9: Magnitudes of the singular values of the input sensitivity function (currently used controller - solid, MIMO LQG - dashed, bandwidth border - dashed-dotted)

Simulating the MIMO controller shows that the steady state error is driven to zero, (Fig. 10). Comparing the simulation with feedforward and the one without feedforward, indicates that the feedforward has a beneficial effect on the performance of the MIMO controller. The settling time for the mass control is very small, while the settling time for the pressure control is longer.

A look at the control signals, Fig. 11, shows that the FCV position changes smoothly and, logically, the coal mass flow is also expected to change similarly smooth. Moreover, the valve opening signal lies far from the saturation limits. Several simulation tests with different parameters suggest that it takes a pressure reference step of about $50kPa$ to drive the PCV into saturation. According to the logged data, such a step is unlikely to occur in practice.

7 Practical tests

In this section, tests on the actual plant are briefly described. A more detailed description and discussion of implementation issues can be found in [3]. For experiments, a standard PC with an A/D-card is used. The software *RegSim*©, [7], is used to perform the real-time experiments. Using buffer amplifiers the A/D-card channels are connected to the plant. The controller is implemented in a *RegSim*© program which can be run in real-time. By means of software switches in the plants control system, the currently used controller is replaced by the MIMO LQG controller.

Besides that data from control experiments with the MIMO LQG controller are logged, data from several injection phases controlled by the currently used controller are logged with the same equipment.

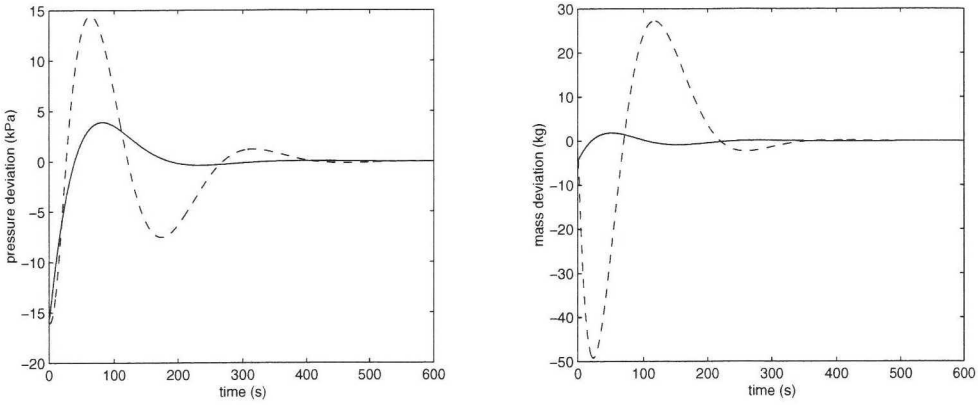

Fig. 10: Simulation of MIMO controller (without feedforward - dashed, with feedforward - solid).

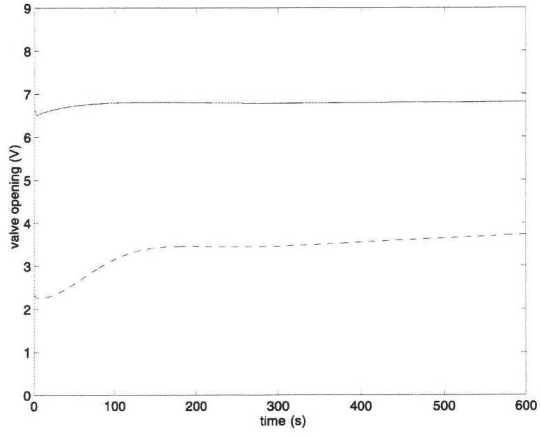

Fig. 11: Simulation of the control signals of the MIMO controller with feedforward (FCV - solid, PCV - dashed).

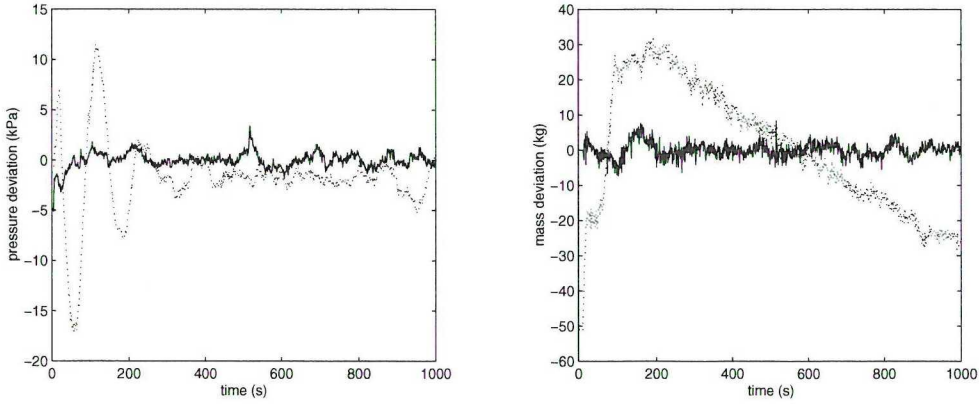

Fig. 12: Comparison of mass and pressure (currently used controller dotted, MIMO LQG solid)

	Currently used controller	MIMO LQG	Improvement
mass $[kg]$	11.3	1.5	79%
pressure $[kPa]$	5.1	1.0	86%
mass flow $\left[\frac{t}{h}\right]$	1.6	1.0	35%

Table 2: Standard deviations of process variables and improvements

Fig. 12 depicts the performance for each controller in terms of mass and pressure deviation. As expected, the MIMO LQG controller yields the better result. Examining the estimated coal mass flow in Fig. 13 leads, in principal, to the same conclusion. Though, the improvement is not that high as in the other two cases, what can be a result of the flow estimation algorithm. The coal mass flow is not measurable and has to be derived from the mass measurement.

Table 2 shows the standard deviations achieved by the corresponding controllers. Once again, it can be seen that the MIMO LQG controller produces the better result. The resulting performance improvements are displayed in column three of Table 2.

8 Conclusions

A multivariable linear quadratic controller design for the coal injection process is discussed. The currently used control strategy is compared with the proposed one by means of sensitivity analysis. Simulation studies and experiments at the plant are performed. It is shown that by use of the new design, the flow and pressure control of the coal injection vessel could be significantly improved. In the proposed control system, the coal mass flow can be used as a control parameter for the blast furnace.

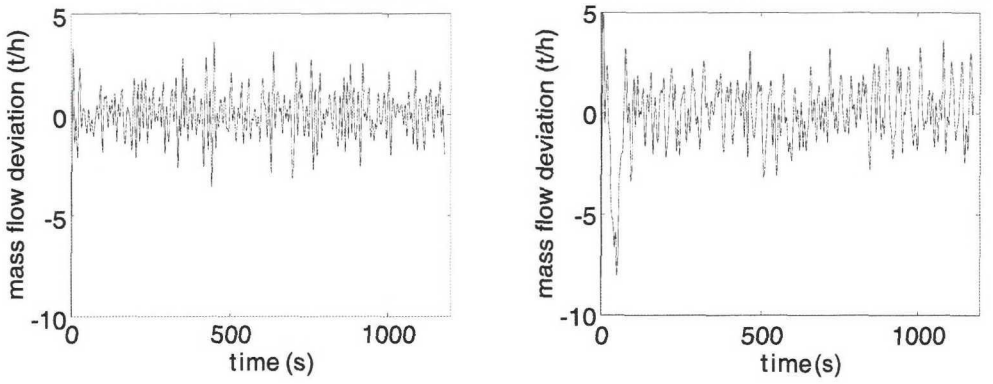

Fig. 13: Comparison of coal mass flow (MIMO LQG left plot, currently used controller right plot)

High injection rates can be used and more coke substituted.

9 Acknowledgment

The authors want to thank SSAB Tunnplåt in Luleå, for making the coal injection plant and maintenance personnel available to us. Particularly, a special thank to Ingemar Lundström and Robert Johansson who helped with the experiments. Financial support of the Center for Process and System Automation (*ProSA*) at Luleå University of Technology provided by *Norrbottens Forskningsråd* and the Swedish National Board for Industrial and Technical Development (NUTEK) is also gratefully acknowledged.

References

[1] K.J. Åström and B. Wittenmark. *Computer Controlled Systems.* Prentice Hall, Inc., 1990.

[2] Wolfgang Birk, Andreas Johansson, and Alexander Medvedev. Control and gas leakage detection in a fine coal injection plant: Design and experiments. In *Proc. of 9th IFAC Symposium on Automation in Mining, Mineral and Metal Processes*, pages 271–276, 1998.

[3] Wolfgang Birk, Andreas Johansson, and Alexander Medvedev. Model-based control for a fine coal injection plant. *IEEE Control Systems Magazine*, 19(1):33–43, February 1999.

[4] K. K. Denoyer and M. K. Kwak. Dynamic modelling and vibration suppression of a slewing structure utilizing piezoelectric sensors and actuators. *Journal of Sound and Vibration*, 189(1):13–31, Jan 1996.

[5] F. Eichinger and M. Rafi. Maintain a very high blast furnace coal injection rate. *Steel times international*, pages 28–29, 1995.

[6] Britta R. Fischer and Alexander Medvedev. Laguerre shift identification of a pressurized process. In *Proc. of the 1998 American Control Conference, Philadelphia*, pages 1933–1942, 1998.

[7] T. Gustafsson. Regsim: A software tool for real time control and simulation. In *Proc. of the 4th IEEE Conference on Control Applications, Albany, New York 1995*, 1995.

[8] Xiang-Dong He, Harry H. Asada, Sheng Liu, and Hiroyuki Itoh. Multivariable control of vapor compression. *HVAC&R Research*, 4(3):205–230, July 1998.

[9] A. Johansson and A. Medvedev. Model based leakage detection in a pulverized coal injection vessel. In *Proc. of the 1998 American Control Conference, Philadelphia*, pages 1742–1746, 1998.

[10] Kenneth B. Lazarus, F. Edward, and Charissa Y. Lin. Multivariable high-authority control of plate-like structures. *Journal of Guidance, Control and Dynamics*, 19(6):1357–1363, Nov-Dec 1996.

[11] S. Skogestad and I. Postlethwaite. *Multivariable Feedback Control - Analysis and Design*. John Wiley & Sons, 1996.

[12] T. Söderström and P. Stoica. *System Identification*. Prentice Hall, 1989.

[13] R.F. Stengel. *Stochastic Optimal Control*. John Wiley & Sons, Inc., 1986.

Paper 2

Sensitivity Analysis of an LQ Optimal Multivariable Controller for a Fine Coal Injection Vessel

Published as

Wolfgang Birk and Alexander Medvedev. "Sensitivity analysis of an LQ optimal multivariable controller for a fine coal injection vessel". *IEEE Transactions on Industry Applications*, 36(3):871–876, May/June 2000.

Sensitivity Analysis of an LQ Optimal Multivariable Controller for a Fine Coal Injection Vessel

Wolfgang Birk and Alexander Medvedev
Control Engineering Group
Luleå University of Technology
SE-971 87 Luleå, Sweden
Wolfgang.Birk@sm.luth.se

Abstract

This paper deals with a sensitivity analysis of an LQ optimal multivariable controller for a fine coal injection vessel used in the blast furnace process. The multivariable controller from a previous work is briefly presented and the closed loop system is studied by means of a sensitivity analysis. Effects of disturbances and uncertainty on the closed loop system are studied basing on analysis of the singular values of the sensitivity and the complementary sensitivity functions, the relative gain array and the minimized condition numbers. Finally, the sensitivity analysis is validated by the use of logged data from test operation at the coal injection plant at SSAB Tunnplåt Luleå, Sweden.

Keywords: Multivariable Control, LQ Control, Sensitivity Analysis, Coal Injection

1 Introduction

Nowadays, iron producers are reducing production costs by replacing the expensive energy carrier coke by other cheaper alternatives. In Luleå, SSAB Tunnplåt AB is partly substituting coke by fine coal, which is 40% cheaper, in their iron production. The economical benefits of pulverized coal injection (PCI) are discussed in [7].

Since fine coal, in its pure form, is highly inflammable even under normal conditions, it is difficult to supply it to the process. Therefore, it is important to keep the fine coal isolated from the air, which can be done by using a pneumatic conveying device (see [6],[10]), where the transportation gas is nitrogen or at least has a higher rate of nitrogen compared to that of the air. The fine coal injection vessel is a part of a coal injection plant for a blast furnace, where fine coal is pneumatically conveyed to the blast furnace and finally injected at tuyere level. The coal injection plant at SSAB Tunnplåt AB in Luleå (Fig. 1), which has been used for the experiments, is described in more detail in [2].

A drawback of substituting coke by fine coal is that it can result in blast furnace instabilities if coal flow outages appear [3]. Hence, a tight and reliable control of the fine coal flow from the injection vessel to the blast furnace becomes necessary.

A combined model-based control and leakage detection system for a fine coal injection plant has been developed in [1]. The designed controller is a linear quadratic (LQ) optimal multivariable controller for the control of the fine coal flow out of the injection vessel. Since the controller is exposed to plant dynamics alternations because of components wear-out, repair and replacement, as well as noise, it is necessary to analyse the sensitivity towards these effects. Typically, sensitivity analysis is used to obtain the necessary information. In [9] some schemes for sensitivity analysis in the multivariable case are given and used for the subsequent sensitivity analysis.

Following up results of experiments and test operation is an essential part of an industrial project, since controller performance specifications have to be checked. From a theoretical point of view such an analysis helps to improve controller designs and pinpoints possible shortcomings in the control strategy. It can also motivate further research in the area. This paper discusses such a follow-up in order to validate theoretical results of a sensitivity analysis.

The paper is organized as follows. In section 2 the controller design is presented. The succeeding section 3 discusses the sensitivity analysis and creates a framework for the follow-up. Finally, in section 4, the acquired data from the tests is used to validate the anteceding analysis.

2 LQ optimal multivariable controller

The multivariable controller is a part of the loop structure depicted in Fig. 2 and is a result of a previous study, [1].

Besides the state vector feedback controller, a Kalman filter, a feedforward controller and an actuator saturation are present in the closed-loop system. Both Kalman filter and multivariable controller design are based on an identified multiple input, multiple output (MIMO) model of the process dynamics.

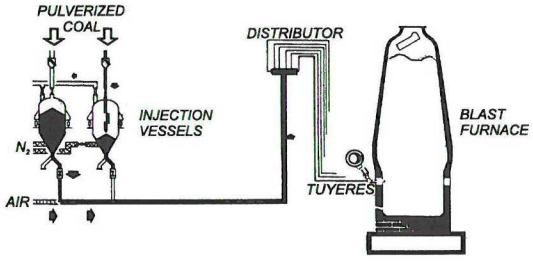

Fig. 1: Coal injection plant (injection vessels, distributor and blast furnace).

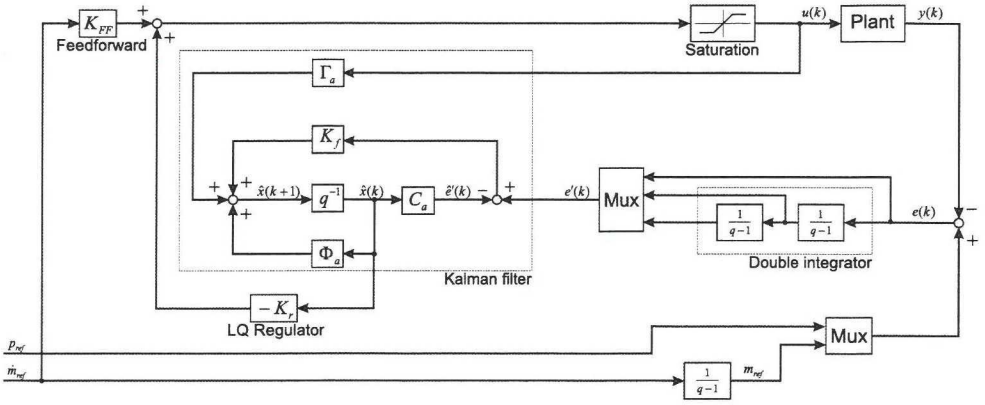

Fig. 2: Block diagram of the closed-loop structure

The structure of an injection vessel can be described by Fig. 3, and is principally a pressurized tank process. During the injection of coal the valves u_I and u_V are closed. Consequently, the two actuators u_N and u_C can be used to control the discharge of the vessel. Measured outputs of the vessel are the net mass m of the vessel. The latter is identical to the sum of the nitrogen mass m_N and the coal mass m_C, and the pressure p in the vessel. Since the injection vessel is injecting coal at a certain flow rate, the net mass of the vessel has to follow a trajectory. Using direct identification, a model describing the process dynamics can be obtained. The identification method and its application to the coal injection plant are discussed in [4], where the subspace identification method *n4sid* is applied to the Laguerre spectra of the input/output data. There, it has been shown that *n4sid* performs better in the Laguerre domain compared to the time domain, when it is used for identification of the injection vessels. The obtained MIMO model is of order two and given by

$$x(k+1) = \Phi x(k) + \Gamma \begin{bmatrix} u_N(k) \\ u_C(k) \end{bmatrix} \tag{1a}$$

$$\begin{bmatrix} p(k) \\ m(k) \end{bmatrix} = Cx(k) + D \begin{bmatrix} u_N(k) \\ u_C(k) \end{bmatrix}, \tag{1b}$$

Since C is invertible, the similarity transformation $x(k) = C^{-1}x'(k)$ can be applied which yields

$$x'(k+1) = C\Phi C^{-1}x'(k) + C \begin{bmatrix} u_N(k) \\ u_C(k) \end{bmatrix} \tag{2a}$$

$$\begin{bmatrix} p(k) \\ m(k) \end{bmatrix} = I_2 x'(k) + D \begin{bmatrix} u_N(k) \\ u_C(k) \end{bmatrix} \tag{2b}$$

Hence, the states of the transformed dynamic system coincide with the outputs.

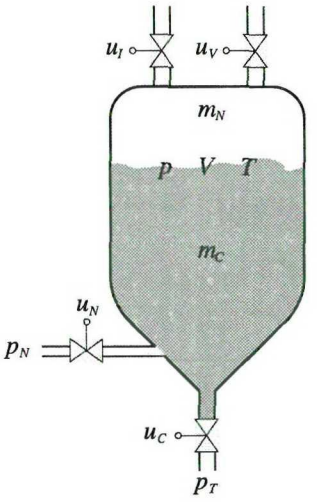

Fig. 3: Simplified injection vessel structure

As mentioned above, the net mass of the injection vessel has to follow a trajectory, which is usually a ramp. For Kalman filter and controller design, the identified model is augmented with a double-integrator for each of the outputs, in order to drive the steady state error to zero. The resulting state space system is given by

$$x_a'(k+1) = \underbrace{\begin{bmatrix} C\Phi C^{-1} & 0 & 0 \\ I_2 & I_2 & 0 \\ 0 & I_2 & I_2 \end{bmatrix}}_{\Phi_a} x_a'(k) + \underbrace{\begin{bmatrix} C\Gamma \\ 0 \\ 0 \end{bmatrix}}_{\Gamma_a} \begin{bmatrix} u_N(k) \\ u_C(k) \end{bmatrix} \tag{3a}$$

$$y(k) = \underbrace{\begin{bmatrix} I_2 & 0 & 0 \\ 0 & I_2 & 0 \\ 0 & 0 & I_2 \end{bmatrix}}_{C_a} x(k) + \begin{bmatrix} D \\ 0 \\ 0 \end{bmatrix} \begin{bmatrix} u_N(k) \\ u_C(k) \end{bmatrix}. \tag{3b}$$

Using the standard LQ design procedure, a MIMO LQ controller with a stationary Kalman filter is obtained (see [2]). The optimal multivariable controller can be written

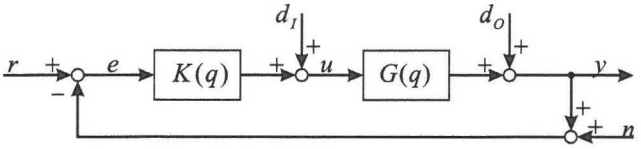

Fig. 4: Closed loop system for sensitivity analysis

in the form:

$$x_c(k+1) = \begin{bmatrix} I_2 & 0 \\ I_2 & I_2 \end{bmatrix} x_c(k) + \begin{bmatrix} I_2 \\ 0 \end{bmatrix} e(k) \tag{4a}$$

$$e'(k) = \begin{bmatrix} 0 & 0 \\ I_2 & 0 \\ 0 & I_2 \end{bmatrix} x_c(k) + \begin{bmatrix} I_2 \\ 0 \\ 0 \end{bmatrix} e(k) \tag{4b}$$

$$\begin{bmatrix} u_N(k) \\ u_C(k) \end{bmatrix} = -K_r \cdot e'(k), \tag{4c}$$

where $e(k) = r(k) - y(k) = \begin{bmatrix} p_{ref}(k) - p(k) \\ m_{ref}(k) - m(k) \end{bmatrix}$. The measurement signal, vector $y(k)$, contains the pressure $p(k)$ and the net mass $m(k)$, whereas the reference signal vector contains the pressure set-point $p_{ref}(k)$ and the net mass trajectory $m_{ref}(k)$.

According to the *separation principle*, the Kalman filter and LQ controller dynamics are not coupled, which allows separate study of their dynamical behaviour. As the feedforward controller is designed for steady state and driven by an external signal (coal flow set point, $\dot{m}_{ref}(k)$), the influence of this controller on the closed loop dynamics can be neglected. Furthermore, it is assumed that the control signals are not saturated.

The resulting closed-loop structure for the controller and the plant is given in Fig. 4, where $K(q)$ denotes the controller in (4), $G(q)$ is the process model in (2) and q is the forward-shift operator. Additional to the loop structure in Fig. 2, disturbance and noise inputs are considered.

3 Sensitivity Analysis

Three sensitivity functions are considered:

- Complementary sensitivity function T, which is the transfer matrix from reference input r to the output y.
- Input sensitivity function S_I describes the transfer matrix from the disturbance input d_I to the control error e.

- Output sensitivity function S_O is similar to S_I but for the disturbance input d_O.

For the sake of simplicity the operator s is dropped.

Analysing the block structure in Fig. 4 the following sensitivity and complementary sensitivity functions are obtained:

$$T = GK(I+GK)^{-1} \quad (5)$$

$$S_I = -G(I+GK)^{-1} \quad (6)$$

$$S_O = -(I+GK)^{-1} \quad (7)$$

It can be mentioned that the sensitivity function for the noise input n to the control error e is identical to S_O, and the sensitivity function from the reference input r to the control error is equal to $-S_O$. Obviously, an analysis of these two more functions would not contribute with more information.

While the sensitivity and the complementary sensitivity functions are directly analysed in the scalar case, the quantities of interest in the multivariable case are the singular values of these functions. However, the role of the sensitivity and the complementary sensitivity functions in both cases are similar, since their magnitudes are usually used to measure stability robustness with respect to modelling uncertainties.

Of great interest in the sensitivity analysis are the suprema of the singular values of the sensitivity functions. High peaks can lead to instability of the closed loop system under perturbation and should be avoided. In the controller design, the characteristics of the singular values can be used to achieve a closed-loop system with minimized peaks in the singular values. Although the magnitudes of the sensitivity and complementary sensitivity functions are not a good measure for the gain of the MIMO system, information on the character of the cross-couplings in the MIMO system can be obtained and exploited in the design process.

Finally, the sensitivity of the plant towards element-by-element uncertainty and input uncertainty is analysed using the relative gain array (RGA) and the minimized condition numbers for the plant and controller.

3.1 Input sensitivity function

Fig. 5 shows the singular values of the input sensitivity function S_I. Obviously, the magnitude is very small compared with the other sensitivity or complementary sensitivity functions (Fig. 6, Fig. 7 respectively). Since disturbances of magnitude larger than one decade are unlikely to occur, the sensitivity to disturbances at the plant inputs can be neglected.

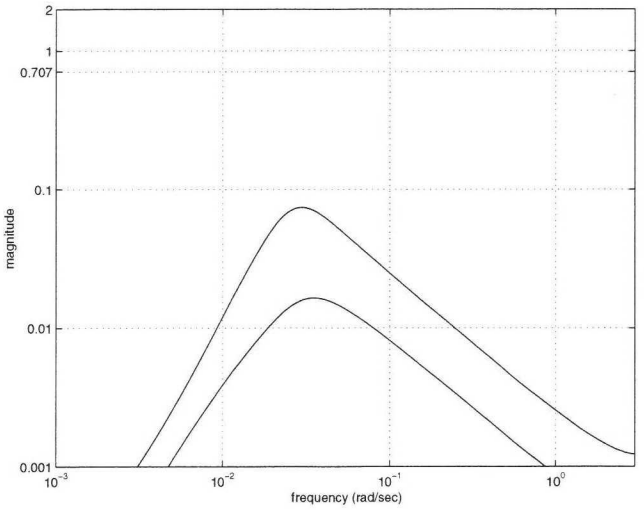

Fig. 5: Singular values of the input sensitivity function S_I.

3.2 Output sensitivity function

Information on the bandwidth of the system with respect to output disturbance attenuation can be obtained from the singular value plot of the output sensitivity function (Fig. 6). Since the bandwidth for a multivariable system depends on the input/output directions, the lowest bandwidth value for output disturbance attenuation should be chosen. To determine the bandwidth of a system the definition in [5] is used. According to Fig. 6, disturbances up to 0.02 rad/sec can be attenuated.

Furthermore, the peak value of the sensitivity function (1.35) is a quite small value which indicates that output disturbances can lead to a slight overshoot in the transient behaviour.

3.3 Complementary sensitivity function

Similarly, the bandwidth for the reference tracking is defined, but here the higher value is chosen. Another important factor is the roll-off, *i.e.* a high negative slope above the cross-over frequency.

Fig. 7 shows the singular values for T. The bandwidth for reference tracking is about 0.095 rad/sec and the closed-loop system has a high negative slope of -2 above the cross-over frequency. The peak value of T is also rather small and is 1.85. According to [9], recommended peak values are less than two.

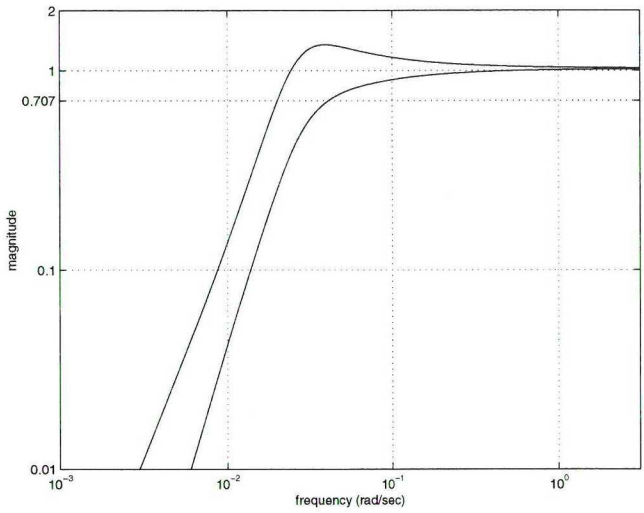

Fig. 6: Singular values of the output sensitivity function S_O.

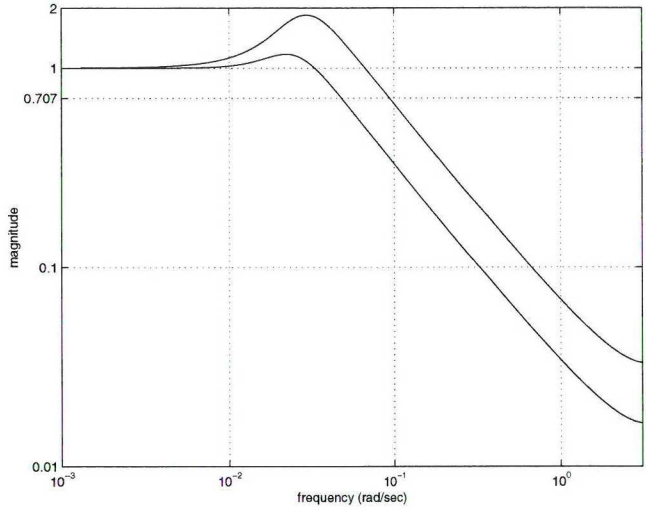

Fig. 7: Singular values of the complementary sensitivity function T.

3.4 Sensitivity to uncertainty

In [9] the RGA and the minimized condition numbers are used to evaluate sensitivity to uncertainty. In this case the MIMO model for design is obtained from direct identification of the plant dynamics. Because of non-linearities as well as disregarded dynamics, the model only approximates the plant behaviour. Hence, uncertainty has to be taken into consideration.

The RGA is given by

$$RGA(G) = G \times (G^{\dagger})^{T},$$

where $\times$ is the Schur product. The RGA is computed at discrete frequency points. Here, the RGA is a symmetric 2×2 matrix of the form

$$\begin{bmatrix} a & b \\ b & a \end{bmatrix}.$$

Large values in the RGA indicate that G will loose rank if the element g_{ij} in G is multiplied by a factor $(1 - \frac{1}{\lambda_{ij}})$, where λ_{ij} is the respective entry in the RGA. Thus, the RGA should contain small values.

In Fig. 8 the entries of the RGA are displayed. Because of the above given form of the RGA, only two values are plotted. The values are small and therefore the closed loop system should not be sensitive to element-by-element changes. An important property of the RGA is that sign changes of entries over the frequency axis indicate the presence of right half plane (RHP) zeroes in G or at least in one subsystem of G. As pointed out in [11] and [8], such non-minimum phase zeroes lead to fundamental performance limitations of the closed-loop system. Since one RGA entry is changing sign (see Fig. 8) at least one subsystem of G has a RHP zero and thus, performance limitations of the closed-loop system exist.

The minimized condition numbers $\gamma_I^*(G)$ and $\gamma_O^*(K)$ are a measure of robust performance to diagonal input uncertainty. According to [9], these condition numbers can be derived as follows:

$$\gamma_I^*(G) = \min_{D_I} \gamma(GD_I)$$

$$\gamma_O^*(K) = \min_{D_O} \gamma(D_O K),$$

where D_I and D_O are scaling matrices. The minimized condition number is the result of a minimization of the condition number over all possible scales.

For the closed-loop system to be insensitive to input uncertainty, the values of $\gamma_I^*(G)$ and $\gamma_O^*(K)$ should be around 2 or smaller in the cross-over region. Both condition numbers are depicted in Fig. 9. In the cross-over region (between 0.024 rad/sec and 0.065 rad/sec), the minimized condition numbers are obviously around 2 (between 1.94 and 2.76), which yields an relative insensitivity of the closed-loop system to input uncertainty.

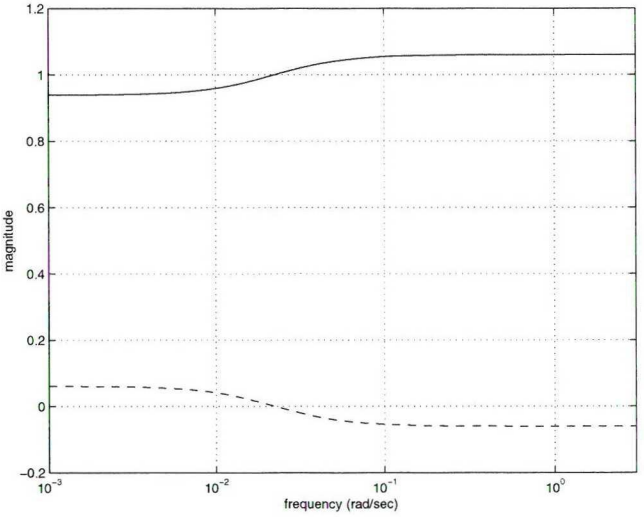

Fig. 8: RGA of G.

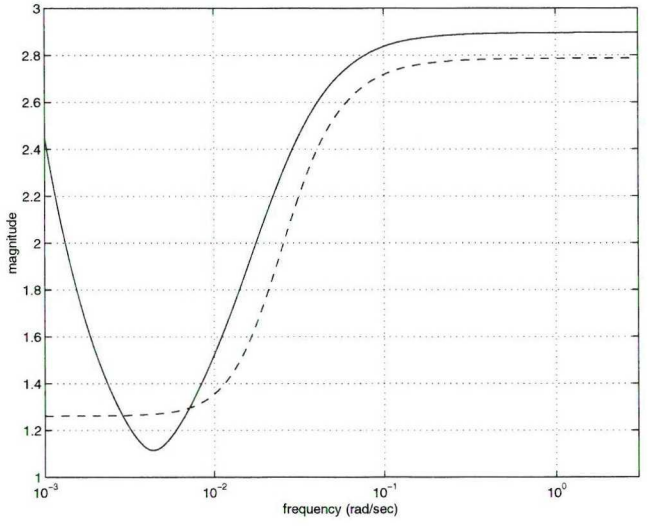

Fig. 9: Minimized condition numbers: $\gamma_I^*(G)$ solid, $\gamma_O^*(K)$ dashed.

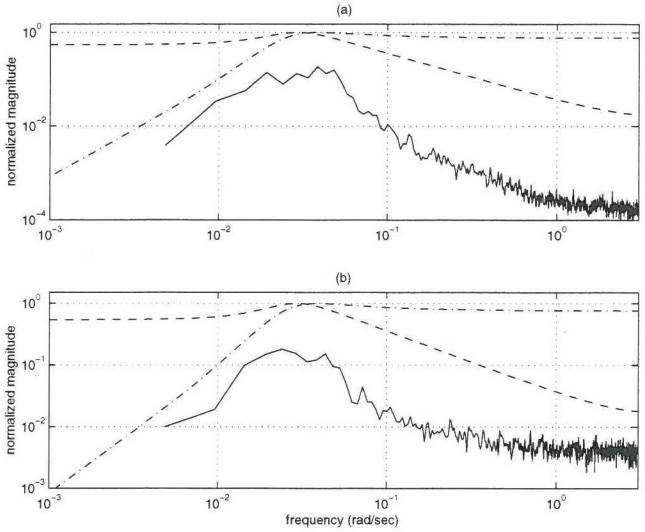

Fig. 10: Power spectral density (solid) versus maximum singular value of T (dashed) and S_O (dashed-dotted). (a) power spectral density of the pressure error, (b) power spectral density of the mass error.

4 Follow-up

The LQ optimal multivariable controller has been tested during a period of two weeks at the coal injection plant. During this period data has been logged. Since two injection vessels are injecting coal alternatingly, the time for one injection phase is limited and depends on the coal flow set-point. Thus, the frequency range is not only bounded from above with half the sampling frequency (π rad/sec) but also from below. The minimum recordable frequency is approximately 0.002 rad/sec.

Several injection series are randomly selected, and the power spectral density is estimated. Then, the expectation value for every frequency point is estimated and plotted versus the maximum singular value of the output sensitivity and complementary sensitivity function (Fig. 10).

Obviously, the peaks in the maximum singular values of S_O and T are in the same frequency range as the ones in the power spectral density of the mass and the pressure deviation. Accordingly, the sensitivity analysis for S_O and T is validated by these results.

Since the input sensitivity function S_I contributes only with a comparably small magnitude, pure data analysis is not sufficient to validate the analysis. Therefore, a disturbance at the plant inputs has to be introduced in an experiment.

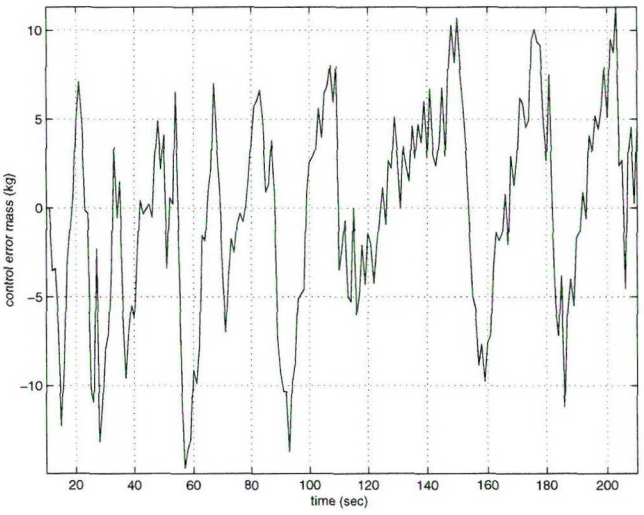

Fig. 11: Control error in the mass for the malfunctioning position control of the valve

In practice, disturbances at the plant inputs are introduced by adding an extra signal to the input of the actuators, which can be achieved by sending a falsified position signal to the valve's position controller. Here, the position sensor signal is simply saturated before reaching its usual upper bound. Therefore, the transmitted position signal is incorrect if the valve has opened more than this artificially introduced upper bound. As a result the valve's position controller is reacting on a non-existing position error and thus, is opening the valve completely as soon as the physical position of the valve exceeds the artificial bound.

Such a situation can occur when the valves position sensor malfunctions or a transmitting buffer amplifier saturates.

During the experiment, the closed-loop system did not loose its stability, but performance losses could be observed (see Fig. 11). In Fig. 12 the position signal from the valve and the control signal to the valves position controller are displayed.

Since these rather extreme input disturbances have not invalidated the analysis of the input sensitivity function, it can be concluded that the analysis is reliable.

In order to test the closed-loop sensitivity for input uncertainty and element-by-element changes in practice, the design is based on a model for one injection vessel but also run on the second injection vessel, which is equipped with a larger sized pressure control valve (u_N). During test-operation no performance losses due to this fact could be recognized.

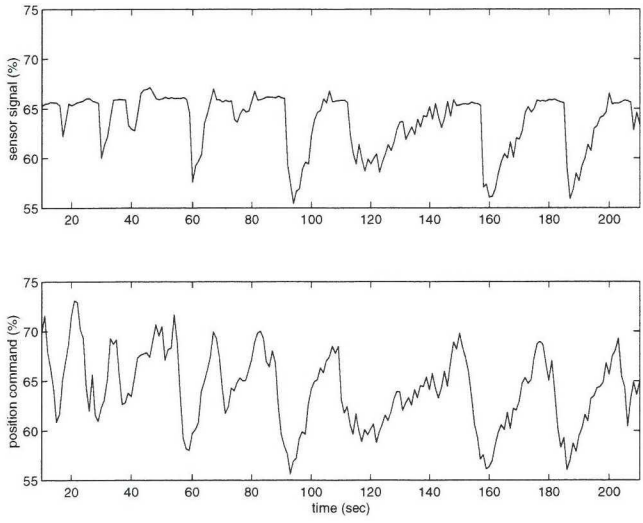

Fig. 12: Simulated malfunction of the position controller of the u_C valve. (a) position signal from the sensor, (b) control signal to the valve

5 Conclusions

In this paper an LQ optimal multivariable controller for a fine coal injection vessel is analyzed. The indications from the theoretical sensitivity analysis are validated through evaluation of data acquired during test operation of the controller at the coal injection plant at SSAB Tunnplåt Luleå, Sweden. It could be shown that the behaviour of the closed-loop system during operation is according to the results from the sensitivity analysis. Therewith, the controller design is validated and reliable enough to be considered for permanent installation. The commercially available control and leakage detection system *SafePCI* is now equipped with the above controller.

Acknowledgement

The authors would like to thank SSAB Tunnplåt AB in Luleå, for making the coal injection plant and maintenance personnel available to us. Financial support of the Center for Process and System Automation (*ProSA*) at Luleå University of Technology provided by *Norrbottens Forskningsråd* is also gratefully acknowledged.

References

[1] Wolfgang Birk, Andreas Johansson, and Alexander Medvedev. Model-based control for a fine coal injection plant. *IEEE Control Systems Magazine*, 19(1):33–43, February 1999.

[2] Wolfgang Birk and Alexander Medvedev. Pressure and flow control of a pulverized coal injection vessel. In *Proc. of the 1997 IEEE International Conference on Control Applications*, pages 127–132, 1997.

[3] F. Eichinger and M. Rafi. Maintain a very high blast furnace coal injection rate. *Steel times international*, pages 28–29, 1995.

[4] Britta R. Fischer and Alexander Medvedev. Laguerre shift identification of a pressurized process. In *Proc. of the 1998 American Control Conference, Philadelphia*, pages 1933–1942, 1998.

[5] Gene F. Franklin, J. David Powell, and Abbas Emami-Naeini. *Feedback Control of Dynamic Systems.* Addison-Wesley, third edition, 1994.

[6] G.E. Klinzing, R.D. Marcus, F. Rizk, and L.S. Leung. *Pneumatic conveying solids - A theoretical and practical approach.* Chapman and Hall, cop., London, 1997.

[7] E. Salvatore, M. Calgani, R. Capriulo, F. Eichinger, and M. Rafi. An integrated coal injection system for blast furnace at ILVA Taranto. In *Proc. of the 52. Ironmaking Conference, Dallas, USA, March 1993*, 1993.

[8] María M. Seron, Julio H. Braslavsky, and Graham C. Goodwin. *Fundamental Limitations in Filtering and Control.* Springer-Verlag, 1997.

[9] S. Skogestad and I. Postlethwaite. *Multivariable Feedback Control - Analysis and Design.* John Wiley & Sons, 1996.

[10] O.A. Williams. *Pneumatic and Hydraulic conveying solids.* Dekker, cop., New York, 1983.

[11] Kemin Zhou. *Robust and Optimal Control.* Prentice Hall, 1996.

Paper 3

Implementation and Industrial Experiences of Advanced Control and Monitoring in Coal Injection

Published as

Wolfgang Birk, Andreas Johansson, Robert Johansson, and Alexander Medvedev. "Implementation and industrial experiences of advanced control and monitoring in coal injection". *Control Engineering Practice*, 8(3):327–335, 2000.

Implementation and Industrial Experiences of Advanced Control and Monitoring in Coal Injection

Wolfgang Birk*† Andreas Johansson†
Robert Johansson‡ Alexander Medvedev†

*Corresponding author: wolfgang@sm.luth.se
†Control Engineering Group, Luleå University of Technology, SE-971 87 Luleå, Sweden
‡IT-Department, SSAB Tunnplåt AB, SE-971 88 Luleå, Sweden

Abstract

This paper summarizes the implementation and industrial experiences of a model-based control and gas-leakage detection system in a coal injection plant. It describes how advanced control and monitoring can be implemented in an industrial environment while taking human-machine interface aspects into consideration. The operation of the advanced and the conventional concept are compared regarding evaluation data, experiences and observations of operators and maintenance personnel. It is shown that the advanced control and monitoring system improves plant performance without disturbing routines in plant operation and, moreover, is positively accepted by the plant operators.

Keywords: Multivariable control; LQG; Fault detection; Fault isolation; Coal injection; Experiences.

1 Introduction

For a long time controllers were used in industry to automate processes, improve product quality and reduce production costs. One of the best known and most used controller types is the PID controller. It is usually employed to control sub-processes of industrial processes in so-called single loops, where the individual controller reacts to deviations from a given set-point or trajectory with movements of a single actuator. This traditional control concept and its possible design approaches are well described in the literature (see *e.g.* [11]; [2] [12]; [8] or [7]), and it is in every control engineer's tool-box.

Since each control loop only deals with one process variable, such a decentralized structure has its pros and cons. One of many advantages of the PID controller is that it seems to be easy to maintain. But there is also a major drawback. Control loops may disturb each other through process couplings, thus preventing the individual loops from achieving their objective. Furthermore, the structure offers only one-degree-of-freedom, as only one actuator is available.

An obvious alternative is a more centralized structure with multiple inputs and multiple outputs (MIMO) which can handle several process variables at a time, a so-called

multivariable controller. One direct result is the increase in the number of degrees-of-freedom. The controller can use multiple actuators to achieve one control objective. Consequently, the design of multivariable controllers depends even more on the characteristics of the plant than in the scalar case, [17]. Moreover, the design procedure is more complex which is reflected in the maintenance of a multivariable control system. This is probably why multivariable control concepts are so rare in industry.

Still, some examples of multivariable control in industry can be found: *e.g.* in vibration suppression [6], in the control of plate-like structures [16] and in the control of vapour compression [13]. In each of these three examples a multivariable linear quadratic gaussian (LQG) controller is used.

Fault detection and isolation is a potentially powerful tool for achieving security and effective maintenance in various types of processes. See [14] for a survey of recent simulations and implementations of fault detection systems.

The basic terminology and techniques for fault detection can be found in the survey by [10]. State estimation by observers is often used. A number of different techniques exist, for example Unknown Input Observers, Dedicated Observers, Parity Space and Kalman Filter Methods. Fault detection in non-linear systems is for example treated in [18] and [19].

In this article multivariable control and fault detection are applied to pulverized coal injection. Since coal is 40% cheaper than coke, injecting pulverized coal instead of using coke is more economical. According to the [1], the market share of pulverized coal for fuel is set to rise from 36% to 50% by the year 2015. This, of course, has consequences for the blast furnace process. From a metallurgical point of view, high coal injection rates lead to sensitivity of the blast furnace process to coal flow variations and outages. Hence, tight control of the coal flow is necessary. Furthermore, gas-leakages can cause unexpected stops in the coal injection, leading to possible instabilities in the blast furnace process. Thus, a gas-leakage detection system should be in place to detect small leakages and thereby enable the plant maintenance to plan inspection stops. Another advantage of an improved coal mass flow to the blast furnace is the increased plant capacity without hardware changes.

During the course of the project *Intelligent alarm management*, funded by the Swedish National Board for Industrial and Technical Development (*NUTEK*), a preliminary study on the control and detection of gas-leakages of fine coal injection vessels was conducted. The results indicated that further research was needed, but should be pursued in a different framework.

Consequently, a pilot project of the Center for Process and System Automation (*ProSA*) at Luleå University of Technology was started, aimed at analysing and redesigning the control system of the coal injection plant at SSAB Tunnplåt AB in Luleå, [3]. In this project, a model-based control and gas-leakage detection system, called *SafePCI*, has been developed, tested and suggested for permanent installation. *SafePCI* consists of a multivariable control concept combined with monitoring, su-

pervision and algorithms for the detection of gas-leakages to and from the injection vessels. Accordingly, *SafePCI* is now permanently installed in SSAB Tunnplåt AB's newly purchased coal injection plant.

When it comes to the implementation of advanced control and monitoring concepts, the design of the human-machine interface becomes crucial. Maintenance and operation of *SafePCI* should be facilitated by an interface that is designed with respect to man-machine aspects. Therefore, it is important to consider the experience of operators and maintenance personnel during the design as well as following up their experiences with *SafePCI*. Moreover, the success of the installation of advanced control and monitoring concepts greatly depends on positive acceptance by the operators. Therefore, thorough testing and caution during start-up is necessary.

The paper is organized as follows. First, the coal injection process is briefly described and a problem definition is given in Section 2. Then, *SafePCI* is presented in Section 3, where the focus is on the design of interfaces and implementation. The design of the multivariable controller and the gas-leakage detection system are only briefly described but further references for the interested reader are given. The operation of *SafePCI* is evaluated and compared with the conventional control concept in Section 4. Finally, the experiences and observations of the operators and maintenance personnel are presented in Section 5, followed by a short summary of the results in Section 6.

2 The process

A coal injection plant is a highly automated plant, where incoming raw coal is stored, ground, dried and finally injected into the blast furnace. During operation, human interaction is only needed for set point adjustments. Fig. 1 shows the structure of the plant, where only the injection vessels, distributor and the blast furnace are depicted. While one vessel is de-pressurized, charged and pressurized the other vessel is injecting pulverized coal. Thus a continuous pulverized coal flow is achieved. The control of the injection process is complicated due to the two phase nature of the injected flow (gas plus particles). In Table 1, the process phases of an injection vessel working cycle (Fig. 2) are summarized. A more detailed picture of an injection vessel, including some of the notations used in the following, is given by Fig. 3.

Continuous injection of coal powder is crucial for blast furnace operation. A sudden loss of coal injection capacity may lead to 'chilled hearth', a condition that can have serious consequences for the blast furnace. Leakages in worn-out valves can make it impossible to maintain the pressure in the injection vessel. This fact, in addition to the cost of lost nitrogen, motivates the development of a fault detection system to detect and isolate leakages. In some coal injection plants, where the injection line contains air, the risk of air leakages into the highly inflammable coal powder is an additional reason for performing leakage detection.

Since coal powder is significantly less expensive than coke, it is desirable to substitute

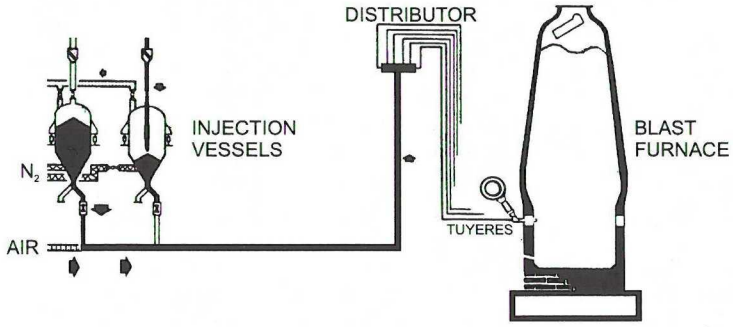

Fig. 1: Coal injection plant (injection vessels, distributor and blast furnace).

Table 1: Process phases

Phase	Name	Description
A	Charging	The unpressurised vessel is filled with coal powder
B	Pressurization	The injection vessel is put under pressure
C	Pressure holding	Standby until the other vessel has finished injection
D	Injection	The coal powder is injected into the blast furnace
E	Ventilation	Depressurization and ventilation of the vessel

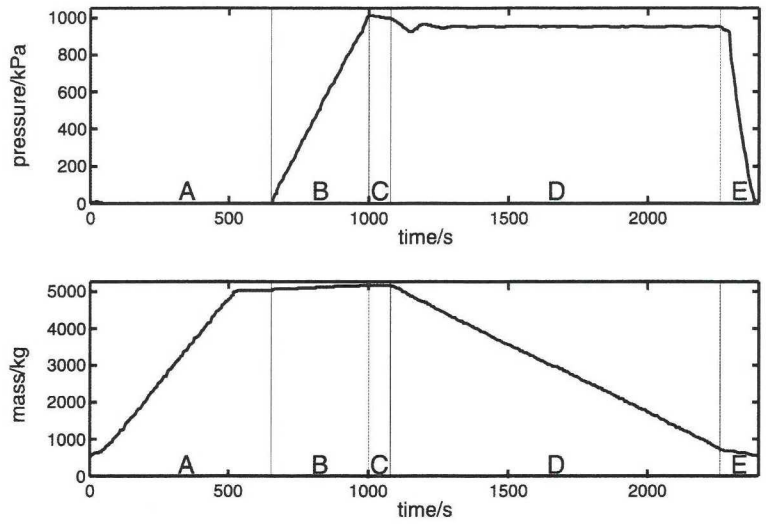

Fig. 2: Pressure and weight evolution during a working cycle.

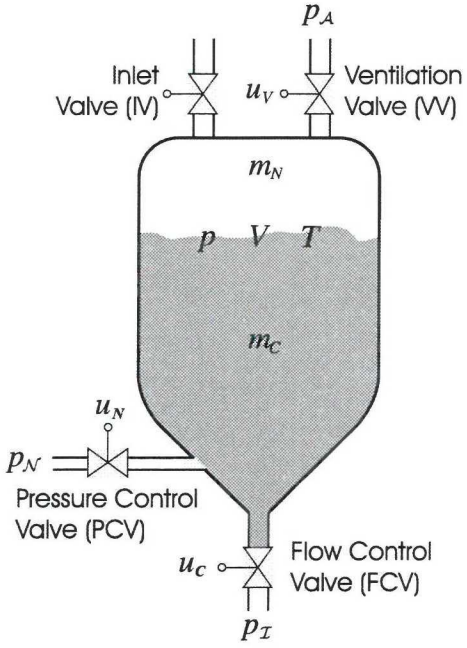

Fig. 3: Schematic drawing of an injection vessel

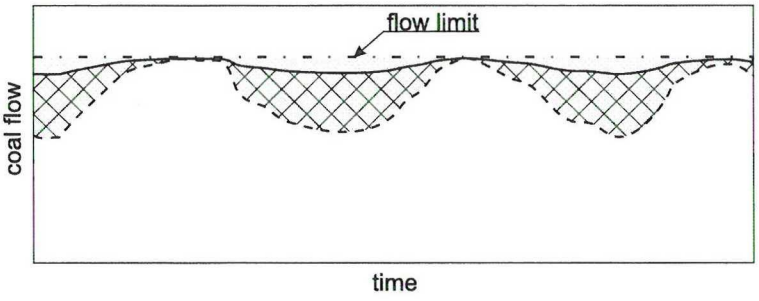

Fig. 4: Benefit of improved control. Limiting mass flow (dashed-dotted), coal mass flow (dashed), improved coal mass flow (solid), benefit (hatched area).

as much as possible of the latter for the former. There is, however, a limit to how much coal powder can be injected at each time instant. Improved control of the injection rate can make it possible to increase the flow closer to this limit and thus give economical benefits, see Fig. 4.

Furthermore, coal powder is used to control the flame temperature in the blast furnace. A certain ratio of coal powder, oxygen enrichment and blast volume is computed in order to achieve a constant temperature. Thus, improved control of the injection rate facilitates flame temperature control.

A particular problem when controlling the coal injection plant is the inherent MIMO nature of the process. Both the position of the flow control valve and the pressure in the vessel affect the flow of coal powder. Furthermore, there exists no measurement of the flow itself but instead the mass of the injection vessel has to be used. These facts explain why good performance cannot be obtained using traditional SISO PI or PID control loops, [5].

3 SafePCI

To minimize coal flow variations, optimize maintenance and reduce unexpected injection stops, a model-based control and gas-leakage detection system, called *SafePCI*, is suggested. In the first design steps the dynamical behaviour of injection vessels is modelled. Two models are developed, a linear model which is obtained from system identification and a non-linear model which is based on the laws of physics. The linear model is used for the design of the multivariable controller and the non-linear model is used for the design of the gas-leakage detection system.

SafePCI is then implemented in the control system of the coal injection plant in two steps which are described in Subsection 3.1. A brief description of the control system used is also given there. In the subsequent subsection, the interfaces to the control

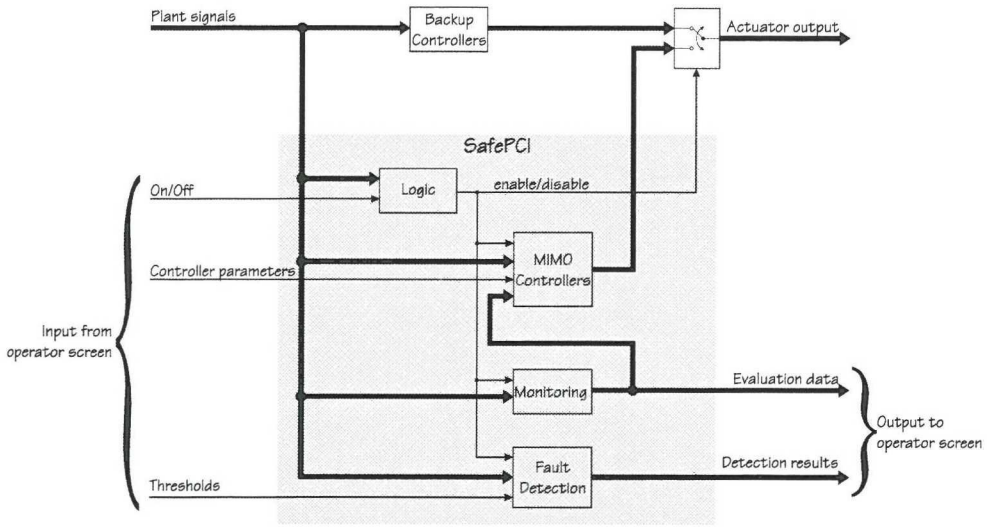

Fig. 5: Structure of *SafePCI* as installed in Honeywell-Measurex TotalPlant AlCont

system and for the plant operators are described. The design of the multivariable controller is given in Subsection 3.3. Finally, the design of supervision, monitoring and the gas-leakage detection system are recapitulated in Subsections 3.4 and 3.5, respectively.

3.1 Structure

SSAB Tunnplåt Luleå AB uses the commonly available control system, Honeywell-Measurex TotalPlant AlCont. It provides the engineer with a standard function block set, from which new blocks with more functionality can be created. Additionally, function blocks can be directly generated from Pascal-code with freely definable input/output interface. These so-called Pascal-blocks are treated in the same way as the standard function blocks by the PLC. The engineer can simulate and test the blocks in an off-line environment and download them to the PLC. Also, signal information in all blocks of the application can be monitored on-line from a Windows NT environment.

Since the coal injection plant is in continuous operation, *SafePCI* is installed as a parallel structure to the conventional controllers of the injection vessels. This enables the engineers to maintain the conventional controllers and *SafePCI* during operation of the plant. Furthermore, the conventional controllers can be used as a backup.

For the installation of *SafePCI* the structure depicted in Fig. 5 is suggested. The gray-shaded area represent the implementation of *SafePCI* with its interfaces to the

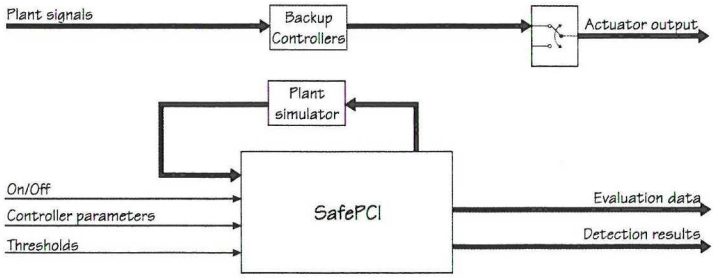

Fig. 6: Structure of *SafePCI* during debugging

operators and to the control system. During debugging of the *SafePCI* implementation, the coal injection plant is replaced by a plant simulator, which models the dynamic, sequential and logical behaviour of the coal injection plant. The structure for debugging is shown in Fig. 6. Setting up such a test structure results in a longer implementation phase on the one hand but on the other hand reduces debugging and the test phase and, most important, system failures during start-up. The simulator provides also a tool for training of plant operators in maintaining the control system.

3.2 Interfaces

SafePCI has two interfaces. In the Honeywell-Measurex TotalPlant AlCont system the interface to the plant is constructed by creating software links to signals from A/D input cards or signals generated in the control system.

A graphical editor can be used to create the display and controls for the operator interface. Software links are introduced to connect the displays and controls with signals to and from *SafePCI*. The control system resolves the software links automatically and provides the necessary data transfers as soon as screens or program blocks are uploaded from the IDE to the control system.

Fig. 7 shows the operator interface. The main switch for *SafePCI* is placed in the upper left corner. Using this switch the operators can choose between the backup controllers and *SafePCI*. The upper left frame contains the controls to adjust control parameters, and the upper right contains the controls for the leakage detection thresholds. Evaluation data is presented to the operator in the lower left frame, where standard deviations, residuals from the state estimation and a coal flow estimation are given. Finally, the results from the leakage detection are presented in the lower right frame.

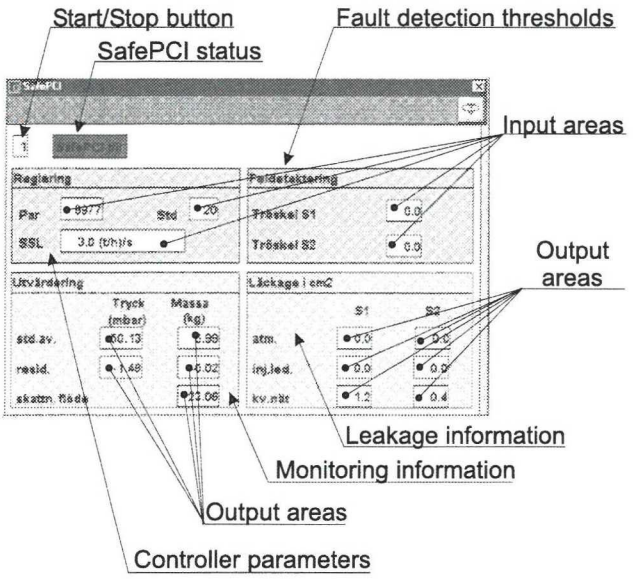

Fig. 7: Operator interface

3.3 The multivariable controller

The multivariable controller is a part of the loop structure depicted in Fig. 8 and is a result of a previous study, [3].

Besides the state vector feedback controller, a Kalman filter, a feedforward controller and an actuator saturation are included in the closed-loop system. Both the Kalman filter and multivariable controller design are based on an identified multiple input, multiple output (MIMO) model of the process dynamics.

The structure of an injection vessel can be described by Fig. 3, and the process is principally a pressurized tank process. During the injection of coal the inlet and ventilation valves are closed. Consequently, the two actuator signals u_N and u_C can be used to control the vessel. Measured outputs of the vessel are the pressure p in the vessel and the net mass m of the vessel. The latter is identical to the sum of the nitrogen mass m_N and the coal mass m_C. Since the injection vessel is injecting coal at a certain flow rate, the net mass of the vessel has to follow a trajectory. Using direct identification, a model describing the process dynamics can be obtained. The identification method and its application to the coal injection plant are discussed in [9], where the subspace identification method *n4sid* is applied to the Laguerre spectra of the input/output data. There was shown that *n4sid* performs better in the Laguerre domain compared to the time domain, when it is used for identification of

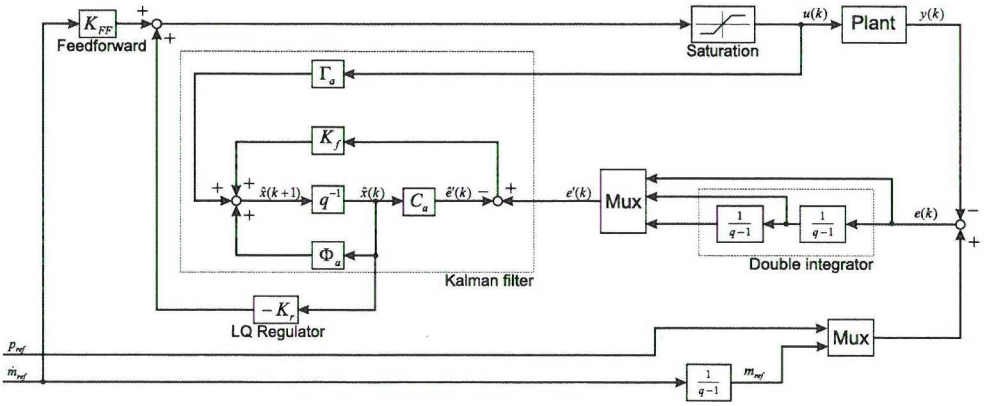

Fig. 8: Block diagram of the closed-loop structure

the injection vessels. The obtained MIMO model is of second order and given by

$$x(k+1) = \Phi x(k) + \Gamma \begin{bmatrix} u_N(k) \\ u_C(k) \end{bmatrix} \tag{1a}$$

$$\begin{bmatrix} p(k) \\ m(k) \end{bmatrix} = Cx(k) + D \begin{bmatrix} u_N(k) \\ u_C(k) \end{bmatrix} \tag{1b}$$

As only the design methodology is outlined here, numerical values are omitted. Since C is invertible, the similarity transformation $x(k) = C^{-1}x'(k)$ can be applied, which yields

$$x'(k+1) = C\Phi C^{-1}x'(k) + C \begin{bmatrix} u_N(k) \\ u_C(k) \end{bmatrix} \tag{2a}$$

$$\begin{bmatrix} p(k) \\ m(k) \end{bmatrix} = I_2 x'(k) + D \begin{bmatrix} u_N(k) \\ u_C(k) \end{bmatrix} \tag{2b}$$

Hence, the states of the transformed dynamic system coincide with the outputs.

As mentioned above, the net mass of the injection vessel has to follow a trajectory, which is usually a ramp. Hence, the open-loop system (controller and plant) needs to include at least two integrators, in order to drive the steady state error to zero. For Kalman filter and controller design, the identified model is augmented with a double-integrator for each of the outputs. The resulting state space system is given

by

$$x'_a(k+1) = \underbrace{\begin{bmatrix} C\Phi C^{-1} & 0 & 0 \\ I_2 & I_2 & 0 \\ 0 & I_2 & I_2 \end{bmatrix}}_{\Phi_a} x'_a(k) + \underbrace{\begin{bmatrix} C\Gamma \\ 0 \\ 0 \end{bmatrix}}_{\Gamma_a} \begin{bmatrix} u_N(k) \\ u_C(k) \end{bmatrix} \tag{3a}$$

$$y(k) = \underbrace{\begin{bmatrix} I_2 & 0 & 0 \\ 0 & I_2 & 0 \\ 0 & 0 & I_2 \end{bmatrix}}_{C_a} x(k) + \begin{bmatrix} D \\ 0 \\ 0 \end{bmatrix} \begin{bmatrix} u_N(k) \\ u_C(k) \end{bmatrix}. \tag{3b}$$

Using the standard LQG design procedure, a MIMO LQG controller with a stationary Kalman filter is obtained (see [4]). The optimal multivariable controller can be written in the form:

$$x_c(k+1) = \begin{bmatrix} I_2 & 0 \\ I_2 & I_2 \end{bmatrix} x_c(k) + \begin{bmatrix} I_2 \\ 0 \end{bmatrix} e(k) \tag{4a}$$

$$e'(k) = \begin{bmatrix} 0 & 0 \\ I_2 & 0 \\ 0 & I_2 \end{bmatrix} x_c(k) + \begin{bmatrix} I_2 \\ 0 \\ 0 \end{bmatrix} e(k) \tag{4b}$$

$$\begin{bmatrix} u_N(k) \\ u_C(k) \end{bmatrix} = -K_r \cdot e'(k), \tag{4c}$$

where $e(k) = r(k) - y(k) = \begin{bmatrix} p_{ref}(k) - p(k) \\ m_{ref}(k) - m(k) \end{bmatrix}$.

The measurement signal vector $y(k)$ contains the pressure $p(k)$ and the net mass $m(k)$, whereas the reference signal vector contains the pressure set-point $p_{ref}(k)$ and the net mass trajectory $m_{ref}(k)$.

3.4 Monitoring and supervision

Malfunction of a controller can be caused by hardware failures in the coal injection plant or a part wearing out. Therefore, operators have to monitor a number of control loops in a plant. Automatic supervision and monitoring supports the operators' work and facilitates the detection of malfunctions.

Hence, *SafePCI* is equipped with automatic monitoring and supervision. In addition to the LQ optimal-multivariable controller, back-up controllers are available. During injection, deviations from set-points and residuals are evaluated. Using pre-defined thresholds, the supervision function is enabled to take decisions on controller malfunction. In case of a detected malfunction, a back-up controller is used instead of the MIMO-LQG controller.

To facilitate supervision and trend analysis by the operators, the control performance is monitored on-line. Throughout operation of the plant evaluation data is computed and presented on the operator screen. The quantities are:

- Standard deviations in mass and pressure
- Mean values of mass and pressure residuals
- Least squares estimate of the coal mass flow

Since the coal mass flow is not directly measured and only an estimate based on differentiation is available, *SafePCI* provides a least squares estimate of the coal mass flow.

3.5 Leakage detection

Leakage detection is performed during the ventilation phase. A non-linear model for the injection vessel during this phase, based on physical principles is given by

$$\begin{aligned} \dot{m}_N &= A_V m_N + B_V f_{\text{gas}}(p, p_{\mathcal{A}}) u_V + q_L \\ \dot{m}_C &= 0 \\ y &= h(m_N, m_C) \end{aligned} \tag{5}$$

where A_V and B_V are constants obtained by identification. The input u_V is the control signal to the ventilation valve and f_{gas} is a function describing the flow of a gas through a pressure drop. The state variables m_C and m_N represent the masses of coal and nitrogen in the vessel and the output vector $y = \begin{bmatrix} m & p \end{bmatrix}^T$ is the mass and the pressure in the vessel, respectively. The transformation $h(m_N, m_C)$ relating the state to the output vector is uniquely invertible [15].

Three different types of leakages are considered (Table 2). The set of leakages is denoted

$$\mathcal{L} \triangleq \{\mathcal{A}, \mathcal{N}, \mathcal{I}, \emptyset\}$$

A leakage can be interpreted as the flow through a valve with an unknown control signal. The nitrogen leakage flow can thus be represented by

$$q_\ell = k_\ell f_\ell(\cdot) \quad \ell \in \mathcal{L} \tag{6}$$

where k_ℓ is an unknown time-varying factor and $f_\ell(\cdot)$ is a function of the pressures on each side of the leakage. The trivial leakage function for the event of 'No Leakage' is $f_\emptyset = 0$. The other leakage functions ($f_{\mathcal{A}}$, $f_{\mathcal{N}}$ and $f_{\mathcal{I}}$) are developed from the non-linear physical model.

A linear observer for (5) was designed and it was shown that the observer residual is an approximation of the leakage flow $\hat{q}_L$ scaled by a constant.

Table 2: Leakages

Leakage	Possible consequence	Notation
To the atmosphere	Loss of nitrogen and pressure drop in the vessel	$\mathcal{A}$
From the nitrogen net	Over-pressurized vessel	$\mathcal{N}$
To/from the injection pipe	Loss of nitrogen and pressure drop in the vessel. Fire if the injection line contains air	$\mathcal{I}$
No Leakage	-	$\emptyset$

The factor k_ℓ in (6) is a measure of the size of the hole through which the leakage flow takes place. This means that k_ℓ varies slowly in time when describing incipient leakages. If k_ℓ is assumed to be constant during a reasonably long period of time (for example a ventilation phase), it can be estimated using the Generalized Likelihood Ratio.

Four hypotheses ($\mathcal{H}_\emptyset$, $\mathcal{H}_\mathcal{A}$, $\mathcal{H}_\mathcal{N}$ and $\mathcal{H}_\mathcal{I}$) are formed in agreement with the leakage events. The three leakage hypotheses are tested one by one against $\mathcal{H}_\emptyset$ using the Generalized Likelihood Ratio (GLR). If $\mathcal{H}_\emptyset$ is rejected in more than one of these tests, the hypothesis with the highest GLR is accepted. The GLR for each leakage hypothesis is

$$\Lambda_\ell\left(\hat{q}_L\right) = \frac{\sup_{k_\ell>0} P_\ell\left(\hat{q}_L\right)}{P_\emptyset\left(\hat{q}_L\right)}$$

where P_ℓ is the likelihood function for hypothesis $\mathcal{H}_\ell$. The restriction on k_ℓ comes from the fact that a negative k_ℓ would imply a leakage flow from a lower pressure to a higher. The leakage type with the highest GLR is chosen and the size of this leakage is compared to the detection threshold set by the operators. If the threshold is exceeded then the null hypothesis is rejected and a leakage has occurred.

See also [15] for more details on the leakage detection scheme.

4 Evaluation

After the parameters adjustment of *SafePCI*, evaluation data is logged using SSAB Tunnplåt's measurement database *MÖSS*. Since *MÖSS* stores data over a long time period it is possible to obtain data sets afterwards. Therefore, adequate data sets for a comparison of the conventional control and *SafePCI* can be chosen. As mentioned above the mass flow is not measured directly. Instead, an estimate based on a numerical differentiation of the mass signal is available in *MÖSS* and will be used for the evaluation.

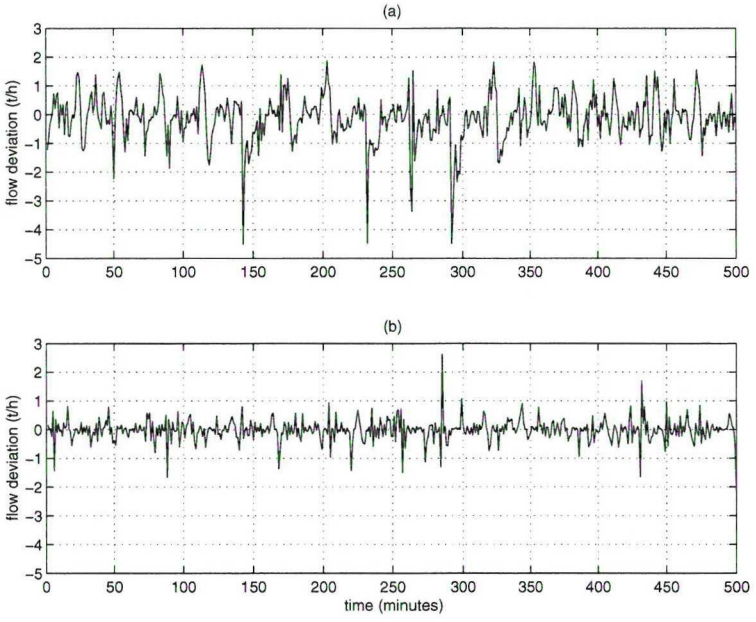

Fig. 9: Comparison of the coal mass flow deviation. (a) conventional control, (b) *SafePCI*.

Since the set point for the coal mass flow varies, specifications for the evaluation data have to be set up. First, the mean value of the coal mass flow set point over the evaluation period must not deviate more than 1 (t/h). Second, the data set should contain high and low injection rates. Furthermore, the data set should be continuous and reflect at least 8 hours of operation.

Fig. 9 shows the absolute deviation of coal mass flow from the set-point for *SafePCI* and the conventional controller. Obviously, the coal mass flow variations are reduced. Apart from some peaks, the deviations are less than 1 (t/h). Comparing the relative deviations of the coal mass flow from the set-point (see Fig. 10) shows that the relative deviations are mostly less than 5%.

For the quantitative analysis, the standard deviation and the maximum deviation are used. These measures are applied to the relative and absolute deviation from the flow set point. Table 3 summarizes the results and gives the percentage improvement achieved by *SafePCI* compared to the conventional control.

During the start-up and the evaluation period *SafePCI* gave some indications on leakages from the nitrogen net. These indications were probably due to temporary clogging of the ventilation valve which, to the detection algorithm, will appear as a leakage into the vessel.

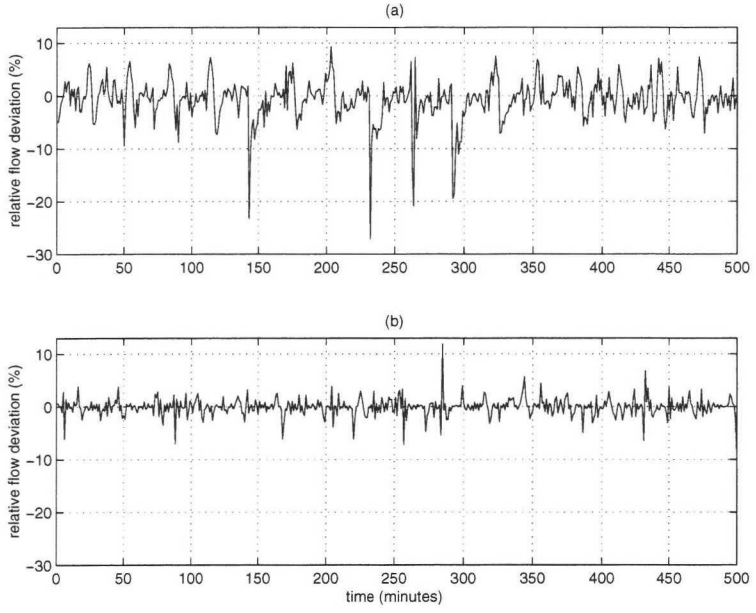

Fig. 10: Comparison of the relative coal mass flow deviation. (a) conventional control, (b) *SafePCI*

Table 3: Quantitative evaluation

	Conventional Control	*SafePCI*	Improvement (%)
Standard deviation (t/h)	0.81	0.40	51.53
Maximum deviation (t/h)	4.51	2.62	41.95
Relative standard deviation (%)	3.88	1.73	55.32
Relative maximum deviation (%)	27.13	11.89	56.19

5 Experiences and observations

To follow-up the installation of *SafePCI*, the operators and maintenance personnel were interviewed about their experiences and observations during the operation of the coal injection plant under *SafePCI*.

The overall opinion was that a smooth transition from the conventional control system to *SafePCI* had been achieved. During start-up and operation no unexpected stops occurred due to a malfunction of *SafePCI*.

It has been observed that vibrations in the injection lines have reduced. According to the operators, this is an indication of an evenly divided flow from the distributor. Furthermore, the mechanical wear-out in the injection pipes is thus reduced.

When clogging occurs in one of the injection pipes, the coal flow is distributed to the remaining unclogged pipes, resulting in an unbalanced distribution of coal in the blast furnace raceway. Consequently, the amount of unburned coal is not evenly distributed and can lead to instabilities in the blast furnace process. Usually, the coal injection is stopped for a short time and the clogged pipe is purged. If clogging is detected in time, blast furnace operation is not affected. Since *SafePCI* was put into operation, the occurrence rate of clogging has reduced.

6 Conclusions

The installation of the model-based control and gas-leakage detection system *SafePCI* in SSAB Tunnplåt's coal injection plant is described. The system comprises an LQ optimal-multivariable controller, with a supervision and a gas-leakage detection system based on a non-linear model for the injection vessels.

SafePCI was then compared with the conventional control concept using evaluation data. The comparison was complemented with an analysis of the operators' experiences and observations during operation of the plant under *SafePCI*.

The short term comparison has shown that advanced control and monitoring concepts improve plant performance, are positively accepted by plant operators and can be installed during normal production in so that plant operation is not disturbed.

References

[1] American Iron and Steel Institute. Steel industry technology roadmap. At *http://www.steel.org/MandT/contents.htm*, February 1998.

[2] K.J. Åström and B. Wittenmark. *Computer Controlled Systems.* Prentice Hall, Inc., 1990.

[3] Wolfgang Birk, Andreas Johansson, and Alexander Medvedev. Model-based control for a fine coal injection plant. *IEEE Control Systems Magazine*, 19(1):33–43, February 1999.

[4] Wolfgang Birk and Alexander Medvedev. Pressure and flow control of a pulverized coal injection vessel. In *Proc. of the 1997 IEEE International Conference on Control Applications*, pages 127–132, 1997.

[5] Wolfgang Birk and Alexander Medvedev. Pressure and flow control of a pulverized coal injection vessel. *IEEE Transactions on Control Systems Technology*, 8(6):919–929, November 2000.

[6] K. K. Denoyer and M. K. Kwak. Dynamic modelling and vibration suppression of a slewing structure utilizing piezoelectric sensors and actuators. *Journal of Sound and Vibration*, 189(1):13–31, Jan 1996.

[7] Richard C. Dorf and Robert H. Bishop. *Modern Control Systems*. Addison-Wesley, 1998.

[8] John C. Doyle, Bruce A. Francis, and Allen R. Tannenbaum. *Feedback Control Theory*. Macmillan Publishing Company, 1992.

[9] Britta R. Fischer and Alexander Medvedev. Laguerre shift identification of a pressurized process. In *Proc. of the 1998 American Control Conference, Philadelphia*, pages 1933–1942, 1998.

[10] P.M. Frank and X. Ding. Survey of robust residual generation and evaluation in observer-based fault detection systems. *J. Proc. Cont.*, 7(6):403–424, 1997.

[11] Gene F. Franklin, J. David Powell, and Abbas Emami-Naeini. *Feedback Control of Dynamic Systems*. Addison-Wesley, third edition, 1994.

[12] Gene F. Franklin, J. David Powell, and Michael Workman. *Digital Control of Dynamic Systems*. Addison-Wesley, 1998.

[13] Xiang-Dong He, Harry H. Asada, Sheng Liu, and Hiroyuki Itoh. Multivariable control of vapor compression. *HVAC&R Research*, 4(3):205–230, July 1998.

[14] Rolf Isermann and Peter Ballé. Trends in the application of model based fault detection and diagnosis of technical processes. In *IFAC World Congress Proceedings*, 1996. CD-ROM.

[15] Andreas Johansson and Alexander Medvedev. Model based leakage detection in a pulverized coal injection vessel. *IEEE Transactions on Control Systems Technology*, in press, 1999.

[16] Kenneth B. Lazarus, F. Edward, and Charissa Y. Lin. Multivariable high-authority control of plate-like structures. *Journal of Guidance, Control and Dynamics*, 19(6):1357–1363, Nov-Dec 1996.

[17] S. Skogestad and I. Postlethwaite. *Multivariable Feedback Control - Analysis and Design.* John Wiley & Sons, 1996.

[18] Jürgen Wünnenberg and Paul M. Frank. Dynamic model based incipient fault detection concepts for robots. In *Preprints of the 11th IFAC World Congress*, volume 3, pages 76–81, 1990.

[19] A. Zhirabok and O. Preobrazhenskaya. Robust fault detection and isolation in nonlinear systems. In *Proceedings of IFAC Symposium "Safeprocess'94"*, pages 244–248, 1994.

Paper 4

A Note on Gramian-Based Interaction Measures

European Control Conference ECC2003, 1-4 September, University of Cambridge, UK

Submitted

A Note on Gramian-Based Interaction Measures

Wolfgang Birk*† and Alexander Medvedev†§

*Corresponding author: eMail: wolfgang@sm.luth.se
§ Information Technology, Uppsala University, Box 337, SE-751 05, Uppsala, Sweden
†Control Engineering Group, Luleå University of Technology, SE-971 87 Luleå, Sweden

Abstract

This note deals with recently developed gramian based interaction measures. The measures are used for the choice of measurement/actuator pairs for decentralized control, where the controller remains unspecified. The theoretical background of these measures is clarified and a geometrical interpretation is given. Moreover, a generalization of the Hankel interaction index array to different gramian based system norms is proposed and it is shown that the introduction of weighted gramians makes the criteria more flexible and superior compared to the augmenting with additional filter dynamics. Finally, some examples are given to illustrate the usefulness of the generalized measures.

1 Introduction

Prediction of interaction present in a control system from an open-loop perspective has been dealt with for a long time. Both steady state and dynamic measures for interaction have been suggested.

The first proposed interaction measures were the *Rijnsdorp interaction measure* [16] and the *relative gain array* (RGA) [3]. These measures are derived from steady-state gain information and are related to each other via a non-linear map [8]. Ever since, the RGA is widely used in industrial applications and has been extended to a dynamic measure [11].

Further development of the RGA became necessary due to the introduction of more advanced control structures. In order for the RGA to be applicable a decentralized controller has to be used and the steady state control error has to be zero. Generally, these assumptions are not fulfilled and thus the indications are not reliable.

This led *e.g.* to the introduction of the block relative gains (BRG) [14] and partial relative gains (PRG) [9]. Thereby, it became possible to get indications for interactions in multivariable control systems with control structures different from decentralized control.

Newly developed measures are a measure based on Hankel singular values [5] and the *Hankel interaction index array* [20], which makes use of the Hankel norm of the scalar sub-systems. Both measures are gramian based and analyze scalar sub-systems of the multivariable system in order to get insight into the system structure and thus draw

a-priori conclusions on interaction in the closed loop system. The Hankel norm is originally used in model reduction [7] and is easily derived from the gramian product.

Since gramian based measures judge the overall dynamic behavior of a system, indications of these measures are realistic even for transient behavior, where many frequencies arise. When these interaction measures are used to make decisions on the measurement/actuator pairs for decentralized control, the problem can be divided into two classes: controller independent and controller dependent. In the controller dependent problem both process model and controller are considered, which is more complex than the controller independent problem where the controller remains unspecified. Here, the controller independent problem is discussed.

Since existing publications do not clarify the geometrical aspects of the gramian based measures, the paper reviews these aspects to get a better understanding of the measures when used for the controller independent problem.

The paper is structured as follows. Starting out from a general description of linear multivariable systems, the notion of gramians is introduced as a tool for function spaces and how it can be applied to linear systems. Moreover, state space realizations of linear systems are introduced and gramians are used to derive subspaces of the state space. It is illustrated how intersections in subspaces are related to interaction in multivariable systems. Thereafter, the connection between gramians and the Hankel operator is discussed and based on the results generalizations of the Hankel interaction index array are derived. Then, weighted gramians are introduced into the interaction measures and their relation to filtering of process dynamics is analyzed. Finally, some examples are given followed by conclusions and outlook.

2 Preliminaries

Interaction concerns input/output behavior of multivariable systems, namely the relation between different channels. A channel is defined as the path from an input to an output. The output of a linear multivariable system is given as the convolution of an input signal with its impulse response function matrix

$$y(t) = \int_{t_1}^{t_2} g(t-\tau)u(\tau)d\tau \tag{1}$$

where $y(t) \in \mathcal{L}_2^p[t_1, t_2]$ and $u(t) \in \mathcal{L}_2^m[t_1, t_2]$. The associated function spaces are denoted $\mathcal{Y}$ and $\mathcal{U}$, respectively. The impulse response function has to be bounded and thus $g(t) \in \mathcal{L}_1^{p\times m}[t_1, t_2]$. The restriction to the time interval $[t_1, t_2]$ makes it possible to consider unstable multivariable systems as long as $g(t)$ is bounded in the interval. For stable systems the interval can be set to $[-\infty, \infty]$.

The frequency domain representation of (1) can be obtained by applying the Laplace transform and is given by

$$Y(s) = G(s)U(s) \tag{2}$$

where s denotes the differential operator and $Y(s)$, $U(s)$ denote the Laplace transform of $y(t)$ and $u(t)$, respectively. $G(s)$ is referred to as the transfer function matrix, which is the Laplace transform of the impulse response function $g(t)$.

Now, the standard inner product of two vectors $\phi(t)$ and $\xi(t)$ in the function space $\mathcal{L}_2^n[t_1, t_2]$ is defined as

$$\langle \phi(t), \xi(t) \rangle = \int_{t_1}^{t_2} \phi^T(t)\xi(t)dt \tag{3}$$

For this inner product a Gram matrix, also referred to as gramian, can be derived by computing the inner product of all combinations of the vector elements $\phi_q(t)$ and $\xi_r(t)$. The elements in the gramian are given by

$$\begin{aligned} [\Gamma]_{qr} &= \langle \phi_q(t), \xi_r(t) \rangle \\ &= \int_{t_1}^{t_2} \phi_q(t)\xi_r(t)dt \end{aligned}$$

Consequently, the gramian can be written as

$$\Gamma = \int_{t_1}^{t_2} \phi(t)\xi^T(t)dt \tag{4}$$

The gramian is the matrix of the inner product relative to the basis in which the vectors ϕ and ξ are expressed, [6]. When the basis is changed using a non-singular transformation matrix T, the corresponding vectors $\phi'(t)$ and $\xi'(t)$ in the new basis are given as

$$\phi'(t) = T\phi(t) \ , \quad \xi'(t) = T\xi(t)$$

The gramian for the transformed vectors is then found as

$$\begin{aligned} \Gamma' &= \int_{t_1}^{t_2} \phi'(t){\xi'}^T(t)dt \\ &= \int_{t_1}^{t_2} T\phi(t)\xi^T T^T(t)dt \\ &= T\Gamma T^T \end{aligned} \tag{5}$$

Thence, the gramian is not invariant to basis changes. Moreover, it is also known that the gramian is symmetric and positive semidefinite. Thus, the eigenvalues of the gramian are all real and non-negative. Following [6], two vectors are linearly independent if the gramian is positive definite or, in other words, has only strictly positive eigenvalues. Gramians have a close relation to the associated function spaces which is stated in the following lemma.

Lemma 1. *A vector $\xi(t)$ lies in the range space of the impulse response function $g(t)$ if and only if it lies in the range space of*

$$\Gamma = \int_{t_1}^{t_2} g(t)g^T(t)dt$$

Proof. A proof is given in [4]. □

Thus, using the eigenvector/eigenvalue decomposition of the gramian an orthonormal basis for the range of $g(t)$ can be derived, namely the eigenvectors associated with the non-zero eigenvalues constitute a basis. An important generalization to the decomposition of gramians is the operator decomposition, namely the derivation of singular values and Schmidt pairs of a compact operator and its adjoint [21].

Often in linear systems analysis the impulse response function $g(t)$ is expressed in terms of a state space realization, which is a set of linear differential equations

$$\dot{x}(t) = Ax(t) + Bu(t) \tag{6a}$$
$$y(t) = Cx(t) + Du(t) \tag{6b}$$

where $A \in \mathbb{R}^{n\times n}$, $B \in \mathbb{R}^{n\times m}$, $C \in \mathbb{R}^{p\times n}$ and $D \in \mathbb{R}^{p\times m}$. The state space realization consists of two equations, the state and the output equation. It is well known, that a state space realization is not unique and they are connected via the similarity transform.

$$z(t) = Tx(t) \tag{7a}$$
$$\dot{z}(t) = TAT^{-1}z(t) + TBu(t) \tag{7b}$$
$$y(t) = CT^{-1}z(t) + Du(t) \tag{7c}$$

Obviously, the state vector can be freely chosen and thereby, the basis for the state space $\mathcal{X} \subseteq \mathcal{L}_2^n[t_1, t_2]$.

The solution of (6) is given by

$$y(t) = Ce^{A(t-t_1)}x(t_1) + \int_{t_1}^{t} Ce^{A(t-\tau)}Bu(\tau)d\tau + Du(t) \tag{8}$$

where $x(t_1)$ is the initial condition. Since interaction concerns the input/output relationship, the initial condition $x(t_1) = 0$ can be assumed without loss of generality. Then, (8) equals (1) for all impulse response functions with $g(t) = 0,\ t < 0$. In the frequency domain, $G(s)$ is given by $C(sI - A)^{-1}B + D$.

Each of the pm scalar subsystems, which describes the behavior from input j to output i, is then defined by either the triple (A, B_j, C_i), $G_{ij}(s)$ or $g_{ij}(t)$. There, B_j is the j^{th} column vector in B and C_i is the i^{th} row vector in C.

3 Subspaces of $\mathcal{X}$

Subspaces are a geometrical construct which is used to divide up a vector space according to properties of its elements like controllability and observability. Subsystems

of a multivariable system are also associated with subspaces and thus, the same framework can be used to analyze the relationship between subsystems in terms of system properties. Thence, subspaces can be used in interaction analysis of multivariable systems.

In order to characterize subspaces that are associated with subsystems of (6), the indices i and j are used, *e.g.* $\mathcal{X}_{12}$ would denote the state space of the scalar subsystem from input 2 to output 1.

3.1 Controllable subspace of $\mathcal{X}$

The state vector $x(t)$ is governed by the differential equation (6a). Thus the state impulse response matrix can be given as

$$X(t) = [X_1(t)\ X_2(t)\ \ldots\ X_m(t)] \tag{9}$$

where $X_j(t) = e^{At}B_j$ is the response to a Dirac delta impulse in $u_j(t)$ with $x(t_1) = 0$. Accordingly, the state impulse response matrix in the frequency domain is obtained as

$$X(s) = (sI - A)^{-1}B \tag{10}$$

According to [15], the controllable subspace $\mathcal{X}_c$ is the subspace of $\mathcal{X}$ of least dimension containing the range of the state impulse response function $X(t)$. The controllable subspace that is associated with input j is denoted $\mathcal{X}_{cj}$.

Applying the definition of the gramian (4) to $X(t)$ the controllability gramian is obtained as

$$\Gamma_c = \int_{t_1}^{t_2} e^{At}BB^T e^{A^T t}dt \tag{11}$$

In the frequency domain, the controllability gramian can be defined by

$$\Gamma_c = \frac{1}{2\pi j}\int_{-j\infty}^{j\infty} (sI - A)^{-1}BB^T(\bar{s}I - A^T)^{-1}ds \tag{12}$$

where $\bar{s}$ denotes the complex conjugate.

For stable systems, the controllability gramians in time domain and frequency domain are connected via Parseval's equality and yield the same result. The controllability gramians for individual inputs are then given by

$$\begin{aligned}\Gamma_{cj} &= \int_{t_1}^{t_2} e^{At}B_jB_j^T e^{A^T t}dt \\ &= \frac{1}{2\pi j}\int_{-j\infty}^{j\infty} (sI - A)^{-1}B_jB_j^T(\bar{s}I - A^T)^{-1}ds\end{aligned}$$

In case of a stable system it can be shown by partial integration that the gramian satisfies

$$A\Gamma_{cj} + \Gamma_{cj}A^T = -B_j B_j^T$$

where $[t_1, t_2]$ is set to $[0, \infty]$.

From Lemma 1 follows that a basis for $\mathcal{X}_{cj}$ can be found via the eigenvector/eigenvalue decomposition of the controllability gramian Γ_{cj}, where the eigenvectors are denoted a_j. Only the eigenvectors associated with the non-zero eigenvalues are considered and they are sorted according to the size of the eigenvalues.

$$\mathcal{X}_{cj} = \text{span}\,\{a_{jr} | r = 1 \ldots dim(\mathcal{X}_{cj})\}$$

According to (5), the controllability gramians of two state space realization are connected via the transform matrix T as

$$\Gamma'_{cj} = T\Gamma_{cj}T^T$$

where Γ'_{cj} is the controllability gramian of the transformed system.

3.2 Observable subspace of $\mathcal{X}$

The characterization of the observable subspace can be done in a similar manner as for the controllable subspace. Thus, some steps in the derivation are superficial for the presentation.

When a state vector $x(t)$ is observable, then it can be reconstructed from the output vector $y(t)$, which is governed by both (6b) and (6a). The output impulse response matrix to an initial condition $x_i(t_1) = 1$ with $u(t) = 0$ can be found as

$$Y(t) = [Y_1(t)\ Y_2(t)\ \ldots\ Y_n(t)] \tag{13}$$

where $Y_i(t) = C_i e^{At}$. Clearly, the Laplace transform of $Y(t)$ is given by $Y(s) = C(sI - A)^{-1}$.

In the case of observability, it is inquired what state function gives rise to the measured output, which is the dual problem to controllability. Therefore, the row space of $Y(t)$ or $Y(s)$ has to be analyzed. Again according to [15], the observable subspace $\mathcal{X}_o$ is the subspace of least dimension containing the row space of the output impulse response matrix $Y(t)$. The observable subspace that is associated with an individual output is denoted $\mathcal{X}_{oi}$.

Analogously, the observability gramians are given by

$$\begin{aligned}
\Gamma_o &= \int_{t_1}^{t_2} e^{A^T t} C^T C e^{At} dt \\
&= \frac{1}{2\pi j} \int_{-j\infty}^{j\infty} (\bar{s}I - A^T)^{-1} C^T C (sI - A)^{-1} ds \\
\Gamma_{oi} &= \int_{t_1}^{t_2} e^{A^T t} C_i^T C_i e^{At} dt \\
&= \frac{1}{2\pi j} \int_{-j\infty}^{j\infty} (\bar{s}I - A^T)^{-1} C_i^T C_i (sI - A)^{-1} ds
\end{aligned}$$

Applying the eigenvector/eigenvalue decomposition the eigenvectors b_i of Γ_{oi} are found and a basis for $\mathcal{X}_{oi}$ is constituted by the b_i associated with the r non-zero eigenvalues. One can write

$$\mathcal{X}_{oi} = \text{span}\,\{b_{ir} | r = 1 \ldots dim(\mathcal{X}_{oi})\}$$

Again, the observability gramian is changed with the application of the similarity transform and Γ'_{oi} of the transformed system is given as

$$\Gamma'_{oi} = T^{-T} \Gamma_{oi} T^{-1}$$

3.3 Controllable and observable subspace $\mathcal{X}_{co}$

The controllable and observable subspace is the intersection of the observable subspace and the controllable subspace, namely $\mathcal{X}_{co} = \mathcal{X}_c \cap \mathcal{X}_o$.

As already known from the minimal realization theory [13] the subspace $\mathcal{X}_{co}$ is associated with a realization of (6) that has the same input-output behavior with least order. Using *e.g.* the Kalman canonical decomposition [22] a realization with $\mathcal{X}_{co}$ as state space can be extracted.

The subspace $\mathcal{X}_{coij}$ is then related to a minimal realization of the scalar subsystem between input j and output i. A characterization of the subspace can be obtained from the associated controllable and observable subspaces.

The subspaces $\mathcal{X}_{cj}$ and $\mathcal{X}_{oi}$ are spanned by $\{a_{j1}, \ldots, a_{jq}\}$ and $\{b_{i1}, \ldots, b_{ir}\}$, respectively. Vectors that lie in the intersection of the two vector spaces can be parameterized in both bases simultaneously.

$$x(t_p) = \sum_{\alpha=1}^{q} a_{j\alpha} \lambda_\alpha = \sum_{\beta=1}^{r} a_{j\beta} \mu_\beta, \quad t_1 \leq t_p \leq t_2$$

The condition can be rewritten to

$$\underbrace{\begin{bmatrix} a_{j1} & \dots & a_{jq} & b_{i1} & \dots & b_{ir} \end{bmatrix}}_{\Upsilon} \begin{bmatrix} \lambda \\ -\mu \end{bmatrix} = 0 \tag{14}$$

According to [17], a basis for the intersection can be found by deriving a set of linearly independent vectors that lie in the null space of Υ. Thus, (14) needs to have non-trivial solutions.

If $\mathcal{X}_{coij} \neq 0$ then the output i is affected by the input j. Furthermore, if there is an input r with $r \neq j$ for which $\mathcal{X}_{coir} \neq 0$, then there are two channels that affect each other in the multivariable system and thus, interaction is present. Consequently, the intersection of controllable and observable subspaces contain information on interaction.

4 Gramians and the Hankel operator

Generally, the input/output behavior of a linear causal system without direct term can be described by a Hankel operator. It is defined by

$$\begin{aligned} \Psi_g &: \mathcal{L}_2(-\infty, 0] \mapsto \mathcal{L}_2[0, \infty) \\ \Psi_g u(t) &= \begin{cases} \int_{-\infty}^{0} C e^{A(t-\tau)} B u(\tau) d\tau & t \geq 0 \\ 0 & t < 0 \end{cases} \end{aligned} \tag{15}$$

Applying the bilateral Laplace transform to (15) a frequency domain representation of the Hankel operator can be derived. The Hankel operator then becomes a strictly proper transfer function matrix.

When a general transfer function matrix G is given, the non-causal and direct part of the transfer function matrix need to be removed. Introducing the orthogonal projection $P : \mathcal{L}_2(-\infty, \infty] \mapsto \mathcal{L}_2[0, \infty)$ and applying it to G the Hankel operator can be stated as

$$\begin{aligned} \Psi_G &: \mathcal{H}_2^{\perp} \mapsto \mathcal{H}_2 \\ \Psi_G U &= P(GU), \text{ with } U \in \mathcal{H}_2^{\perp} \end{aligned}$$

There, the spaces $\mathcal{H}_2^{\perp}$ and $\mathcal{H}_2$ are the counterparts of $\mathcal{L}_2(-\infty, 0]$ and $\mathcal{L}_2[0, \infty)$ in the frequency domain, respectively.

Furthermore, the adjoint of the Hankel operator can be defined as

$$\begin{aligned} \Psi_g^* &: \mathcal{L}_2[0, \infty) \mapsto \mathcal{L}_2(-\infty, 0] \\ \Psi_g^* y(t) &= \begin{cases} \int_{0}^{\infty} B^T e^{A^T(t-\tau)} C^T y(\tau) d\tau & \tau \leq 0 \\ 0 & \tau > 0 \end{cases} \end{aligned} \tag{16}$$

Singular values and Schmidt pairs of the Hankel operator can now be derived from $\Psi_g^*\Psi_g$. The Schmidt pairs are a generalization of eigenvectors and $\Psi_g^*\Psi_g$ can be interpreted as a generalization of a gramian. Thus, two operators can be defined in terms of the Hankel operator and its adjoint

$$\begin{aligned} \Gamma_\Psi &: \mathcal{L}_2(-\infty,0] \mapsto \mathcal{L}_2(-\infty,0] \\ \Gamma_\Psi u &= \Psi_g^*\Psi_g u \qquad (17a) \\ \Gamma_\Psi^* &: \mathcal{L}_2[0,\infty) \mapsto \mathcal{L}_2[0,\infty) \\ \Gamma_\Psi^* u &= \Psi_g\Psi_g^* u \qquad (17b) \end{aligned}$$

When (17a) or (17b) are applied on a Dirac delta impulse function and the resulting functions are evaluated at 0, the following gramians can be obtained.

$$\begin{aligned} \Gamma_{in} &= \int_0^\infty B^T e^{A^T t} C^T C e^{At} B dt \\ &= B^T \Gamma_o B \\ \Gamma_{out} &= \int_0^\infty C e^{At} B B^T e^{A^T t} C^T dt \\ &= C \Gamma_c C^T \end{aligned}$$

These gramians can be used to derive bases for the range or row space of the impulse response function $g(t)$. Descriptions for the frequency domain can be obtained as well, but are omitted here.

In contrary to the controllability and observability gramians, Γ_{in} and Γ_{out} do not depend on the choice of the state vector and are directly related to the $\mathcal{H}_2$-norm via the relationship

$$||G(s)||_2 = \sqrt{tr(B^T \Gamma_o B)} = \sqrt{tr(C \Gamma_c C^T)}$$

When scalar subsystem are analyzed, the gramians Γ_{out} and Γ_{in} reduce to scalars. Naturally, if $\Gamma_{out,ij} = C_i \Gamma_{cj} C_i^T$ is different from zero, then the output i is affected by the input j. Thence, interaction can be expected if there is at least another input r with $\Gamma_{out,ir} \neq 0$. Similar statements can be given for Γ_{in}. Of course, for the subsystems one can derive subspaces of $\mathcal{Y}$, but these subspaces are all either one dimensional or the null space. Thus, sufficient information is already provided by the gramians.

5 Quantification of interaction

Clearly, gramians are a useful tool to derive geometrical and quantitative information on multivariable system. From gramians subspaces can be parameterized and whilst

they are closely connected to system norms. Thus, a quantification should be derived from the gramians.

Interaction measures are usually purpose dependent tools, which makes them hard to compare. Measures that are suited for decentralized control structure design, usually do not need to be effective tools for partial multivariable control structure design or for prediction of interaction in the closed loop. Thus, the quantification discussed here, is aimed for decentralized control structure design.

When a decentralized controller is designed, the choice of the measurement/actuator pair is a crucial task. The achievable performance of the closed loop system usually depends on this choice. For this end, it is necessary to identify the combinations where the actuator has significant impact on the measured output.

In [20] and [5] the proposed gramian based measures are applied on the scalar subsystems of a multivariable process. Thereby, every measurement/actuator combination is tested for its viability to control the measured output. The advantage of gramian based measures is their ability to judge the overall dynamics of a combination of frequencies and not only in a very narrow frequency band, *e.g.* at steady state.

Two well-known system norms that can be directly derived from the gramians are the Hankel-norm and the $\mathcal{H}_2$-norm

$$\begin{aligned} ||G(s)||_H &= \sqrt{\rho(\Gamma_c\Gamma_o)} \\ ||G(s)||_2 &= \sqrt{tr(B^T\Gamma_o B)} = \sqrt{tr(C\Gamma_c C^T)} \end{aligned}$$

Although the Hankel norm is derived from the gramian product, which does depend on the state vector choice, the eigenvalues of the product do not depend on the chosen state space realisation. Moreover, it relates to the $\mathcal{X}_{co}$ subspaces of the state space, and thus is suited as a quantification.

Using the gramian product the $\mathcal{H}_\infty$-norm can be bounded according to [22] in the form

$$||G(s)||_H \leq ||G(s)||_\infty \leq 2\sum_i \sqrt{\sigma_i(\Gamma_c\Gamma_o)} \triangleq \overline{||G(s)||}_\infty$$

where $\sigma_i(\Gamma_c\Gamma_o)$ denotes the eigenvalues of the product.

In [20] the normalized Hankel Interaction Index Array (HIIA) was suggested to solve the measurement/actuator pairing problem for decentralized control

$$[\Sigma_H]_{ij} = \frac{||G_{ij}(s)||_H}{\sum_{q,r}||G_{qr}(s)||_H} \tag{18}$$

Using the above results, the HIIA can be generalized to the use of different gramian

based norms, namely

$$[\Sigma_2]_{ij} = \frac{||G_{ij}(s)||_2}{\sum_{q,r} ||G_{qr}(s)||_2} \tag{19}$$

$$[\Sigma_\infty]_{ij} = \frac{\overline{||G_{ij}(s)||}_\infty}{\sum_{q,r} \overline{||G_{qr}(s)||}_\infty} \tag{20}$$

The generalized measures have the same properties as the original HIIA. Still, the interaction measures need to be validated, in order to see the effect of different norms on the measurement/actuator pairing.

As the matrix D is not considered in the computation of gramians, any gramian based measure has the drawback of ignoring a direct term. In other words, plants with $G(\infty) \neq 0$ have an HIIA which does not reflect that part of the dynamics. In cases, where the interaction is purely caused by the direct term and not by the causal part of the dynamics, the indications derived from the HIIA might be wrong.

The problem can be solved for the $\mathcal{H}_2$-norm based HIIA by considering the direct term in the computation of the system norm. The needed modification is rather easy implemented in (19)

$$[\Sigma_{\tilde{2}}]_{ij} = \frac{||G_{ij}(s)||_2 + ||G_{ij}(\infty)||_2}{\sum_{r,q} ||G_{rq}(s)||_2 + ||G_{rq}(\infty)||_2} \tag{21}$$

where the norm on the direct term is simply the 2-norm for matrices.

The new measures can now be used to find appropriate measurement/actuator pairs, according to the methodology described in [20].

5.1 Weighted gramians and filtering

Not in all application it is desired to judge the overall dynamics but instead focus on certain frequency regions. Especially, if the multivariable system has largely varying dynamics for different frequency bands.

In [19] it has also been pointed out that interaction measures should considered frequency regions where control is active. Hence, filtering should be applied and there are two different kinds of approach. Firstly, the filter dynamics can be augmented to the system dynamics, either at the input or the output side of the multivariable system. This approach is utilized in [20]. Secondly, a weighting function that corresponds to the filter dynamics can be introduced in the computation of the gramians, which is discussed here.

Assuming a scalar causal filter with the transfer function $F(s)$ is used and a minimal realization of the filter is given as

$$F(s) = C_f(sI - A_f)^{-1}B_f + D_f$$

The filtered state impulse response function can then be expressed by

$$X^f(s) = X(s)F(s) = (sI - A)^{-1}B\left(C_f(sI - A_f)^{-1}B_f + D_f\right)$$

and the resulting controllability gramian is obtained as

$$\begin{aligned}\Gamma_c^f &= \frac{1}{2\pi j}\int_{-j\infty}^{j\infty} X(s)F(s)\bar{F}(s)X^H(s)ds \\ &= \frac{1}{2\pi j}\int_{-j\infty}^{j\infty} X(s)X^H(s)|F(s)|^2 ds \end{aligned} \tag{22}$$

where $X^H(s)$ denotes the complex conjugate transpose of $X(s)$. Clearly, the gramian of the filtered system can be directly obtained by introducing a weight into the controllability gramian. Thus, the weight provides an extra degree of freedom into the criteria.

The filtered controllability gramian can be evaluated as the upper left submatrix of the Lyapunov equation [18]

$$\begin{bmatrix} A & BC_f \\ 0 & A_f \end{bmatrix}\begin{bmatrix} \Gamma_c^f & \Gamma_{12} \\ \Gamma_{21} & \Gamma_{21} \end{bmatrix} + \begin{bmatrix} \Gamma_c^f & \Gamma_{12} \\ \Gamma_{21} & \Gamma_{21} \end{bmatrix}\begin{bmatrix} A & BC_f \\ 0 & A_f \end{bmatrix}^T = -\begin{bmatrix} BD_f \\ B_f \end{bmatrix}\begin{bmatrix} BD_f \\ B_f \end{bmatrix}^T \tag{23}$$

Resolving all matrix multiplications, (23) can be rewritten into four dependent matrix equations

$$A\Gamma_c^f + \Gamma_c^f A^T = -\left(BC_f\Gamma_{21} + \Gamma_{21}(BC_f)^T\right) \tag{24a}$$

$$A\Gamma_{12} + \Gamma_{12}A_f^T = -BC_f\Gamma_{22} \tag{24b}$$

$$A_f\Gamma_{21} + \Gamma_{21}A^T = -\Gamma_{22}(BC_f)^T \tag{24c}$$

$$A_f\Gamma_{22} + \Gamma_{22}A_f^T = -B_fB_f^T \tag{24d}$$

As $\Gamma_{12} = \Gamma_{21}^T$, (24b) and (24c) are equivalent. Consequently, three equations have to be solve in order to obtain a solution for Γ_c^f via (24).

Obviously, (24a) and (24d) are Lyapunov equations, while (24b) is a Sylvester equation. In order that the equations have a unique solution, the matrix A_f of the chosen weighting function needs to fulfill certain requirements.

First, $\lambda_i(A)$ and $\mu_i(A_f)$ denote the eigenvalues of A and A_f, respectively. Then according to [10], the Lyapunov equations have a unique solution if and only if $\lambda_i(A) + \lambda_j(A) \neq 0, \forall i, j$ and $\mu_i(A_f) + \mu_j(A_f) \neq 0, \forall i, j$. A unique solution for the Sylvester equation is obtained if and only if $\lambda_i(A) + \mu_j(A_f) \neq 0, \forall i, j$. This implies, that for a stable multivariable system any stable weighting function yields a unique solution for the equations and thus for the gramians.

Clearly, the size of Γ_c is maintained for Γ_c^f and thus, only the criteria is changed and not the multivariable system. For the weighted observability gramian Γ_o^f similar equations can be stated.

In the time domain, filtering with $F(s)$ connotes convolution with the impulse response function $f(t)$. Since gramians are directly connected with the inner product defined in the function space, the introduction of the weight $f(t)$ leads to the weighted inner product.

$$\langle \phi(t), \xi(t) \rangle_f = \int_{t_1}^{t_2} \int_{t_1}^{t_2} \int_{t_1}^{t_2} f(t-\mu)\phi(\mu)\xi^T(\nu)f(t-\nu)d\mu d\nu dt \tag{25}$$

where $\phi(t)$ and $\xi(t)$ are vectors in weighted $\mathcal{L}_2^n[t1, t2]$. It can be seen that the standard scalar product is obtained if the impulse response function of the filter is a Dirac delta impulse $f(t) = \delta(t)$.

Due to the convergence requirement of the integrals, the weighting function should be chosen so that the cascaded system, scalar filter and multivariable system, are strictly proper. Thus, the scalar filter can be used to bound the integrals, which enables the application of the criteria on multivariable systems that are not strictly proper.

The use of weighted gramians as underlying structure for gramian based norms leads to different results than augmenting the multivariable system with additional filter dynamics. Thus a direct comparison of the two concepts is not possible, see Example 2. Additionally, through the weighting functions model uncertainties can be considered in the interaction measures, see Example 1. A drawback of the weighted gramians approach is the restriction to scalar filter functions.

6 Examples

The aim of the examples is to illustrate the usage of the gramian-based measures on a real-life process and on a discrete time example. The gramian based measures are used to find appropriate measurement/actuator pairs for decentralized control.

First, the linearized physical model of a coal injection vessel, which is an example for a continuous time 2×2 servo system, is studied. Secondly, the 3×3 system from [20] is revisited and the generalized versions of the HIIA are applied.

The examples are examined in the following way. First, the dynamic RGA for the process is analyzed and the pairs whose elements have the closest value to 1 are chosen. Then, the gramian based measures are computed with no filtering according to (18), (20) and (21). Pairs that yield the largest sum are chosen and compared with the RGA based choice. Since in both examples filtering is needed, appropriate filters are chosen and the gramian based measures are computed via weighted gramians (23). Finally, the performance of the measures is evaluated according to the correctness of the indications.

Example 1 (Coal injection vessel). The coal injection vessel is a pressurized multivariable tank system which is discussed in [12], [1] and [2]. There, models for the

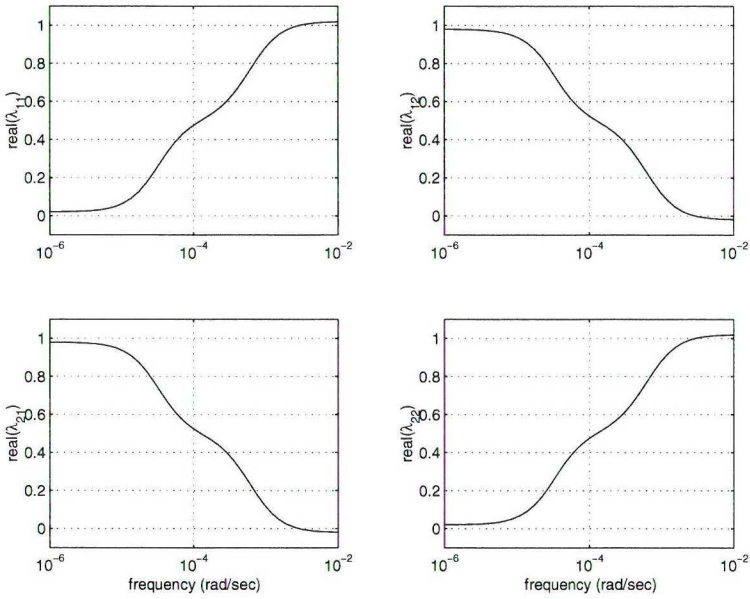

Fig. 1: Real part of the RGA for the coal injection vessel over frequency.

process are derived and successfully used for the design and analysis of multivariable controllers and a gas-leakage detection system.

A linear physical model for the coal injection vessel is given by

$$\dot{x}(t) = 10^{-3}\begin{bmatrix} -0.3234 & 0.3604 \\ 0.2128 & 0.2963 \end{bmatrix} x(t) + \begin{bmatrix} -0.4878 & 0.6816 \\ 0.5721 & -0.3043 \end{bmatrix} u(t) \quad (26a)$$

$$y(t) = \begin{bmatrix} -0.8379 & 0.6477 \\ -0.0237 & -0.0198 \end{bmatrix} x(t) \quad (26b)$$

where the input $u(t)$ is the opening of the pressure control and flow control valve in respective row. The output $y(t)$ consists of the pressure in the vessel and the net weight, again, in respective row.

Fig. 1 shows a plot for the real parts of the RGA elements over frequency. Clearly, the measurement/actuator pairing changes from anti-diagonal to diagonal from low to high frequencies. Drawing conclusions on the pairing from the static RGA, the anti-diagonal pairing should be favored, which means the pressure is stabilized with the flow control valve and the weight is controlled with the pressure control valve. According to knowledge of the process, this is an unconventional choice.

Computation of the gramian based interaction measures Σ_H, Σ_2, Σ_∞ yields the

following arrays

$$\Sigma_H = \begin{bmatrix} 0.3740 & 0.5297 \\ 0.0500 & 0.0463 \end{bmatrix}$$
$$\Sigma_2 = \begin{bmatrix} 0.4676 & 0.5043 \\ 0.0133 & 0.0148 \end{bmatrix}$$
$$\Sigma_\infty = \begin{bmatrix} 0.4680 & 0.4676 \\ 0.0335 & 0.0309 \end{bmatrix}$$

First of all, the gramian based measures do not differ much, although different norms were used. When a pairing decision should be taken according to Σ_H and Σ_2 the anti-diagonal pairing is favored again, while a distinction based on Σ_∞ cannot be made. Thus, more knowledge of the process is needed to make a clear decision.

Due to the character and operation of the coal injection process and model uncertainties, the linear model is not reflecting the plant dynamics in frequency ranges below 10^{-4} rad/sec. Therefore, high pass filtering should be applied.

In order to avoid non-strictly proper weighting functions, the following band pass filter is chosen instead.

$$F(s) = \frac{s^2}{s^4 + 2.02s^3 + 1.04s^2 + 0.0202s + 0.0001}$$

The filter has the break frequencies 0.01 rad/sec and 1 rad/sec. Using the filter as weight in the gramians, the HIIA are recomputed

$$\Sigma_H = \begin{bmatrix} 0.5001 & 0.4931 \\ 0.0003 & 0.0065 \end{bmatrix}$$
$$\Sigma_2 = \begin{bmatrix} 0.5002 & 0.4931 \\ 0.0002 & 0.0065 \end{bmatrix}$$
$$\Sigma_\infty = \begin{bmatrix} 0.5001 & 0.4930 \\ 0.0004 & 0.0065 \end{bmatrix}$$

Obviously, the gramian based measures have changed and now $\Sigma_H \approx \Sigma_2 \approx \Sigma_\infty$. In all three cases the diagonal pairing should be chosen for decentralized control. According to knowledge on the process the diagonal pairing should be favored and has been successfully used for decentralized control of the process. □

Example 2 (Discrete time 3×3 system). The multivariable system is given in the transfer matrix representation

$$G(z) = \begin{bmatrix} \frac{-0.7987z+0.7673}{z^2-1.575z+0.6065} & \frac{0.04758}{z-0.9048} & \frac{-0.09516}{z-0.9048} \\ \frac{0.1813}{z-0.8187} & \frac{1.517z-1.457}{z^2-1.489z+0.5488} & \frac{0.09063}{z-0.8187} \\ \frac{-0.1814}{z-0.7408} & \frac{0.2592}{z-0.7408} & \frac{2.163z-2.077}{z^2-1.411z+0.4966} \end{bmatrix} \quad (27)$$

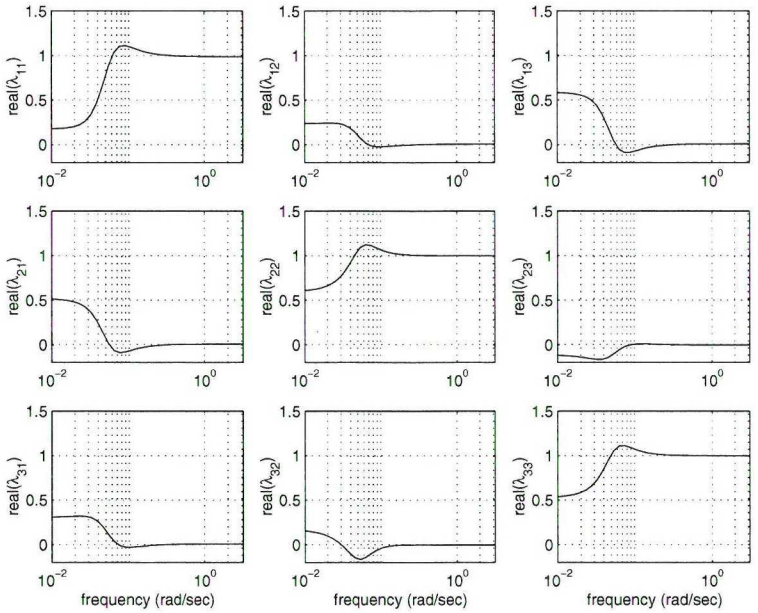

Fig. 2: Real part of the RGA for the 3×3 example over frequency.

From Fig. 2 it is clear that for low frequencies the anti-diagonal pairing should be favored, but the diagonal pairing should be chosen for higher frequencies. In [20] it is shown that the anti-diagonal pairing decision leads to unstable controllers and has to be avoided.

Again, the gramian based measures can be computed and yield

$$\Sigma_H = \begin{bmatrix} 0.1428 & 0.0295 & 0.0589 \\ 0.0617 & 0.2437 & 0.0309 \\ 0.0451 & 0.0645 & 0.3229 \end{bmatrix}$$

$$\Sigma_2 = \begin{bmatrix} 0.1488 & 0.0165 & 0.0329 \\ 0.0465 & 0.2675 & 0.0233 \\ 0.0398 & 0.0569 & 0.3678 \end{bmatrix}$$

$$\Sigma_\infty = \begin{bmatrix} 0.1468 & 0.0214 & 0.0428 \\ 0.0449 & 0.2733 & 0.0224 \\ 0.0328 & 0.0469 & 0.3687 \end{bmatrix}$$

It is rather obvious, that the diagonal pairing yields the highest values and thus, is the correct choice. When it is necessary to focus on the low frequency region, the low pass filter $F(z) = \frac{0.01}{z-0.99}$ is applied. Here, the gramian based measures are re-computed firstly, with the weighted gramians and secondly, with additional filter

dynamics augmented to $G(z)$.

Weighted gramians:

$$\Sigma_H = \begin{bmatrix} 0.1488 & 0.0654 & 0.1309 \\ 0.0721 & 0.2182 & 0.0360 \\ 0.0358 & 0.0512 & 0.2416 \end{bmatrix}$$

$$\Sigma_2 = \begin{bmatrix} 0.1372 & 0.0564 & 0.1128 \\ 0.1155 & 0.1557 & 0.0577 \\ 0.0815 & 0.1164 & 0.1668 \end{bmatrix}$$

$$\Sigma_\infty = \begin{bmatrix} 0.1540 & 0.0640 & 0.1279 \\ 0.0704 & 0.2206 & 0.0352 \\ 0.0350 & 0.0501 & 0.2428 \end{bmatrix}$$

$G(z)$ augmented with filter dynamics:

$$\Sigma_H = \begin{bmatrix} 0.1223 & 0.0705 & 0.1409 \\ 0.1368 & 0.1170 & 0.0684 \\ 0.0945 & 0.1351 & 0.1146 \end{bmatrix}$$

$$\Sigma_2 = \begin{bmatrix} 0.1372 & 0.0564 & 0.1128 \\ 0.1155 & 0.1557 & 0.0577 \\ 0.0815 & 0.1164 & 0.1668 \end{bmatrix}$$

$$\Sigma_\infty = \begin{bmatrix} 0.1268 & 0.0675 & 0.1351 \\ 0.1277 & 0.1322 & 0.0638 \\ 0.0873 & 0.1247 & 0.1349 \end{bmatrix}$$

In case of the weighted gramians the diagonal pairs should be chosen, although the distinction is not that clear anymore. It can also be observed, that the HIIA for the augmented system differ much and, as already stated in [20], a distinction from Σ_H can not be made. Clearly, Σ_∞ does not improve the situation.

In contrary, Σ_2 still indicates a diagonal pairing. An evaluation of the sum of the elements for the different pairings shows, that the diagonal pairing accounts for 0.4597, while the anti-diagonal yields a value of 0.3558. □

From the examples it can be seen, that the generalized gramian measures can be used to improve the decision process for measurement/actuator pairing. Still knowledge of the process and model uncertainties is needed to make the correct choice for weighting functions.

7 Conclusions

The theoretical background for the gramian based interaction measures is discussed. It is shown that the gramian based approach to interaction is closely related to inter-

sections of subspaces of function spaces. The relation between the Hankel operator and the gramian based measures is clarified and an extension to the use of different norms is given.

Moreover, it can be suggested that filtering of model dynamics should be introduced in the tool by the use of weighting functions. Thereby, the model dynamics are not augmented with additional dynamics and model uncertainty can be considered.

The measures are then applied to two examples, where the gained improvements via the use of different norms is rather small, which stresses the Hankel norm as a good choice. Furthermore, the use of the weighted gramians in the underlying computation has shown to yield correct results.

Although the measures give a solution for the pairing problem in decentralized control the controller is not yet considered in the measures, which could lead to further improvements and understanding of interaction in multivariable systems. It should therefore be investigated how gramians in closed loop system relate to those in the open loop case. Then, it should be possible to integrate interaction measures directly into the controller design process.

References

[1] Wolfgang Birk and Alexander Medvedev. Pressure and flow control of a pulverized coal injection vessel. *IEEE Transactions on Control Systems Technology*, 8(6):919–929, November 2000.

[2] Wolfgang Birk and Alexander Medvedev. Sensitivity analysis of an LQ optimal multivariable controller for a fine coal injection vessel. *IEEE Transactions on Industry Applications*, 36(3):871–876, May/June 2000.

[3] E.H. Bristol. On a new measure of interaction for multivariable process control. *IEEE Transactions on Automatic Control*, 11:133–134, January 1966.

[4] Roger W. Brockett. *Finite Dimensional Linear Systems.* John Wiley and Sons, Inc, 1970.

[5] Arthur Conley and Mario E. Salgado. Gramian based interaction measure. In *Proc. of the 2000 Conference on Decision and Control, Sydney*, 2000.

[6] C. Nelson Dorny. *A Vector Space Approach to Models and Optimization.* Robert E. Krieger Publishing Company, Malabar, Florida, reprint with corrections edition, 1986.

[7] K. Glover. All optimal hankel-norm approximations of linear multivariable system and their $\mathcal{L}_\infty$-error bounds. *International Journal of Control*, 39:1115–1193, 1984.

[8] Pierre Grosdidier and Manfred Morari. The μ interaction measure. *Ind. Eng. Chem Res.*, 26:1193–1202, 1987.

[9] Kurt E. Häggblom. Control structure analysis by partial relative gains. In *Proc. of the 36th Conference on Decision & Control, San Diego, USA*, pages 2623–2624, December 1997.

[10] Roger A. Horn and Charles R. Johnson. *Topics in Matrix Analysis.* Cambridge University Press, 1991.

[11] M. Hovd and S. Skogestad. Simple frequency-dependent tools for control systems analysis, structure selection and design. *Automatica*, 28(5):989–996, 1992.

[12] Andreas Johansson and Alexander Medvedev. Model based leakage detection in a pulverized coal injection vessel. *IEEE Transactions on Control Systems Technology*, 7(6):675–682, November 1999.

[13] T. Kailath. *Linear Systems.* Prentice Hall, Inc., 1980.

[14] Vasilios Manousiouthakis, Robert Savage, and Yaman Arkun. Synthesis of decentralized process control structures using the concept of block relative gain. *AIChE Journal*, 32(6):991–1003, 1986.

[15] Bruce C. Moore. Principle component analysis in linear systems: Controllability, observability, and model reduction. *IEEE Transactions on Automatic Control*, 26(1):17–31, February 1981.

[16] J.E. Rijnsdorp. Interaction on two-variable control systems for distillation columns. *Automatica*, 1(1):15–28, 1965.

[17] Gilbert Strang. *Linear Algebra and its Applications.* Harcourt, Inc., third edition, 1988.

[18] Lothar Thiele. On the sensitivity of linear state-space system. *IEEE Transactions on Circuits and Systems*, 33(5):502–510, May 1986.

[19] M.F. Witcher and T.J. McAvoy. Interacting control systems: Steady-state and dynamic measurement of interaction. *ISA Transactions*, 16(3):35–41, 1977.

[20] Björn Wittenmark and Mario E. Salgado. Hankel-norm based interaction measure for input-output pairing. In *Proc. of the 2002 IFAC World Congress, Barcelona*, 2002.

[21] Nicholas Young. *An Introduction to Hilbert Space.* Cambridge University Press, 1988.

[22] Kemin Zhou. *Robust and Optimal Control.* Prentice Hall, 1996.

Paper 5

Improving Control Structures in Multivariable Control Systems

Submitted

Improving Control Structures in Multivariable Control Systems

Wolfgang Birk*† and Alexander Medvedev†§

*Corresponding author: eMail: wolfgang@sm.luth.se
§ Information Technology, Uppsala University, Box 337, SE-751 05, Uppsala, Sweden
†Control Engineering Group, Luleå University of Technology, SE-971 87 Luleå, Sweden

Abstract

This paper deals with interaction in multivariable control systems and the improvement of control structures from a closed loop perspective. A dynamic quantification of interaction in a closed loop system is derived and validated through an example. Then, the structural mismatch of a decentralized control scheme is quantified in terms of transfer function matrices. Norms of these matrices are used to derive indications for possible control structure improvements. It shown that indications can be derived from process data by means of system identification. Finally, the method is applied to the control of a coal injection vessel, where the interaction measure is used as a validation criterion.

1 Introduction

Traditionally, the control structures for large scale industrial plants are dictated by the plant vendors. During the life cycle of an industrial plant, physical changes are incorporated in order to fulfill new standards and improve plant performance, i.e. rectified energy conservation.

Usually, the control system is left unchanged, even though structural changes in the plant might alter dynamic couplings in process variables. Such changes can lead to deteriorated plant performance which can not be compensated for by re-tuning of the existing control scheme. Only structural changes in the control system can restore plant performance or might even improve it.

Assessment of interaction present in a control system from an open-loop perspective has been dealt with for a long time. Both steady state and dynamic measures for interaction have been suggested. The first proposed interaction measures were the *Rijnsdorp interaction measure* [22] and the *relative gain array* (RGA) [4]. These measures are derived from steady-state gain information and are related to each other via a non-linear map [10]. Ever since, the RGA is widely used in industrial applications and has been extended to a dynamic measure [12]. Further development of the RGA became necessary due to the introduction of more advanced control structures. This led *e.g.* to the introduction of the block relative gains (BRG) [19] and partial relative gains (PRG) [11]. Thereby, it became possible to get indications for interactions in multivariable control systems with control structures different from decentralized

control. Newly developed measures are a measure based on Hankel singular values [6] and the *Hankel interaction index array* [26], which makes use of the Hankel norm of the scalar sub-systems. Both measures analyze sub-systems of the multivariable plant in order to get insight into the structure and thus draw a-priori conclusions on interaction in the closed loop system.

A drawback of the above interaction measures is that stability of the closed loop system is not guaranteed. On the contrary, the *Niederlinski index* [21] gives a steady state stability condition for decentralized controllers. Later the *μ-interaction measure* [10] was introduced as a tool providing information on closed loop stability and performance loss due to control structure selection. Another stability condition for decentralized controllers that considers RGA and Niederlinski index is discussed in [5].

A common result is that the control structure selection has a large effect on the closed loop behavior of multivariable control system. Thus, suitable tools are needed to select the appropriate control structure. Since the decentralized control structure is widely spread and often preferred by plant operators due to its simplicity in design and maintenance, many tools were created to solve the variable pairing problem. Criterions that rely on the RGA and the Niederlinski index are presented in [29, 23]. A Variable pairing criterion that is based on Rijnsdorps interaction measure is discussed in [28]. There, the relative interaction array (RIA) is introduced. In [14] an algorithmic implementation of a pairing criterion using RGA and RIA is presented. A method that combines the ideas behind the RIA and the μ interaction method is derived in [8], where an attempt is made to introduce dynamic interaction and controller structure in the μ synthesis framework. And finally, the Hankel interaction index array can also be effectively used to solve the pairing problem.

Apparently, the focus has been on decentralized control structures and only little has been suggested for more complex control structures. The μ interaction measure is used in [15] to derive methods to screen control structures for multivariable systems. There, tools that are dependent as well as independent of the design approach are suggested. Another tool that can consider complex control structure makes use of the Hankel singular values and derives so-called participation matrices [6].

Still, there is a common problem. A dynamic description of interaction that considers the controller is only available for a special case, *i.e.* two inputs and two outputs system with a decentralized controller [27]. Thus, a generalization to larger systems and different control structures is needed. Then, interaction properties of different control structures become comparable and can be used as a controller design criterion.

Moreover, all the given measures and methods rely on either empirical or physical dynamic models for the processes at hand. When these models are obtained from closed loop process data, they are often uncertain and make the above mentioned measures unreliable or hard to interpret. Therefore, the closed loop dynamics should be evaluated for its interaction properties. Then, controller and process are jointly

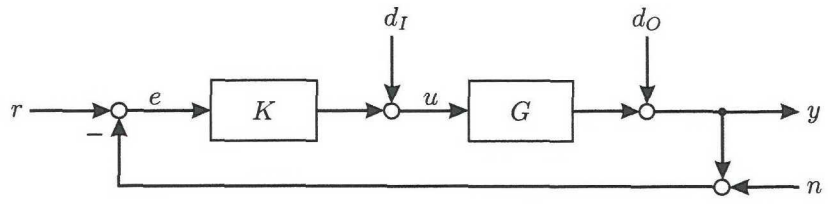

Fig. 1: General multivariable control system

considered and indications from the interaction properties for controller improvement can be derived.

The paper is arranged as follows. Firstly, some known results are summarized and the terminology important for the sequel is introduced in Section 2. Then a dynamic description of interaction is derived in Section 3 that quantifies the interaction in the closed loop system. The measure is validated through an example and then used as a validation criterion for control structure improvements in the case study. In Section 4 a method is proposed that evaluates interaction properties in terms of complementary sensitivity functions of the control system. The section is followed by a case study in Section 5, where the method is applied to a real-life example. Finally, some conclusions and an outlook are given.

2 Preliminaries

A multivariable control system with process $G(s)$ and controller $K(s)$ is depicted in Fig. 1, where $G(s)$ has n actuators and m measurement outputs. In the sequel, if not stated otherwise, square systems are considered, namely $n = m$.

Thus, $G(s)$ and $K(s)$ can be given in transfer function matrix notation:

$$G(s) = \begin{bmatrix} G_{11}(s) & \cdots & G_{1n}(s) \\ \vdots & \ddots & \vdots \\ G_{m1}(s) & \cdots & G_{mn}(s) \end{bmatrix}$$

$$K(s) = \begin{bmatrix} K_{11}(s) & \cdots & K_{1m}(s) \\ \vdots & \ddots & \vdots \\ K_{n1}(s) & \cdots & K_{nm}(s) \end{bmatrix}$$

For the sake of simplicity, the Laplace operator s will be dropped in the sequel. Furthermore, G_{ij} denotes the transfer function from input u_j to output y_i and similarly, K_{ji} denotes the transfer function from control error e_i to the actuator u_j. The index j and i refer to the corresponding elements in the vectors u, y and e.

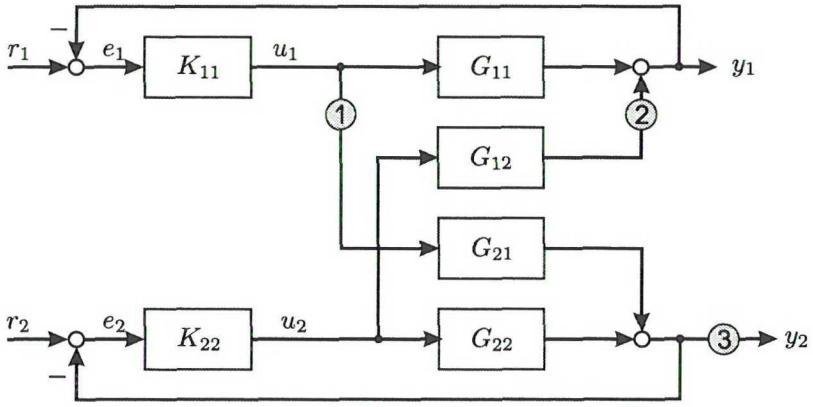

Fig. 2: Simplified multivariable control system for a 2×2 process under decentralized control

For the closed loop system the complementary sensitivity transfer matrix T and the sensitivity transfer matrix S are defined as

$$T = (I + GK)^{-1} GK \tag{1}$$

$$S = I - T = (I + GK)^{-1} \tag{2}$$

Both T and S are transfer matrices in the closed loop system depicted in Fig. 1 and reflect the relative sensitivity of the closed loop system to changes in G. The following relationships can be easily verified

$$y = Tr - Tn + SGd_I + Sd_O \tag{3}$$

$$e = Sr - Sn - SGd_I - Sd_O \tag{4}$$

$$u = KSr - KSn - KSGd_I - KSd_O \tag{5}$$

When the multivariable system is under decentralized control, *i.e.* the controller K is diagonal and the process G is square, the cause of interaction is the off-diagonal elements in the process G. Fig. 2 shows a simplified block diagram for a 2×2 process. Suppose, the controllers K_{11} and K_{22} are designed to achieve a certain behavior of y_1 and y_2, respectively, and the elements G_{12} and G_{21} are neglected during the design. Then the channels (e_1, y_1) and (e_2, y_2) are used to specify the performance of the control system and the design yields two sub-systems A and B.

Depending on the structure of G, the sub-systems are connected with each other and interaction of the sub-systems occurs. Then, two case have to be considered:

1. There is a path from A to B, see Fig. 3a.
   Then A acts as a disturbance on B, but not vice versa. Usually, B can be designed so that the effect of A is attenuated, see [20].

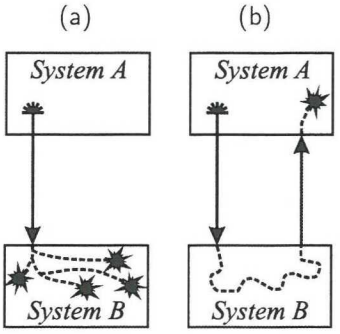

Fig. 3: Effects of interaction in multivariable systems

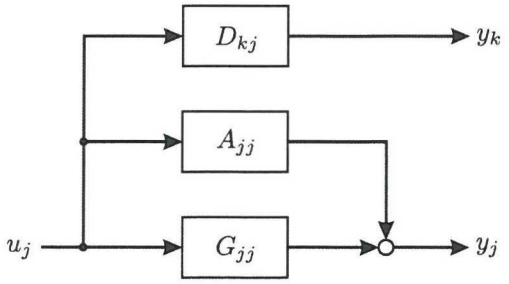

Fig. 4: Representation of interaction

2. There exists a loop from A via B back to A, see Fig. 3b.
   Then the dynamics of A are altered, which can have an effect on the stability of the closed loop system. This effect can first be studied after A and B are designed, which complicates controller synthesis.

The effects from paths and loops for the system in Fig. 2 can be described by transfer functions. The loop effect for channel (e_1, y_1) is described by the transfer function between the points $(1, 2)$ and the path effect for channel (e_2, y_2) is described by the transfer function between the points $(1, 3)$. This decomposition is suggested in [27], and yields a decomposed system for the multivariable control system, see Fig. 4. There, A_{jj} and D_{kj} denote the effects from loops and paths, respectively.

It can be verified that the process transfer function matrix has a triangular structure if there are no loops. Then the sequential loop closing method [18, 23] yields good design results for decentralized controller structures.

3 Quantification of interaction

In [27, 28] a dynamic description of interaction in a 2×2 multivariable control system is derived for a decentralized control structure. A generalization of this approach to arbitrarily sized systems and different control structures yields a design criterion for control structures and a quantification of the overall interaction.

3.1 Interaction transfer function matrix

Clearly, the transfer functions $A_\bullet$ and $D_\bullet$ describe the absolute interaction in a multivariable control system. For a decentralized control system these scalar transfer functions can be arranged as the following square transfer function matrix

$$\Upsilon = \begin{bmatrix} A_{11} & D_{12} & \cdots & D_{1n} \\ D_{21} & A_{22} & & D_{2n} \\ \vdots & & \ddots & \vdots \\ D_{n1} & D_{n2} & \cdots & A_{nn} \end{bmatrix}$$

As $A_\bullet$ and $D_\bullet$ are functions of G and K, Υ is also a function of G and K. It is then denoted $\Upsilon(G,K)$ in the sequel and called the interaction transfer function matrix (ITFM). Moreover, the ITFM depends on the choice of the channels and fully describes the interaction effects in a multivariable control system.

Using the decomposition in Fig. 4 the output y is given by

$$y = (\mathrm{diag}(G_{11}, \ldots, G_{nn}) + \Upsilon(G,K))\, u \tag{6}$$

According to [23], if the multivariable process is not properly scaled the interaction terms become hardly comparable with each other. Therefore, the relative interaction is derived by weighting the absolute interaction terms with the inverse of the corresponding process dynamics [28]

$$\Phi_{ij} = \begin{cases} \frac{A_{ij}}{G_{ii}} & i = j \\ \frac{D_{ij}}{G_{ii}} & \text{otherwise} \end{cases}$$

Accordingly, Φ is then the relative ITFM. Clearly, Υ or Φ are unique for a pair (G,K) and have to be computed anew if the controller K and/or process model G are changed. Subsequently, no conclusions on the ITFM can be drawn from the open-loop process model without setting requirements on the controller. This suggests an iterative procedure, where the ITFM is used as a design criterion.

3.2 ITFM for arbitrary system size

In the 2×2 case, the elements of Υ can be easily obtained using the block diagram Fig. 2. Already for a 3×3 system, the derivation from a block diagram becomes tedious. Thus, a general way of computation based on matrix manipulation is needed.

Introducing block transfer matrices, the transfer matrices G and K can be partitioned as follows

$$G = \left[\begin{array}{c|ccc} G_{11} & G_{12} & \cdots & G_{1n} \\ \hline G_{21} & G_{22} & \cdots & G_{2n} \\ \vdots & \vdots & \ddots & \vdots \\ G_{n1} & G_{n2} & \cdots & G_{nn} \end{array}\right] = \left[\begin{array}{c|c} G_{11} & G'_{12} \\ \hline G'_{21} & G'_{22} \end{array}\right]$$

$$K = \left[\begin{array}{c|ccc} K_{11} & 0 & \cdots & 0 \\ \hline 0 & K_{22} & \cdots & 0 \\ \vdots & \vdots & \ddots & \vdots \\ 0 & 0 & \cdots & K_{nn} \end{array}\right] = \left[\begin{array}{c|c} K_{11} & 0 \\ \hline 0 & K'_{22} \end{array}\right]$$

Thereby, one gets back to a 2×2 case, where some elements are transfer function matrices. Without loss of generality, the derivation is only pursued for the first column and row. The terms A_{11} and $D'_{21} = [D_{21} \ldots D_{n1}]^T$ can be derived using the block diagram Fig. 2 as

$$A_{11} = -G'_{12}K'_{22}(I + G'_{22}K'_{22})^{-1}G'_{21} \tag{7}$$

$$D'_{21} = (I + G'_{22}K'_{22})^{-1}G'_{21} \tag{8}$$

According to Fig. 4, the response y on the input u_1 can be reconstructed from

$$y = \left[\begin{array}{c} G_{11} + A_{11} \\ D'_{21} \end{array}\right] u_1 \tag{9}$$

Thus, the first column of $\Upsilon(G, K)$ is derived. Consequently, n iterations are required to completely obtain $\Upsilon(G, K)$. Instead of computing Υ columnwise, the rows of $\Upsilon(G, K)$ can be obtained by deriving $D'_{12} = [D_{12} \ldots D_{1n}]$ as follows

$$D'_{12} = (1 + G'_{11}K'_{11})^{-1}G'_{12} \tag{10}$$

Finally, Φ can be derived from Υ according to the definition.

Applying a system norm to Υ or Φ a measure for the amount of interaction in the multivariable control system determined by G and K is found. Since interaction is only of interest in frequency bands where the actuator has significant energy, *i.e.* singular values of G and K are larger than 1, the interaction measure should reflect that [25, 7].

One solution would be to introduce a filtered version of the interaction measures. Introducing the scalar bandpass filter F, the filtered ITFM are obtained as

$$\tilde{\Upsilon} = \Upsilon F \tag{11}$$
$$\tilde{\Phi} = \Phi F \tag{12}$$

A drawback of this approach is the augmenting of the ITFM with additional filter dynamics.

Another solution is to apply weighted system norms [3]. There weighted gramian based norms are suggested to introduce filtering as an additional parameter in the computation of system norms.

3.3 ITFM for multivariable controllers

Multivariable controllers are usually designed to exploit the multivariable nature of the process in order to improve performance of the closed loop system. Since the off-diagonal elements in the controller transfer function matrix are non-zero, the controller contributes to interaction in the closed loop system.

Therefore, in order to achieve a loop decomposition with multivariable controllers the loop transfer matrix $L = GK$ is considered instead. Consequently, in (7), (8) and (10) the process transfer matrix G is replaced by L and the controller transfer matrix is replaced by an identity matrix I, which yields

$$A_{11} = -L'_{12}(I + L'_{22})^{-1}L'_{21} \tag{13}$$
$$D'_{21} = (I + L'_{22})^{-1}L'_{21} \tag{14}$$
$$D'_{12} = (1 + L_{11})^{-1}L'_{12} \tag{15}$$

The construction of Υ and Φ from the A and D terms is not affected by this change, and hence the above methodology applies. The absolute or relative ITFM that is derived from process transfer matrix G and multivariable controller K is then a function of L and I, namely $\Upsilon(L, I)$ or $\Phi(L, I)$, respectively.

In many cases, the loop transfer matrix of a multivariable control system is square, even if the process transfer matrix is non-square. Hence, the ITFM can be derived even for non-square multivariable processes, which widens the application area.

Clearly, decentralized controllers are a special case of a multivariable controller and thus, can be evaluated in the same framework. Thereby, it is possible to compare

decentralized and multivariable control structures according to interaction properties of the closed loop system.

3.4 Example

The ITFM is now derived for a multivariable system with different types of controllers and compared with each other. It is shown that the intuitive expectations are confirmed by the analysis of Υ.

The example system and controllers are taken from [9]. Consider a two-input, two-output multivariable system with the transfer function matrix

$$G(s) = \begin{bmatrix} \frac{2}{s^2+3s+2} & \frac{-2}{s+1} \\ \frac{0.75}{s^2+2s+1} & \frac{6}{s^2+5s+6} \end{bmatrix} \tag{16}$$

A decentralized controller is designed with the input/output pairings: $(1,1)$ and $(2,2)$. The off-diagonal elements in $G(s)$ are ignored during the design and the controllers are designed so that the following complementary sensitivity transfer function for the pairing selections are achieved

$$T_{11}(s) = T_{22}(s) = \frac{9}{s^2 + 4s + 9} \tag{17}$$

The controller transfer matrix is then found as

$$K(s) = \frac{1}{s(s+4)} \begin{bmatrix} 4.5(s^2 + 3s + 2) & 0 \\ 0 & 1.5(s^2 + 5s + 6) \end{bmatrix} \tag{18}$$

If the process is non-interacting, *i.e.* the off-diagonal elements in $G(s)$ are zero, then Υ becomes a zero matrix, which is due to (7) and (8). Hence, Υ reflects that the multivariable control system is a collection of scalar control systems.

Now, the step responses of the desired control system and the real control system are depicted in Fig. 5. Since the off-diagonal elements are ignored during the design, the desired closed loop performance is not met by the control system. Obviously, the interaction in the control system has caused performance loss.

Fig. 6 depicts $\Upsilon(GK, I)$ in comparison with the loop transfer matrix GK. In the region where control is effective, *i.e.* the frequency is less than 2 rad/sec, the magnitude of $\Upsilon(GK, I)$ is large and in some cases larger than the magnitude of loop transfer function. An analysis of the decomposed loop transfer functions shows that interaction has caused a reduction of the phase margin in each loop, see Fig. 7, and is associated with the loop effect. Thus, larger overshoots and more oscillations should be observed, which is reflected in Fig. 5. Consequently, a controller re-design is necessary to achieve performance improvements of the control system.

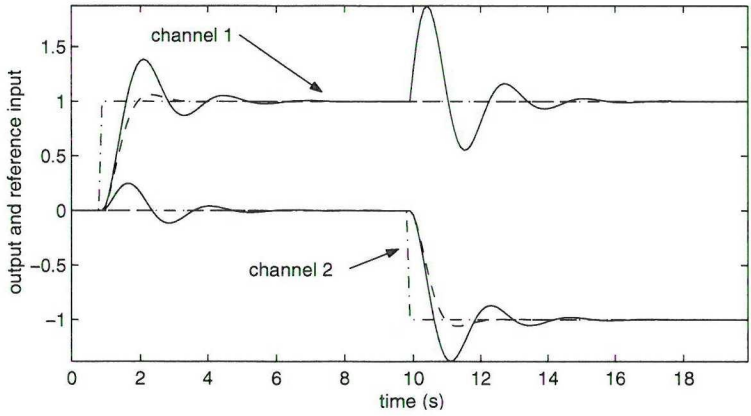

Fig. 5: Step response of the closed loop system. Reference input (dashed), desired output (dashed-dotted), real output of the control system (solid).

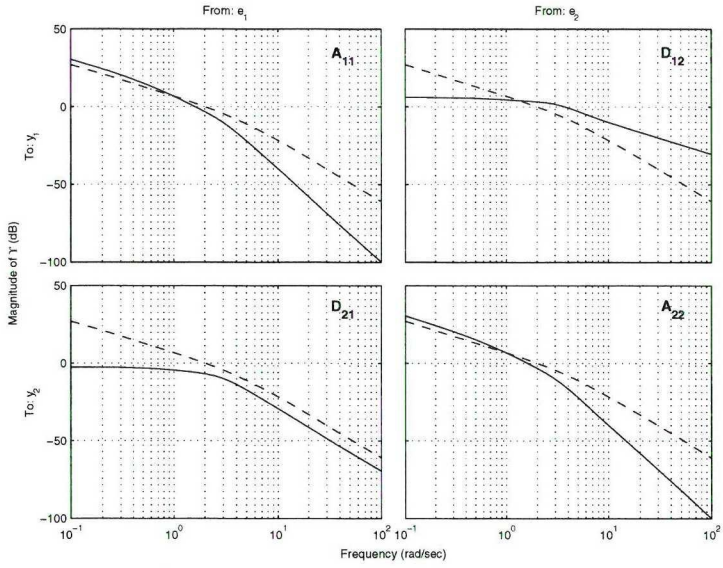

Fig. 6: Magnitude of ITFM $\Upsilon(GK, I)$ (solid) and of the loop transfer functions (dashed)

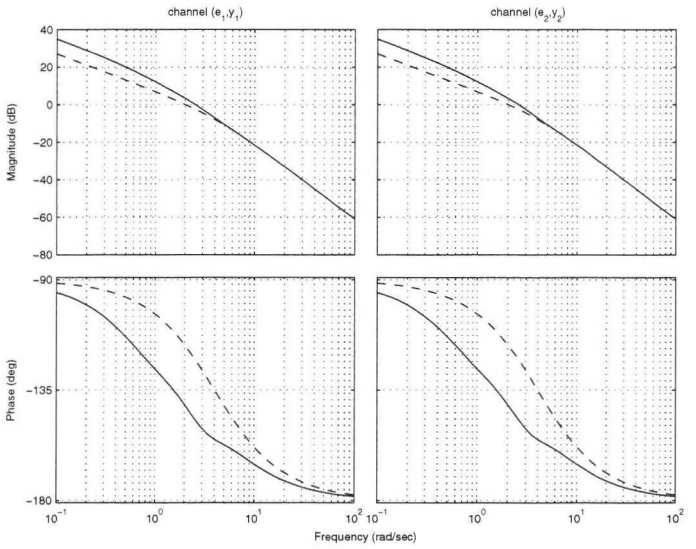

Fig. 7: Bode plot for the decentralized control system. Desired loop transfer functions (dashed), Decomposed loop transfer functions (solid)

Principally, there are two ways to improve the performance of the control system. One, the controllers are tuned so that the interaction reduces, which usually only leads to minor improvements. Two, a multivariable controller is designed that considers the couplings in the process.

Here, the second approach is chosen to improve the performance of the closed loop system. The simplest choice of a multivariable controller is the same decentralized controller in combination with a pre-compensating steady-state decoupling network. In that case the new controller transfer matrix becomes

$$K_d(s) = \frac{1}{s(s+4)} \begin{bmatrix} 1.8s^2 + 5.4s + 3.6 & 1.2s^2 + 6s + 7.2 \\ -1.35s^2 + 4.05s - 2.7 & 0.6s^2 + 3s + 3.6 \end{bmatrix} \tag{19}$$

Clearly, the introduction of the steady-state decoupling network has improved the performance of the control system, Fig. 8.

According to Fig. 9, the magnitude of the elements in $\Upsilon(GK_d, I)$ has reduced compared to the loop transfer functions, which indicates less loop interaction. Furthermore, $\Upsilon(GK_d, I)$ tends to zero for low frequencies, which is an indication for perfect decoupling at steady state. Thus, the ITFM reflects what should be expected from the design approach. Although perfect decoupling is only achieved at steady state, a wider frequency range is positively affected by the introduction of the decoupling

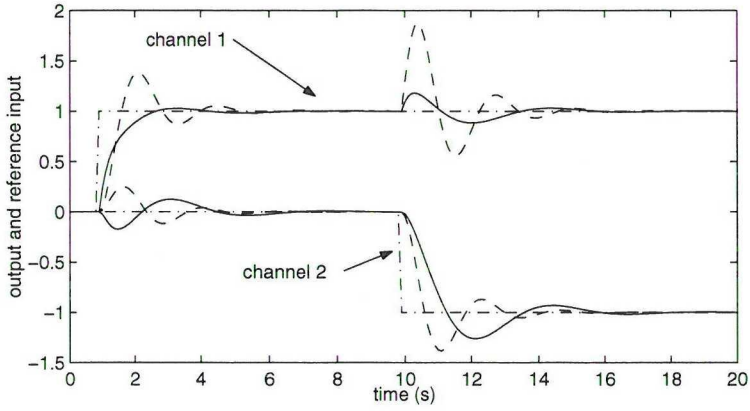

Fig. 8: Step response of the closed loop system. Reference input (dashed-dotted), output of the steady-state decoupled control system (solid), output of interacting control system (dashed).

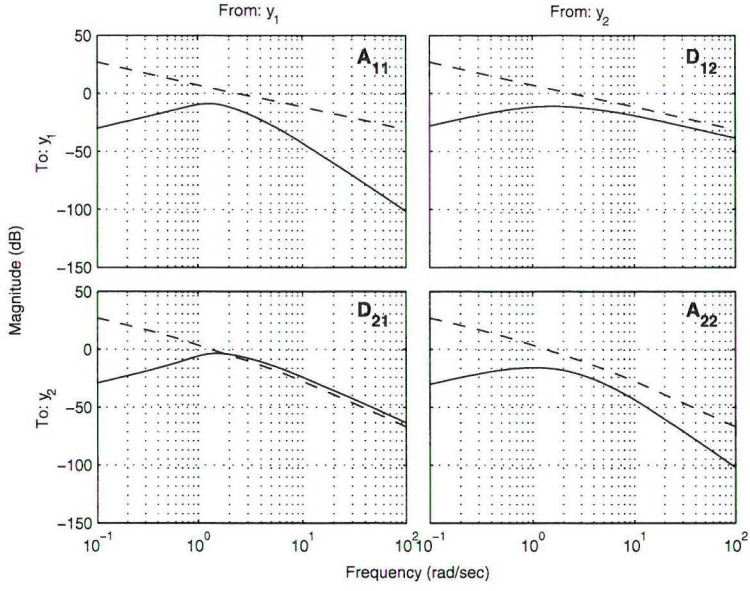

Fig. 9: Magnitude of $\Upsilon(GK_d, I)$ (solid) and of the loop transfer functions (dashed)

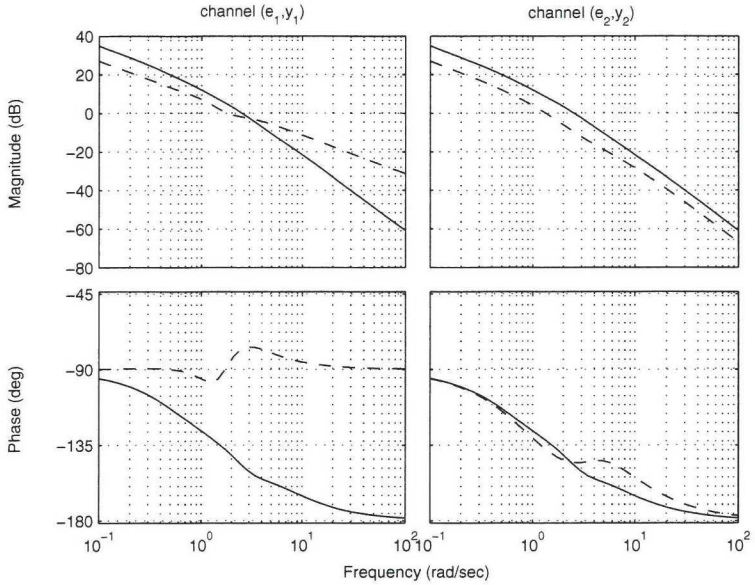

Fig. 10: Bode plot of decomposed loop transfer functions for the decoupled versus the decentralized control system. Decentralized control (solid), Decoupling control (dashed)

network.

A Bode plot of the decomposed loop transfer function is depicted in Fig. 10. Obviously, the phase margin has increased due to the introduction of the decoupling network. The increase of the phase margin is also reflected in the simulation of the control system.

Finally, it can be concluded that the ITFM can be used as a design criterion for multivariable control systems. It should also be noted, that multivariable controllers are usually not only meant for interaction reduction but also to make use of interaction. Thus, the ITFM should be considered where loop interaction should be avoided.

4 Control structure improvement

The most widespread control structure is the decentralized controller, due to its simplicity of design, implementation and maintenance. When a decentralized control structure is evaluated and a performance assessment is conducted, the adequacy of the control structure should be analyzed at the same time.

The analysis of the control structure should be based on closed loop contiguities and

consider the structural mismatch in the controller design. Implications of the analysis are either re-design of individual controllers or re-design of the control structure. The latter usually yields better results. It has to be pointed out that the described methodology is exclusively aimed at the evaluation of decentralized control structures.

4.1 Structural mismatch

When decentralized control, *i.e.* K is diagonal, is applied to a multivariable process G the controller design is based on the model

$$\hat{G} \triangleq \text{diag}(G_{11}, \ldots, G_{nn}) \tag{20}$$

It implies that the off-diagonal elements of G are small or zero, and thus have little effect on the closed loop performance of the control system. The structural mismatch between G and $\hat{G}$ is given by

$$\tilde{G} \triangleq G - \hat{G} \tag{21}$$

The sensitivity function matrices $\hat{T}$ and $\hat{S}$ are a function of K and $\hat{G}$. Clearly, $\hat{T}$ and $\hat{S}$ coincide with T and S only if $\tilde{G} = 0$. Moreover, $\hat{T}$ and $\hat{S}$ are usually determined by performance specification for the closed loop system and the controller K is designed according to them.

Consequently, the mismatch between $\hat{T}$ and T is caused by $\tilde{G}$ or by uncertainties that perturb $\hat{G}$. If $\hat{G}$ is perturbed by uncertainties then $\hat{T}$ is also perturbed.

Firstly, it is assumed that there are no uncertainties in $\hat{G}$. Then, the sensitivity function matrices T and S of the closed loop system can be derived in terms of $\hat{S}$, $\hat{T}$ and the mismatch $\tilde{G}$.

Proposition 1. *The sensitivity function matrix S can be derived in terms of $\hat{S}$ and a multiplicative uncertainty as*

$$S = (I + \Delta)^{-1} \hat{S}$$

where $\Delta = \hat{S}\tilde{G}K$.

Proof.

$$\begin{aligned} S &= (I + GK)^{-1} \\ &= \left(I + \tilde{G}K + \hat{G}K\right)^{-1} \\ &= \left\{\left(I + \hat{G}K\right)\left(\hat{S} + \hat{S}\tilde{G}K + \hat{T}\right)\right\}^{-1} \\ &= \left(I + \hat{S}\tilde{G}K\right)^{-1} \hat{S} \\ &= (I + \Delta)^{-1} \hat{S} \end{aligned}$$

□

Proposition 2. *The complementary sensitivity function matrix T can be expressed in terms of $\hat{T}$ using the uncertainty term $\Delta = \hat{S}\tilde{G}K$*

$$T = (I + \Delta)^{-1}\left(\Delta + \hat{T}\right) \tag{22}$$

Proof. The proof follows immediately from $T = I - S$ and $\hat{T} = I - \hat{S}$. □

Clearly, Δ gives a description for the mismatch between T and $\hat{T}$, and is denoted as the structural mismatch. Moreover, Δ has a nice structural property, which is due to the special structure of $\hat{S}$, $\tilde{G}$ and K. Since both $\hat{S}$ and K are diagonal transfer function matrices and $\tilde{G}$ has zero diagonal elements, it can be shown that Δ has the same structure as $\tilde{G}$. The elements of Δ are given by

$$[\Delta]_{ij} = \begin{cases} 0, & i = j \\ \hat{S}_{ii}G_{ij}K_{jj}, & \text{otherwise} \end{cases} \tag{23}$$

Hence, each off-diagonal element in Δ is a filtered version of the corresponding off-diagonal element in G

$$[\Delta]_{ij} = G_{ij}\frac{K_{jj}}{1 + G_{ii}K_{ii}}, \quad \text{with } i \neq j \tag{24}$$

Thus, Δ quantifies the effect of off-diagonal elements in a decentralized control system. If Δ is zero, then T coincides with $\hat{T}$. Otherwise, a minimization of the elements in Δ minimizes the interaction in a closed loop system.

Furthermore, the relationship (22) can be rewritten to

$$\Delta S = \hat{T} - T \tag{25}$$

The output $\hat{y}$ of the desired closed loop system can be computed from $\hat{y} = \hat{T}r$. Consequently, the output of ΔS is the residual $\tilde{y} = \hat{y} - y$ and Δ represents the transfer function matrix from the control error e to the residual $\tilde{y}$. Thus, Δ can be directly retrieved from process data by applying system identification algorithms.

Moreover, if S is close to diagonal, the off-diagonal elements can be ignored and the following approximation holds

$$\Delta\,\mathrm{diag}(S) \approx \hat{T} - T \tag{26}$$

The transfer function matrix $\Delta\,\mathrm{diag}(S)$ has the same properties as Δ, *i.e.* all diagonal elements are equal to zero. Consequently, if (26) holds, then the residuals $\tilde{y}$ contain information on the structural mismatch of control structure and again, the approximation of Δ can be identified from process data.

Until now, uncertainties were not considered. Suppose, $\hat{T}$ is uncertain due to modelling errors in $\hat{G}$, then (25) or (26) cannot be used to describe Δ. If an upper bound

for the uncertainty in $\hat{T}$ is given by an additive diagonal uncertainty term Δ_T, then (25) can be modified to

$$\Delta S = \hat{T} - T + \Delta_T \tag{27}$$

For the approximation this yields

$$\Delta \operatorname{diag}(S) \approx \hat{T} - T + \Delta_T \tag{28}$$

Thus, the uncertainty term Δ_T is reflected as non-zero diagonal elements in the structural mismatch.

Consequently, the transfer function matrix $\tilde{T} = \hat{T} - T$ contains information on the uncertainty in $\hat{T}$ in its diagonal elements and on the mismatch between T and $\hat{T}$ in the off-diagonal elements.

4.2 Evaluation of the mismatch

The transfer matrix Δ quantifies the mismatch between $\hat{T}$ and T and can be approximation by $\tilde{T}$. Contrary to Δ, $\tilde{T}$ additionally contains a description for the uncertainty in $\hat{T}$. Thus, $\tilde{T}$ should be considered as the first hand choice for the evaluation of the mismatch.

Clearly, the approximation (26) has to be valid. But, if the approximation (26) does not hold, then due to (25), the diagonal elements in $\tilde{T}$ relate to a combination of elements in $\tilde{G}$. Thus, the diagonal elements of $\tilde{T}$ are different from zero, even if $\hat{T}$ is certain. Therefore, the magnitude of the diagonal elements can be used as an indicator for the validity of the approximation.

Naturally, the following indicator κ can be introduced

$$\kappa = \max_i \left\| \tilde{T}_{ii} \right\|_N \tag{29}$$

where N denotes a system norm. Thereby, the indicator κ considers the overall dynamics of the diagonal elements and can be used as a minimal threshold for the evaluation of $\tilde{T}$.

When the off-diagonal elements of $\tilde{T}$ are evaluated, then the following can be suggested. A structural mismatch appears as a non-zero $\tilde{T}$ as soon as $\tilde{G}$ is non-zero. Due to (23), if the element in $\tilde{G}_{ij}$ has significant impact on the output, then the element $\tilde{T}_{ij}$ has large magnitude. In terms of system norms this means that if $\|\tilde{G}_{ij}\|_N$ is large then $\|\tilde{T}_{ij}\|_N$ is large. Thus, the element G_{ij} should be considered in the controller design. This motivates the following rule.

Decision rule. The performance of the closed loop system can be improved by considering the dynamics from input j to output i in the controller design, if

$$\left\| \tilde{T}_{ij} \right\|_N > \tau, \quad i \neq j$$

where N is a system norm and τ a threshold. □

The quantification of the possible performance improvement of the closed-loop system in terms of the magnitude of $\tilde{T}_{ij}$ can be used to choose a threshold τ. This unsolved problem has yet to be addressed. However, a lower bound for τ is given by κ, as κ is an upper bound for the uncertainty in $\hat{T}$. Thus, τ can be chosen so that uncertainties and disturbances are not interpreted as a structural mismatch.

For evaluation purposes the following structure array can be defined.

Definition. Let P be an $n \times m$ transfer function matrix. The structure array $\mathcal{S}_N(P)$ with system norm N is a real $n \times m$ matrix, where the elements are defined as

$$[\mathcal{S}_N(P)]_{ij} = \|P_{ij}\|_N$$

□

Now it can be concluded that from inspection of $\mathcal{S}_N(\tilde{T})$, the following conclusions can be drawn:

- If κ is large, then the uncertainties in $\hat{T}$ have to be reduced by re-designing the individual controllers or by modifying the performance specification $\hat{T}$. If a reduction is not yield, then Δ has to be analyzed instead.
- If $\|\tilde{T}_{ij}\|_N > \kappa$ then the dynamics of G_{ij} should be modelled and the controller for multivariable system has to be designed anew.

As stated in [25, 7], the effect of interaction on a control loop is largest in the frequency region where control is active, namely in the cross-over region. Therefore, the evaluation of Δ and $\tilde{T}$ should focus on this region. In [3] weighted system norms are suggested as a tool where certain frequency regions should be emphasized in the analysis of system norms. Hence, the structure array is preferably derived with weighted system norms.

It is still an open question which system norm should be preferred in the evaluation of Δ and $\tilde{T}$. Thence, for the sequel, the $\mathcal{H}_2$-norm is chosen as system norm for the structure array.

4.3 Identification of Δ and $\tilde{T}$

When control structure evaluation is applied on-line, a model of Δ and $\tilde{T}$ can be obtained by applying system identification algorithms to process data. The theory of system identification is well-developed and many methods for model estimation are available, see *e.g.* [24] and [16]. Moreover, implementations of these algorithms in Matlab are given in [17].

For the identification of Δ, the input signal vector and the output signal vector are chosen as control error e and residual $\tilde{y}$, respectively. Obviously, this is a closed-loop

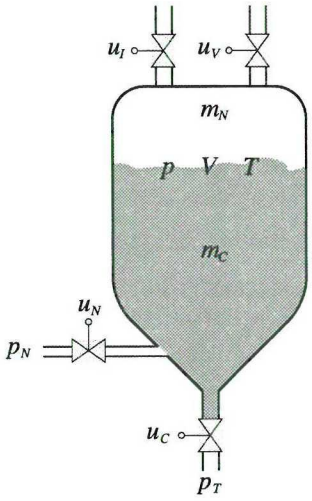

Fig. 11: Schematic drawing of a coal injection vessel

identification problem. In contrary to the identification of Δ, the identification data sets for $\tilde{T}$ have open-loop character, as the input signal vector becomes r instead of e. Both the open and closed-loop identification problem are studied thoroughly and algorithms are available. A further discussion is not pursued here.

5 Case study

In this case study the control of a coal injection vessel is addressed. First, the coal injection process is shortly introduced and decentralized control of the process is presented. Second, the control structure evaluation methodology is applied to a process model and to process data. Finally, the control structure is improved according to the indications and the re-designed closed loop system is then analyzed.

5.1 The process

The coal injection vessel is a pressurized multivariable tank system which is discussed in [13], [1] and [2]. There, models for the process are derived and successfully used for the design and analysis of multivariable controllers and a gas-leakage detection system.

In Fig. 11 a schematic drawing of a coal injection vessel is given. The process can be described shortly as follows. During the injection phase of the vessel, the pressure control valve u_N and the flow control valve u_C are used to release a constant coal

flow from the vessel. The coal flow cannot be measured directly. The available measurements are the net weight m_T of the vessel, which is the sum of the nitrogen weight m_N and the fine coal weight m_C, and the pressure in the vessel p. A linear physical model for the coal injection vessel for the injection phase is given by

$$\dot{x}(t) = 10^{-3}\begin{bmatrix} -0.3234 & 0.3604 \\ 0.2128 & 0.2963 \end{bmatrix} x(t) + \begin{bmatrix} -0.4878 & 0.6816 \\ 0.5721 & -0.3043 \end{bmatrix} u(t) \quad (30a)$$

$$y(t) = \begin{bmatrix} -0.8379 & 0.6477 \\ -0.0237 & -0.0198 \end{bmatrix} x(t) \quad (30b)$$

where $u(t) = [u_N(t)\ u_C(t)]^T$ and $y(t) = [p(t)\ m_T(t)]^T$. It is important to note, that the model uncertainty is large for frequencies below 10^{-4} rad/sec.

5.2 Control structure evaluation

The conventional way to control the vessel with a decentralized controller is to stabilize the pressure by means of the pressure control valve and to retain a constant flow using the flow control valve. A possible controller can be given in the transfer function representation as

$$K(s) = \frac{1}{s}\begin{bmatrix} 0.04s + 0.001 & 0 \\ 0 & -(2s + 0.05) \end{bmatrix} \quad (31)$$

In Fig. 12, a simulation of coal injection vessel with the controller $K(s)$ is displayed. First, a step in both pressure and mass is applied and later only a step in the mass is applied. Clearly, the control system exhibits slight overshoots and retains a zero steady state control error. Furthermore, it can be seen that pressure loop is largely affected by control action in the mass loop.

A Bode magnitude plot of Δ and $\tilde{T}$ is depicted in Fig. 13. Clearly, the diagonal elements in Δ are zero, which is not the case for $\tilde{T}$. Since $\hat{T}$ is perfectly known, the diagonal elements indicate the validity of the approximation. Moreover, it can be observed, that the off-diagonal elements of $\tilde{T}$ and Δ coincide for frequencies above 0.03 rad/sec. Consequently, approximation (26) holds for that region.

Now the structure arrays for both Δ and $\tilde{T}$ using the $\mathcal{H}_2$-norm are derived

$$\mathcal{S}_2(\Delta) = \begin{bmatrix} 0.0000 & 8.4029 \\ 0.0003 & 0.0000 \end{bmatrix}, \qquad \mathcal{S}_2(\tilde{T}) = \begin{bmatrix} 0.0026 & 8.0261 \\ 0.0000 & 0.0038 \end{bmatrix}$$

In both cases the off-diagonal element $(1,2)$ is large compared to all the other elements. Moreover, the value for κ is 0.0038 which is very small. Consequently, the dynamics from u_C to p should be considered in the controller design. Intuitively, opening the flow control valve introduces a gas flow out of the vessel, which discharge the pressure control loop should compensate for.

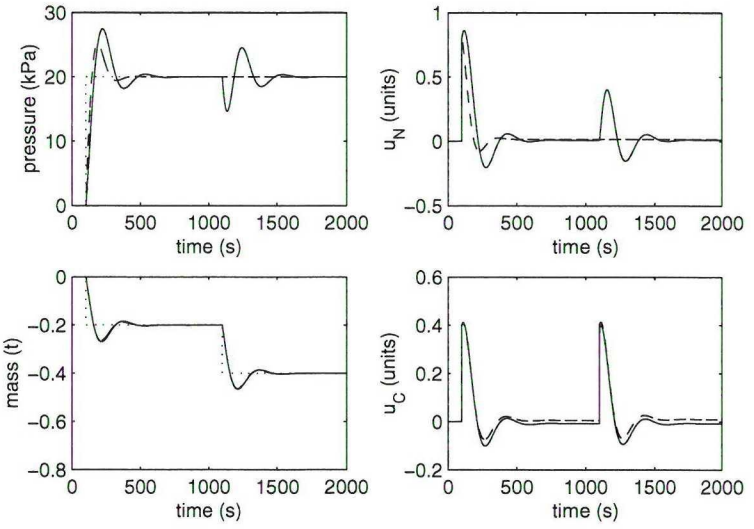

Fig. 12: Simulation of step responses of the coal injection vessel with a decentralized PI controller. Reference signal (dotted), output of $\hat{T}$ (dashed), output of T (solid)

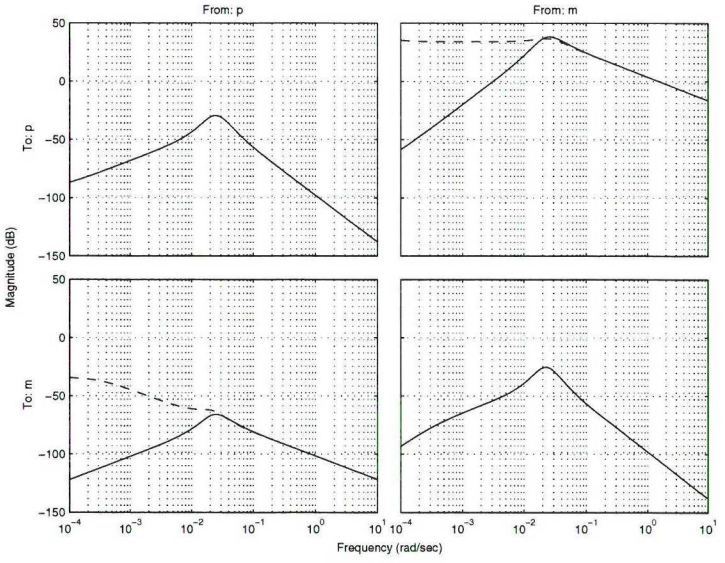

Fig. 13: Bode magnitude plot of Δ (dashed) and $\tilde{T}$ (solid).

From the analysis of $\hat{S}$ and $\hat{T}$ it can be seen, that the cross-over region of the scalar control loops is between 0.01 rad/sec and 0.1 rad/sec. In order to emphasize the evaluation on the cross-over region, the following weighting function is chosen

$$F(s) = \frac{0.032s^2(s+0.057)(s+0.017)}{(s+0.195)(s-0.1)^2(s-0.01)^2(s+0.005)}$$

Now the structure arrays can be re-computed with the weighted $\mathcal{H}_2$-norm

$$\mathcal{S}_{2F}(\Delta) = \begin{bmatrix} 0.0000 & 10.440 \\ 0.0001 & 0.0000 \end{bmatrix}, \qquad \mathcal{S}_{2F}(\tilde{T}) = \begin{bmatrix} 0.0026 & 9.0882 \\ 0.0000 & 0.0037 \end{bmatrix}$$

The usage of the weighted system norms yields the same result as above, namely the off-diagonal element $(1,2)$ has to be considered. Already from Fig. 13, it can be concluded that all elements have nearly the same break frequencies, namely about 0.03 rad/sec. Thus, the usage of the weighted system norms lead to the same conclusions in this case.

5.3 Application to process data

The control structure evaluation is now applied to process data from a PCI vessel at SSAB Tunnplåt AB in Luleå, Sweden. A decentralized PI controller is used to control the pressure in the vessel and the coal mass flow out of the vessel. The data is collected at a sample rate of 1 Hz from the plant control system. Fig. 14 shows measured output versus set point for pressure and coal mass flow.

For the decentralized control system the desired closed-loop performance is given by $\hat{T}$

$$\hat{T}_{11} = \frac{0.001941z + 0.001883}{z^2 - 1.910z + 0.9139}, \quad \hat{T}_{22} = \frac{0.001966z + 0.001934}{z^2 - 1.947z + 0.9512} \tag{32}$$

Now, a model for $\tilde{T}$ is derived from the process data by means of system identification. Since input and output signals are r and $\tilde{y}$, respectively, this is an open-loop identification problem. After $\tilde{y}$ is computed, a model is estimated with the subspace algorithm $n4sid$.

Then, the structure matrix of $\tilde{T}$ is obtained as

$$\mathcal{S}_2(\tilde{T}) = \begin{bmatrix} 1.5353 & 14.4396 \\ 0.1931 & 0.0761 \end{bmatrix} \tag{33}$$

The threshold for the decision rule has to be chosen larger than $\kappa = 1.5353$. Applying the decision rule suggests that the process coupling from u_C to p should be considered for the control of the process, as the element $(1,2)$ is significantly larger than κ. Thus, the decision in Section 5.2 is confirmed by the application to process data from the plant.

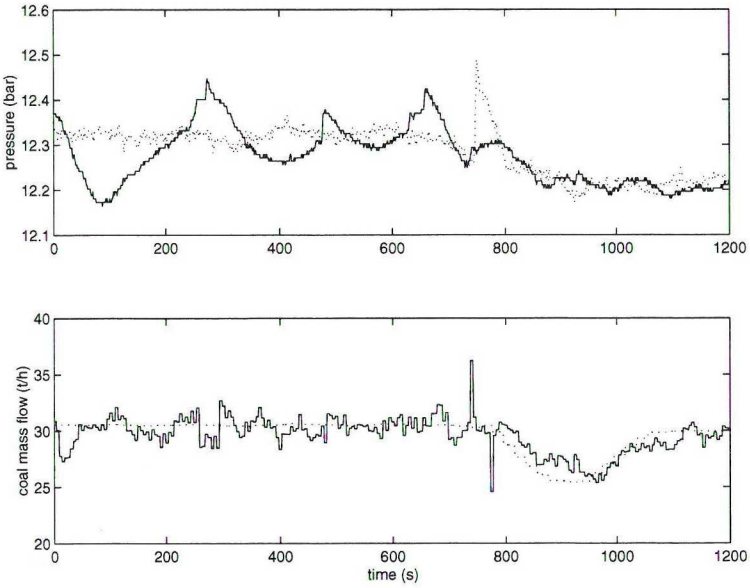

Fig. 14: Collected process data during the injection phase of the PCI vessel. Measured output (solid), set point (dotted).

5.4 Improved control structure

In order to consider the dynamics from the flow control vessel to the pressure, a dynamic compensation that considers mass flow controller and process dynamics is introduced. Consequently, a triangular controller structure can be chosen as

$$K_2(s) = \frac{1}{s} \begin{bmatrix} 0.04s + 0.001 & -(1.44s + 0.036) \\ 0 & -(2s + 0.05) \end{bmatrix} \tag{34}$$

A new simulation with the triangular controller (34) is performed and displayed in Fig. 15. Obviously, the performance of the mass loop has not changed and the performance in the pressure loop is improved. A drawback of the improved control structure is a more intensive control action in the pressure control valve. In Fig. 16 it can be seen that the interaction in the pressure and the mass loop have reduced slightly. Thus, the triangular control structure improves performance and reduces interaction in the multivariable control system.

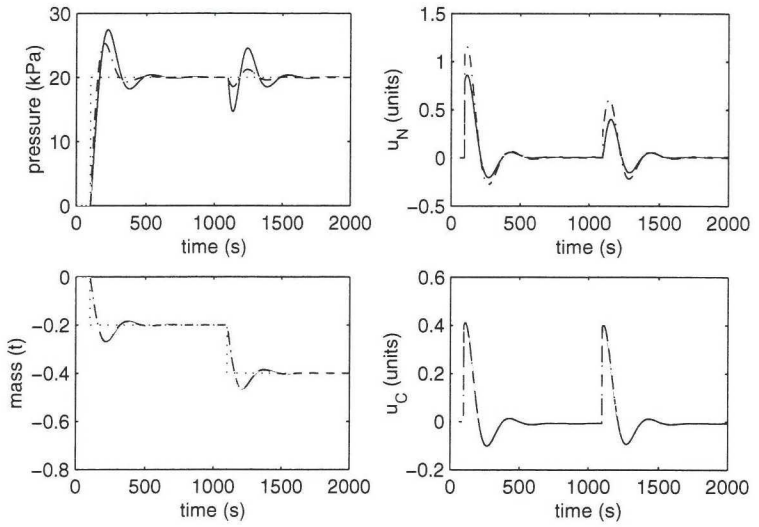

Fig. 15: Triangular controller versus decentralized PI controller. Reference signal (dotted), triangular controller (dashed-dotted), decentralized controller (solid)

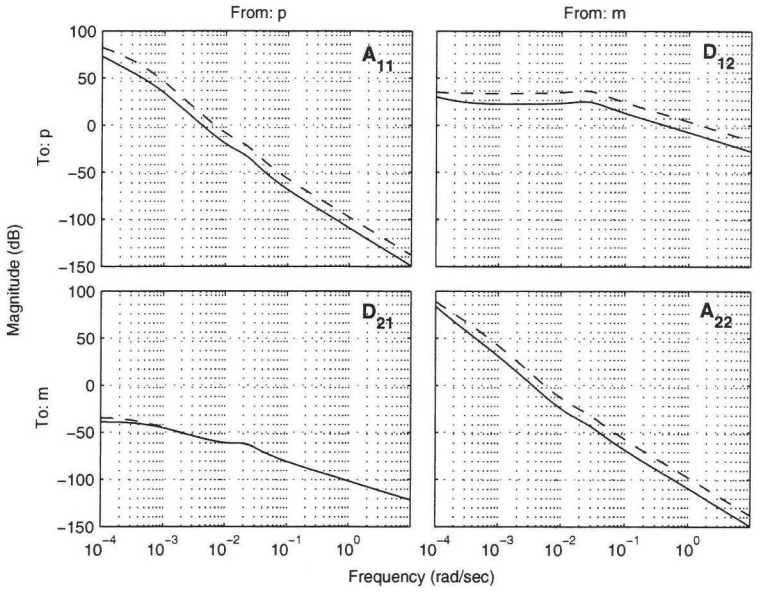

Fig. 16: ITFM of the triangular controller versus decentralized PI controller. Triangular controller (solid), decentralized controller (dashed)

6 Conclusions

In this paper interaction in multivariable control systems and the evaluation of a decentralized control structure from a closed-loop perspective is discussed.

First a dynamic measure that quantifies interaction in a closed-loop system in terms of process model and controller is presented. The measure expresses the amount of interaction as the interaction transfer function matrix (ITFM), which is a linear time invariant system. The ITFM can be used to compare different controllers for a multivariable system with respect to the interaction that the closed-loop control system exhibits. An example is given that illustrates the capabilities of the ITFM. The ITFM is used to display the reduction of interaction due to the control structure re-design.

Then, based on the structural mismatch between desired control loop design and achieved control loop design a method for the evaluation of a decentralized control structure in multivariable control is derived. It is shown that the structural mismatch can be described as a transfer function matrix that directly relates to the ignored off-diagonal elements in the process model. The system norm of the elements in the transfer function matrix are arranged in a so-called structure array. An interpretation of the structure array is discussed and a decision rule is given. In the case study it is shown that the method can be effectively used to improve the control structure of multivariable control systems.

It has still to be investigated how uncertainties in $\hat{T}$, disturbances and non-linearities effect the modelling of Δ and $\tilde{T}$. Additionally, it has to studied how thresholds for the structure evaluation are related to performance improvements and in what way the threshold selection can be automated.

References

[1] Wolfgang Birk and Alexander Medvedev. Pressure and flow control of a pulverized coal injection vessel. *IEEE Transactions on Control Systems Technology*, 8(6):919–929, November 2000.

[2] Wolfgang Birk and Alexander Medvedev. Sensitivity analysis of an LQ optimal multivariable controller for a fine coal injection vessel. *IEEE Transactions on Industry Applications*, 36(3):871–876, May/June 2000.

[3] Wolfgang Birk and Alexander Medvedev. A note on gramian-based interaction measures. Paper no. 4 in Wolfgang Birk, "Industry Applications of Multivariable Control´´, PhD Thesis, Luleå University of Technology, September 2002.

[4] E.H. Bristol. On a new measure of interaction for multivariable process control. *IEEE Transactions on Automatic Control*, 11:133–134, January 1966.

[5] Men-Sin Chiu and Yaman Arkun. A new result on relative gain array, Niederlinski index and decentralized stability condition: 2×2 plant cases. *Automatica*, 27(2):419–421, 1991.

[6] Arthur Conley and Mario E. Salgado. Gramian based interaction measure. In *Proc. of the 2000 Conference on Decision and Control, Sydney*, 2000.

[7] J.-P. Gagnepain and D.E. Seborg. Analysis of process interactions with applications to multiloop control system design. *I&EC Process Design & Development*, 21(5), 1982.

[8] E. Gagnon, A. Desbiens, and A. Pomerleau. Selection of pairing and constrained robust decentralized PI controllers. In *Proc. of American Control Conference, San Diego, USA*, June 1999.

[9] Graham C. Goodwin, Stefan F. Graebe, and Mario E. Salgado. *Control System Design.* Prentice Hall, 2000.

[10] Pierre Grosdidier and Manfred Morari. The μ interaction measure. *Ind. Eng. Chem Res.*, 26:1193–1202, 1987.

[11] Kurt E. Häggblom. Control structure analysis by partial relative gains. In *Proc. of the 36th Conference on Decision & Control, San Diego, USA*, pages 2623–2624, December 1997.

[12] M. Hovd and S. Skogestad. Simple frequency-dependent tools for control systems analysis, structure selection and design. *Automatica*, 28(5):989–996, 1992.

[13] Andreas Johansson and Alexander Medvedev. Model based leakage detection in a pulverized coal injection vessel. *IEEE Transactions on Control Systems Technology*, 7(6):675–682, November 1999.

[14] I.K. Kookos and A.I. Lygeros. An algorithmic method for control structure selection based on the RGA and RIA interaction measures. *Trans IChemE*, 76, Part A:458–464, 1998.

[15] Jay H. Lee, Richard D. Braatz, Manfred Morari, and Andrew Packard. Screening tools for robust control structure selection. *Automatica*, 31(2):229–235, 1995.

[16] Lennart Ljung. *System Identification: Theory for the User.* Prentice Hall, 2 edition, 1999.

[17] Lennart Ljung. *System Identification Toolbox: For use with Matlab.* The MathWorks Inc., 2000.

[18] J.M. Maciejowski. *Multivariable Feedback Design.* Addison-Wesley, 1989.

[19] Vasilios Manousiouthakis, Robert Savage, and Yaman Arkun. Synthesis of decentralized process control structures using the concept of block relative gain. *AIChE Journal*, 32(6):991–1003, 1986.

[20] A. Medvedev and G. Hillerström. An external model control system. *Control Theory Adv. Tech.*, 10(4, part 4):1643–1665, 1995.

[21] A. Niederlinski. A heuristic approach to the design of linear multivariable interacting control systems. *Automatica*, 7:691–701, 1971.

[22] J.E. Rijnsdorp. Interaction on two-variable control systems for distillation columns. *Automatica*, 1(1):15–28, 1965.

[23] S. Skogestad and I. Postlethwaite. *Multivariable Feedback Control - Analysis and Design*. John Wiley & Sons, 1996.

[24] T. Söderström and P. Stoica. *System Identification*. Prentice Hall, 1989.

[25] M.F. Witcher and T.J. McAvoy. Interacting control systems: Steady-state and dynamic measurement of interaction. *ISA Transactions*, 16(3):35–41, 1977.

[26] Björn Wittenmark and Mario E. Salgado. Hankel-norm based interaction measure for input-output pairing. In *Proc. of the 2002 IFAC World Congress, Barcelona*, 2002.

[27] Zhong-Xiang Zhu. Loop decomposition and dynamic interaction analysis of decentralized control systems. *Chemical Eningeering Science*, 51(12):3325–3335, 1996.

[28] Zhong-Xiang Zhu. Variable pairing selection based on individual and overall interaction measures. *Ind. Eng. Chem. Res.*, 35(1):4091–4099, 1996.

[29] Zhong-Xiang Zhu and Arthur Jutan. A new variable pairing criterion based on the Niederlinski index. *Chem. Eng. Comm.*, 121:235–250, 1993.

Paper 6

Foam Level Control in a Water Model of the LD Converter Process

In print

Part of a special section in *Control Engineering Practice*
Revised version of: W. Birk, I. Arvanitidis, A. Medvedev and P. Jönsson "Foam Level Control in a Water Model of the LD Converter Process", in *Proceedings of the 10th IFAC Symposium on Automation in Mining, Mineral and Metal Processes* in Tokyo, Japan, September 4-6, 2001

Foam Level Control in a Water Model of the LD Converter Process

W. Birk[†⋆], I. Arvanitidis[‡], A. Medvedev[†§], and P. Jönsson[‡]

[†]Control Engineering Group, Luleå University of Technology, SE-971 87 Luleå, Sweden
§ Uppsala University, Box 337, SE-751 05, Uppsala, Sweden
[‡]Department of Metallurgy, Royal Institute of Technology, SE-100 44 Stockholm, Sweden
[⋆]Corresponding author: wolfgang.birk@sm.luth.se

Abstract

This paper deals with estimation and control of foam level in dynamic foaming. An improved foam level estimation methodology from a microphone signal and its automatic calibration is presented. The dynamical reaction of the foam level on air lance movements is modelled using system identification. Based on the resulting mathematical model, a controller for foam level stabilisation is designed and applied to a water model, representing the LD converter process. It is shown that the foam level can be controlled using a microphone as the measurement device and air lance movement as the actuator.

Keywords: Level control, Dynamic foaming, Water model, LD Converter process, Soft sensing, Slopping

1 Introduction

Steel is widely produced from hot metal and scrap. Hot metal with about 4-5% C is produced from iron oxide pellets and coke by the blast furnace. After the blast furnace, the hot metal is poured into a ladle, sulfur is removed from the hot metal by a reaction with lime. Thereafter, the hot metal can be converted into steel by a top blown basic oxygen furnace (BOF). Oxygen is supplied through a lance from above and is jetted onto the metal bath at supersonic speed. Scrap, slag forming agents and hot metal are charged to the vessel and, thereafter, the lance is lowered with oxygen blown through. The oxygen jet forms a cavity at the bath surface where Fe, Si, Mn and C are oxidised. Metal droplets are splashed and mixed together with the slag. Carbon dissolved in the metal phase reacts with FeO to form carbon monoxide.

This means that a foam containing metal droplets, metal oxides (slag) and CO bubbles is formed. The effective surface area of this foam is large and thereby the chemical reactions involved in this process are fast. To make this process effective, a large foam volume is needed. However, if the foam level is too high, slopping occurs causing reduction in metal exchange and environmental pollution. The formation of the foam is manually controlled by adjusting the oxygen lance level. The foam level in the vessel is nearly impossible to measure, but there has been somewhat successful methods

using radio waves and sonic meters. Optical methods based on laser technology have been tried with bad results because of the strong dust formation during the foaming.

A very simple and continuous method to estimate foam level is to use a microphone and measure the sound intensity at certain frequency bands. As the foam level increases, the sound intensity decreases. Microphones or sonic meters have been widely used since 1970 in many steel plants. However, the sound signal generated is seldom used in order to automatically control the foam level. Piombino Steel shop, ILVA Taranto and British steel are some examples where the sound signal is used as control signal [3, 1, 2], but not for dynamic control, as continuous lance movements are not supported by the actuator and slag properties are often unknown.

In [9], the sonic meter signal is estimated from off-gas flow rate and CO content in the gas. There, the deviation of estimated signal from measured signal is used to detect slopping, combining sonic meter and gas-analysis.

In order to study the process water models are used. The disadvantage with water models are that only a few parameters of the real high temperature process can be studied. In the case of the study of foam level control in the LD-process it was felt to use a water model with large height to diameter ratio. For a detailed descriptions of the water model see [4]. Moreover, a brief introduction to foaming and first results on foam level estimation are given there.

The purpose of the present work is to improve the formerly introduced foam level estimate algorithm and supply an automatic strategy to calibrate the estimation algorithm. Another goal is to demonstrate the possibility of closed loop control of the foam level in the water model using the sound signal as measurement. Foam level control in a LD-converter can be used to automatically avoid slopping.

2 Foam level estimation

In [4] an estimation algorithm for the foam level based on a microphone signal is derived. There, the foam level is computed from the short time sound spectra as

$$\hat{h}(t,\omega) = \frac{\ln(I_0(\omega)) - \ln(I(h(t),\omega))}{\hat{\beta}_F(\omega)}, \tag{1}$$

where $I_0(\omega)$ is the magnitude of the sound spectra without foam and $I(h(t),\omega)$ is the magnitude of the sound spectra at different foam levels. Furthermore, $\hat{\beta}_F(\omega)$ is the attenuation coefficient, which is frequency dependent.

In the sequel, the following fluids are used in the foaming experiments

Fluid	Viscosity [Cp]	Foam life τ [s]	Surface tension [N/m]
A	3.1	3448	0.27
B	1.0	189	0.49

During the design of the foam level estimation, data from a foaming experiment with fluid A are used. Under the experiments the sound signal from the microphone is logged and the foam level is manually read off. The data set is used in the subsequent three subsections and all plots refer to this data set.

Foam generated from fluid A has a higher stiffness and better sound damping capabilities compared to fluid B, as fluid B generates foam faster than fluid A. These contradictory characteristics will be exploited to validate the estimation algorithm.

2.1 Improved estimation

As the sound spectra are estimated from sampled data, the accuracy of the estimate directly affects the foam level estimate. According to [8], the confidence interval in dB for the sound spectra estimate of M frequency bands from a sequence of N samples is given by

$$R_x \approx K \left(\frac{N}{M} - 0.833 \right)^{-0.5} \tag{2}$$

where

x	80%	90%	96%	98%
K	11.2	14.1	17.7	20.5

Hence, frequency resolution has to be traded off against confidence interval for the estimate. The formerly presented estimation scheme is continuously calculating an estimate every second with a frequency resolution of 1 Hz, which means N is equal to M and gives a confidence interval of $R_{90\%} \approx 34.5\ dB$. By increasing the frequency resolution from 1 Hz to 10 Hz, the confidence interval can be narrowed to $R_{90\%} \approx 3.2\ dB$. Consequently, the foam level estimate can be improved by reducing the frequency resolution.

Moreover, the power spectral density (PSD) is a better measure than magnitude of the Fourier transform as it is based on the power of the signal, which is always bounded, and in contrary to the Fourier transform, does not depend on the stochastic properties of the sound signal.

Consequently, the estimation algorithm has to be reformulated using the PSD. Experiments have shown that the dynamic behaviour of the foam is rather slow and the estimation frequency f_{PSD} is set to $1Hz$. Between the estimation instances, the sound signal is sampled at the much higher frequency f_s, which is chosen according to the microphone performance and the sound signal content. Logged sound signals from foam experiments are analysed and a sampling frequency $f_s = 8\ kHz$ appeared to be sufficient.

The PSD of the sound source can be computed as the Fourier transform of the autocorrelation function of the sound sequence between the estimation instances. While

N is given by f_s/f_{PSD}, the number of frequency bands M has to be chosen. Here, M is chosen as $N/20 = 400$ which corresponds to a frequency resolution of 10 Hz. Thus, the confidence interval becomes $R_{90\%} \approx 3.2\ dB$.

The sampled autocorrelation function of the sound sequence is given by

$$\begin{aligned} \phi(t,m) &= \frac{1}{N-m} \sum_{n=0}^{N-m-1} S_n S_{n+m} \\ m &= 0,1,\ldots,M \end{aligned} \tag{3}$$

where S_i are the samples and t is the time instance when the PSD is computed. By applying the Fourier transform to (3), the PSD is found

$$\begin{aligned} \Phi(t,\omega_n) &= \frac{1}{f_s}\left[\phi(t,0) + 2\sum_{m=1}^{M} \phi(t,m) x_m \cos\frac{mn\pi}{M}\right] \\ x_m &= \frac{1}{2}\left[1+\cos\frac{m\pi}{M}\right];\quad m = 0,1,\ldots,M \\ \omega_n &= \frac{f_s n\pi}{M} \\ n &= 0,1,\ldots,M-1 \end{aligned} \tag{4}$$

Here, x_m is the Hanning window, which is used to smooth the spectra. Fig. 1 shows the estimated power spectral density of the design data set.

Accordingly, (1) can be modified to use the PSD instead of the magnitude of the Fourier transform

$$\hat{h}(t,\omega) = \frac{\ln(\Phi_0(\omega_n)) - \ln(\Phi(t,\omega_n))}{\hat{\beta}_F(\omega_n)} \tag{5}$$

2.2 Automatic calibration

Several parameters have to be calibrated in the estimation algorithm. The parameters β_F and Φ_0 have to be identified and the frequency bands which fit best should be chosen. To facilitate calibration, an automatic calibration scheme has to be available, which provides the user with candidate frequencies and a parameter set for each frequency.

Since there is no automatic procedure to measure the foam level, time marked manually observed foam levels have to be used for the calibration. In the water model, foam level can be easily read using a ruler, which is attached to the water model, Fig. 2. Then, the observed foam level points are interpolated over time using cubic splines and sampled at the same frequency as Φ is available.

Assuming that Φ and the observed foam level h are available as a time series with p points, then for each frequency ω_n fixed, $\ln(\Phi(t,\omega_n))$ can be fitted to $h(t)$ in a least

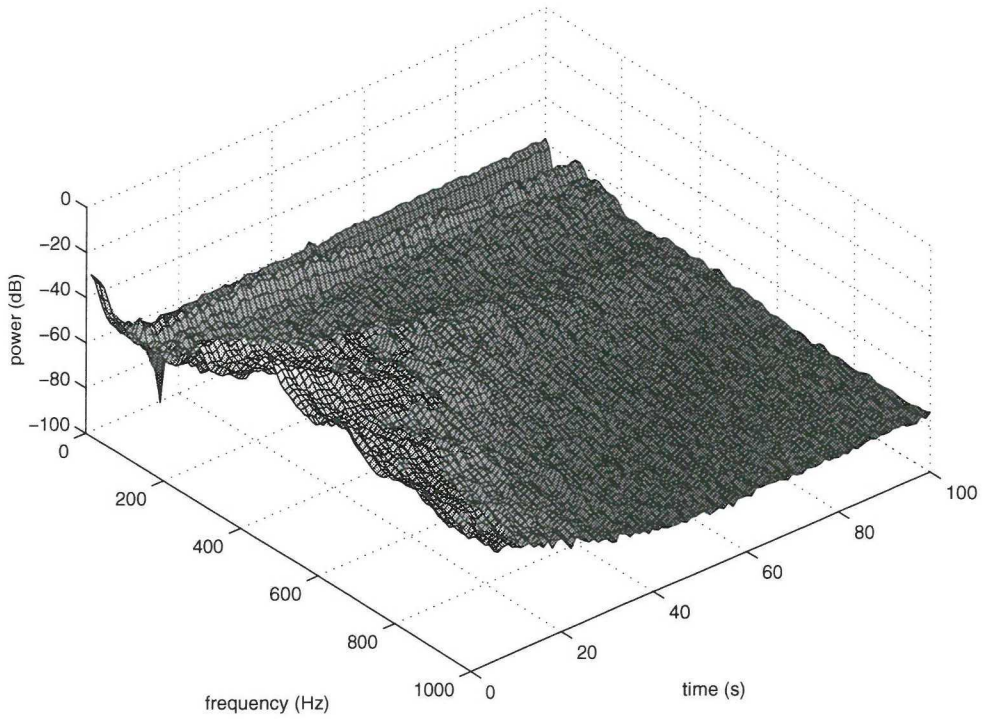

Fig. 1: Power spectral density of the design data set (fluid A).

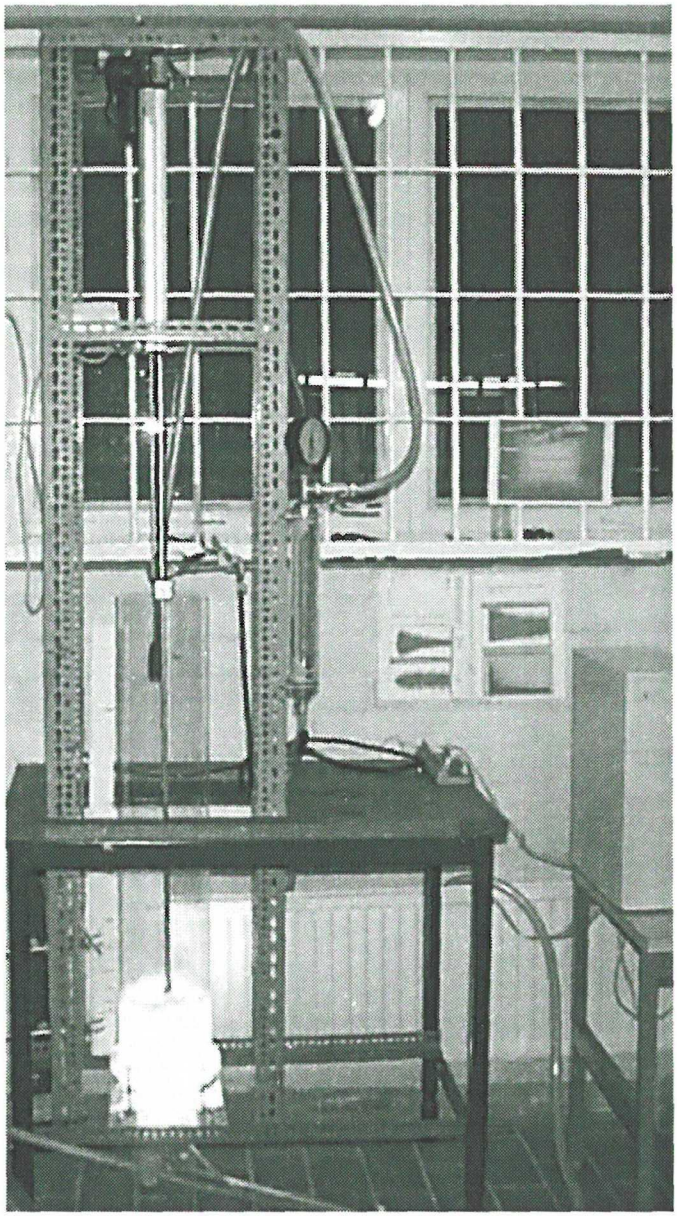

Fig. 2: Photo of the water with the ruler attached to the reactor

squares sense. Rewriting (5) to

$$\hat{h}(t,\omega_n) = \underbrace{-\frac{1}{\beta(\omega_n)}}_{\theta_1} \ln(\Phi(t,\omega_n)) + \underbrace{\frac{\ln(\Phi_0(\omega_n))}{\beta(\omega_n)}}_{\theta_2}$$

the following regressor can be set up for each ω_n

$$\begin{bmatrix} h(t_1) \\ \vdots \\ h(t_p) \end{bmatrix} = \begin{bmatrix} \ln(\Phi(t_1,\omega_n)) & 1 \\ \vdots & \vdots \\ \ln(\Phi(t_p,\omega_n)) & 1 \end{bmatrix} \begin{bmatrix} \theta_1 \\ \theta_2 \end{bmatrix},$$

and the least squares estimate for parameters θ_1 and θ_2 is given by

$$\begin{bmatrix} \hat{\theta}_1 \\ \hat{\theta}_2 \end{bmatrix} = \begin{bmatrix} \ln(\Phi(t_1,\omega_n)) & 1 \\ \vdots & \vdots \\ \ln(\Phi(t_p,\omega_n)) & 1 \end{bmatrix}^{\dagger} \begin{bmatrix} h(t_1) \\ \vdots \\ h(t_p) \end{bmatrix},$$

where $\dagger$ denotes the pseudo-inverse.

Evaluating the standard deviation of the estimation error ϵ, frequencies for foam level estimation can be chosen. Since $\epsilon(\omega_n)$ characterizes the sound attenuation behaviour of the foam, a finger print of the foam is found, Fig. 3.

Fig. 4 shows the estimated foam level using the best fitting frequency. There, ϵ is 17.9 mm and follows rather precisely the confidence interval of the estimate, which becomes ± 19.5 mm for the used frequency.

2.3 Optimal weighted estimate

Since several frequencies can give good fits for the foam level estimation, the weighted sum of those frequencies introduces redundancy and robustness against changes of the foam characteristics.

In order to find the optimal weighted estimate, which even includes the optimal number of frequencies to use, the set of frequencies is re-ordered according to their ability to fit the observed foam level. As ordering measure $\epsilon(\omega_n)$ is used. The ordered set is denoted $\mathcal{F}$ and $\mathcal{F}_i$ denotes the i^{th} best fitting frequency.

Using the weighting scheme

$$w(\omega_n) = \frac{1}{\mathrm{std}(\epsilon(\omega_n))}$$

the weighted foam level estimate composed of r frequencies is given by

$$\hat{h}_r(t) = \frac{1}{\sum_{i=1}^{r} w(\mathcal{F}_i)} \sum_{i=1}^{r} w(\mathcal{F}_i)\hat{h}(t,\mathcal{F}_i) \tag{6}$$

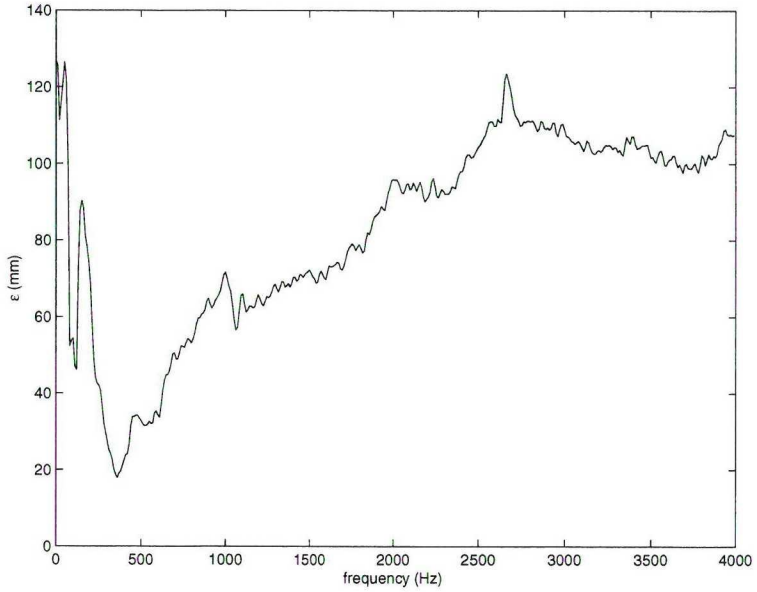

Fig. 3: Plot of ϵ (Finger print of the foam) for fluid A

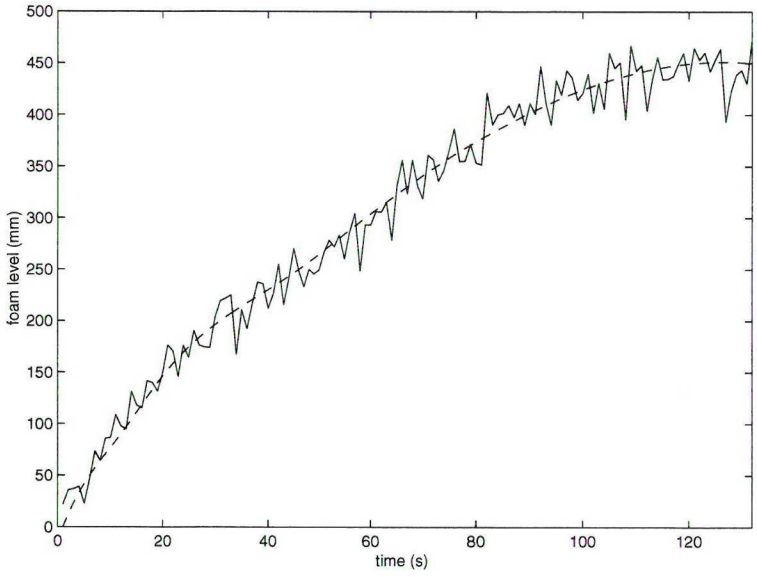

Fig. 4: Foam level estimated (solid) versus observed foam level (dashed) using the best fitting frequency band (fluid A).

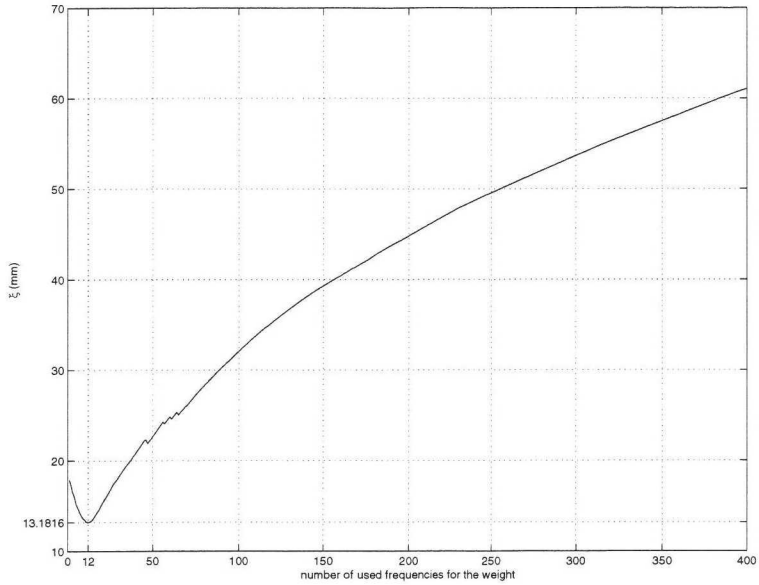

Fig. 5: Plot of ξ (Optimality measure) for fluid A

Deriving the standard deviation of the estimation error for the weighted estimate as above and denoting it $\xi(r)$, an optimality measure for the weighted estimate is found. Hence, searching for $\min_{1\leq i\leq M} \xi(i)$ the best choice for r is obtained.

Consequently, the optimal weighted estimate is given by $\hat{h}_r(t)$ for which $\xi(r) = \min_{1\leq i\leq M} \xi(i)$. Fig. 5 shows a plot for ξ. Obviously, the optimal number of frequencies to use is 12, which reduces the standard deviation of the estimation error from 17.9 *mm* down to 13.2 *mm*. The resulting optimal weighted estimate is shown in Fig. 6.

2.4 Validation

In order to validate the estimation, a different fluid with less attenuation capability is used (fluid B). Furthermore, the generated foam has a shorter foam life τ [4] and will break down considerably faster than the foam generated from fluid A.

Since, the accuracy of the estimation directly depends on the attenuation capability of the foam. Hence, reliability of the estimation concept is tested. Fig. 7 shows the results from the application of the estimation concept. Obviously, the performance is reduced for low and high foam levels. Still, the estimation is reasonably good although the prerequisites are worse.

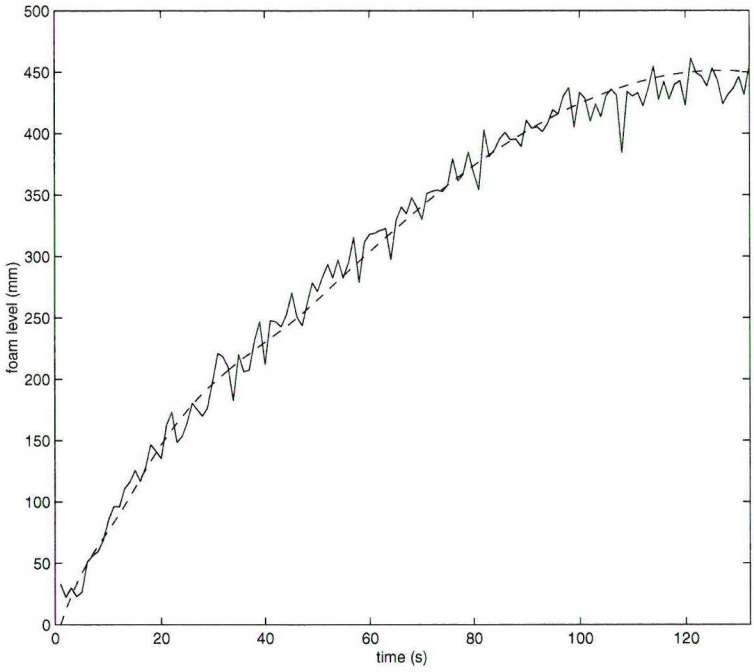

Fig. 6: Optimal weighted foam level estimate for fluid A

3 Foam level control

According to [4], there are several potential actuators to control the foam level in the LD converter. Since the gas-flows to the converter should be constant, their usage as actuator would cause major changes in the converter process.

Hence, the position of the oxygen lance appears to be the natural choice. In manually operated foaming experiments in the water model the foam level could be affected by lance movements.

Thus, a series of foaming experiments has been conducted, where the lance position is only changed between the experiments. In each experiment the steady state value of the foam level is read off.

Fig. 8 shows the lance position versus the steady state value of the foam level. Apparently, the curve reflects the DC-gain from the lance position to the foam level. Important to notice are two areas: below and above 40 mm. At 40 mm a sign change of the DC-gain occurs, and thus actuator movement in the two areas result in different impact on the foam. Additionally, the area below 40 mm is very narrow, which can lead to prevalent saturation.

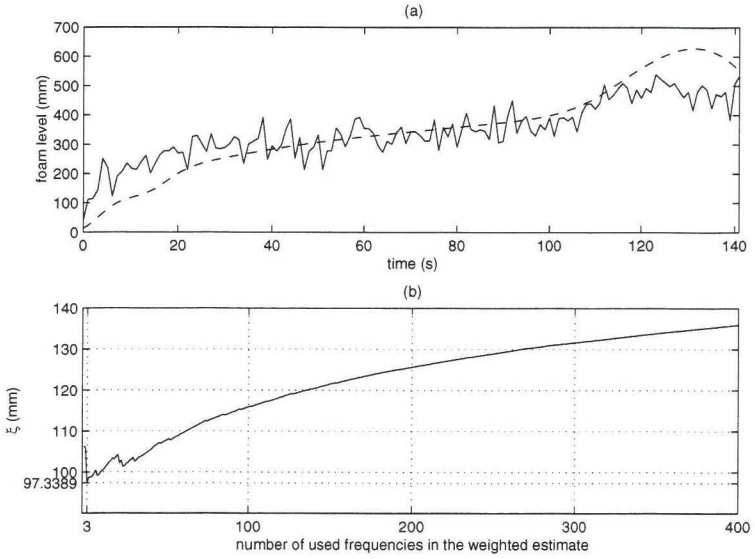

Fig. 7: Estimation with fluid B. (a) Estimated foam level (solid) versus observed foam level (dashed) using the optimal weighted estimate. (b) Optimality measure ξ

3.1 Identification of the foam dynamics

From the static foam experiments it can be expected that the foam dynamics can be approximated by a linear model for the area above 40 mm. For the use in the controller design, a linear mathematical model is identified from input-output data. During a foaming experiment, a pseudo random noise sequence is send to the lance actuator and the resulting estimated foam level is recorded.

As the lance movement has velocity saturation and the dynamical behaviour of the foam is rather slow, the sampling time is chosen to 2 s. Hand driven foam control trials have shown that the sampling time for control purposes can be increased to around 6 s.

Fig. 9 shows input and output signal. There, it can be observed that increasing the distance from the fluid surface does reduce the foam level.

Using the subspace identification algorithm $n4sid$ of the system identification toolbox [6], a linear state space model of order 4 appeared to perform well on the recorded data set. The resulting model will be denoted $G(q)$, where q represents the forward shift operator.

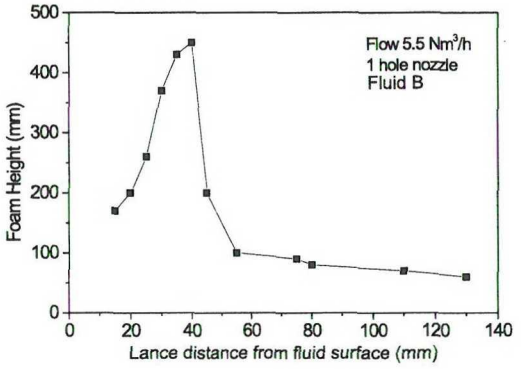

Fig. 8: Dependency of steady state foam level on the lance nozzle distance from fluid surface

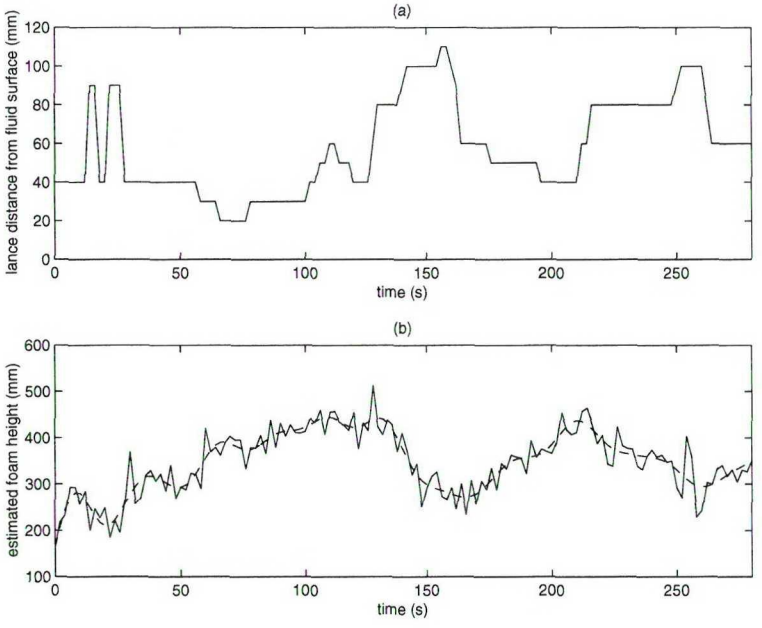

Fig. 9: Identification data. (a) Pseudo random noise as actuator movement. (b) Estimated foam level (solid), filtered version (dashed).

3.2 Design and analysis

In a first attempt to control the foam level, a PI controller in a one degree of freedom control configuration is designed. For this end, an iterative design process is used, where the closed-loop poles are placed so that the output sensitivity function of the closed-loop does not exhibit peaks larger than two. The output sensitivity function, which is the transfer function from output disturbance to output signal, is given by

$$S(q) = \frac{1}{1 + G(q)C(q)},$$

where $C(q)$ denotes the controller. The sensitivity function specification can be written as

$$M_S = \sup_{0 \leq \omega \leq \pi/T_s} |S\left(\exp(-j\omega T_s)\right)| \leq 2$$

It can be shown that the relative stability margin M_S yields a gain margin of at least 2 and a phase margin of more than 30 degrees. Furthermore, plant perturbations of less than 0.5 in magnitude will not affect closed loop stability.

Using the linear model $G(q)$ from the identification, the PI controller $C(q)$ is designed via the root-locus method. The resulting sensitivity function $S(q)$ exhibits a small peak, Fig. 10. Accordingly, the closed loop system is robustly stable for even rather large uncertainties, [7].

Since the movement of the lance has to be restricted to the area above 40 mm, saturation phenomena have to be considered. In order, to prevent integrator wind-up, the PI controller has to be implemented with an anti-windup scheme. The designed closed loop system is depicted in Fig. 11.

4 Experiments

Both foam level estimation and controller are implemented on the DSP of the water model. The control loop is running at a sampling time of 6 s, while the estimation algorithm is run with 2 s.

The reference value during a control experiment could be changed via the user interface. Hence, arbitrarily chosen fixed reference values could be tested and transient behaviour observed. Fig. 12 shows the performance of the closed loop system after a reference value change. It can be seen that the controller is able to drive the control error to zero. The standard deviation of the control error in the displayed range accounts for up to 46 mm.

During the control experiments spot tests of the foam level are taken. A bias between estimated and observed foam height appears, which is a result of the changes in the lance position. Naturally, the lance position should affect the foam level estimation, as the sound source is moving with the position changes of the lance.

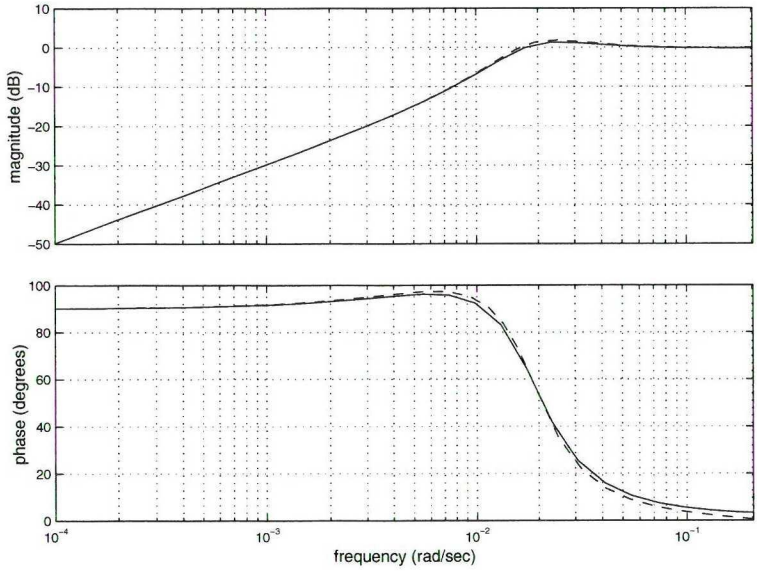

Fig. 10: Bode plot of the output sensitivity function of the closed loop system. Sample time 2 s (solid), sample time 6 s (dashed).

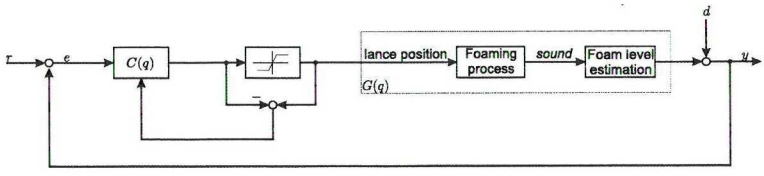

Fig. 11: Block diagram of the closed loop system with PI controller and anti-windup.

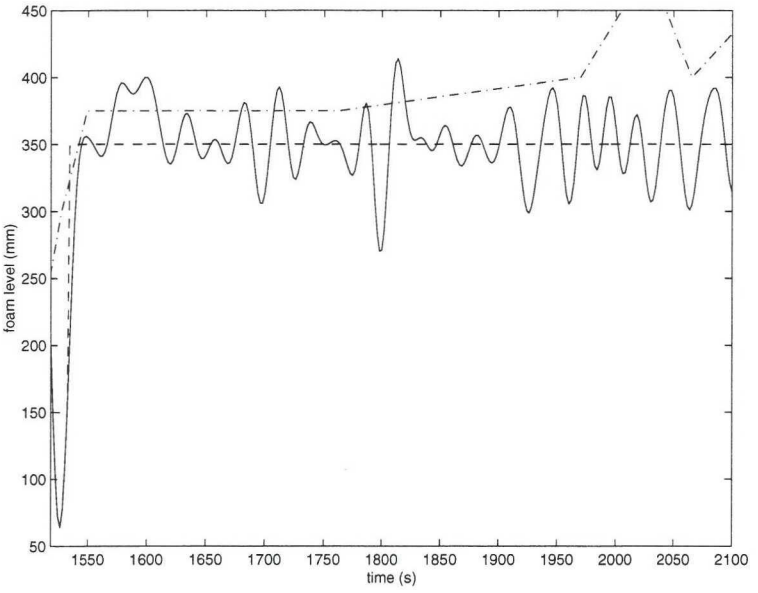

Fig. 12: Performance of the closed loop system with fluid A. Foam level reference value (dashed), Filtered foam level estimate (solid), Observed foam level (dashed-dotted).

5 Comparison between the water model and steel converter

The main process in the LD converter is the decarburization of pig iron whose physics and chemistry differs a lot from the water model. There are many chemical reactions taking place during decarburization in the LD converter changing both chemical composition and temperature of the process. The LD converter is run at temperatures above 1500°C and is very difficult to model. The surface tension and the viscosity depend on the temperature and chemical composition. This implies that the condition for foaming changes during the operation during steel making compared to the foaming in the water model.

The foam in the LD converter consists of three phases, namely slag, iron and gas. Today, there are no reliable models that can predict the effective viscosity of this three-phase foam, which makes it very difficult to model the LD process. If one wants to model the foaming using water model experiments it is also impossible to predict the effective viscosity for a three phase-foam.

In this work it was thought that the foam level in the water model is one of the most important process parameters. The first approach is to study the effect of foam level on the attenuation of the sound generated when the nozzle jet interacts with the

water bath. The principles of how the foam is generated are not studied. Thus, it is not necessary to have access to information on viscosities for the three-phase foam. It is believed, despite the above differences, that the way of automatically control the foam level developed from the water model could be used in a LD converter.

Shifting the control method from water model to LD converter will cause trouble with dust, sound distortion, heat and a continuously changing foam. Future work will be required to address these problems.

6 Conclusions

The estimation of foam level in a water model of an LD converter process from microphone signals is discussed. It is shown how the estimation algorithm can be automatically calibrated. The estimation concept is applied to foaming experiments which are conducted in the water model. Tests with different fluids are performed and prove that the estimation scheme can cope with a wide range of fluids.

Furthermore, the estimated foam level is then used as a measurement signal for closed loop control of the foam level using a PI controller. Control experiments are conducted in the water model and indicate that foam level control using lance positioning is possible. Still, it has to be analysed how dynamical changes in the lance position affect the foam level estimation, since a bias appeared during the control experiments.

In order to be able to apply closed loop control of the foam level in the LD converter the following issues have to be discussed. Firstly, the experiments with the water model do not reflect how properties of the chemical reaction or the slag influence estimation and control of the foam level. Therefore, a high temperature model of the LD-converter should be used to validate both estimation and control. Secondly, most converters are not equipped with lance actuators that can provide continuous motion of the lance. Thus, the LD-converter lance actuator has to be changed in order to be usable for dynamic foam level control.

Despite these portability issues, dynamic control of the foam level has the potential of preventing slopping in the LD-converter process. Finally, if applied in combination with carbon content estimation, [5], automatic control of the LD-converter process would be possible.

References

[1] A. Abbatangelo, M. Dalla Rena, M. Palchetti, and L. Zampetti. Blowing pattern computerised control at Taranto Steelshop. In *Steelmaking Conference Proceedings*, pages 337–342, 1990.

[2] D. Anderson, C. M. Barnes, and H. J. Whittaker. Fully dynamic process control of the BOS in British Steel. In *Steelmaking Conference Proceedings*, pages 379–387, 1991.

[3] C. Bencini and A. Poli. Automation for refining and slag control in LD process at AFP/Piombino Steel Shop. In *Steelmaking Conference Proceedings*, pages 193–198, 1993.

[4] Wolfgang Birk, Ioannis Arvanitidis, Pär Jönsson, and Alexander Medvedev. Physical modelling and control of dynamic foaming in an LD-converter process. In *Proc. of the IEEE Industry Applications Society 35th Annual Meeting, Sheraton Roma Hotel 8-12 October 2000 Rome Italy*, 2000.

[5] A. Johansson, A. Medvedev, and D. Widlund. Model-based estimation of decarburization rate and carbon content in the basic oxygen steelmaking process. In *Proc. of the IEEE Industry Applications Society 35th Annual Meeting, Sheraton Roma Hotel 8-12 October 2000 Rome Italy*, 2000.

[6] Lennart Ljung. *System Identification Toolbox: For use with Matlab.* The MathWorks Inc., 2000.

[7] S. Skogestad and I. Postlethwaite. *Multivariable Feedback Control - Analysis and Design.* John Wiley & Sons, 1996.

[8] Samuel D. Stearns. *Digital Signal Analysis.* Hayden Book Company, Inc. Rochelle Park, NJ., USA, 2 edition, 1975. Digital signal analysis.

[9] D. Widlund, A. Medvedev, and R. Gyllenram. Towards model-based closed-loop control of the basic oxygen steelmaking process. In *Proc. of the 9th IFAC Symposium on Automation in Mining, Mineral and Metal Processing 1998, Cologne, Germany, 1-3 September 1998*, pages 69–74, 1998.

Paper 7

Video Monitoring of Pulverized Coal Injection in the Blast Furnace

Published as

Wolfgang Birk, Olov Marklund, and Alexander Medvedev. "Video monitoring of pulverized coal injection in the blast furnace". *IEEE Transactions on Industrial Applications*, 38(2):571–576, 2002.

Video Monitoring of Pulverized Coal Injection in the Blast Furnace

Wolfgang Birk*†, Olov Marklund†, and Alexander Medvedev†‡

*Corresponding author: wolfgang.birk@sm.luth.se
†Department of Comp. Science and Electrical Eng., Luleå University of Technology, SE-971 87 Luleå, Sweden
‡Department of Systems and Control, Uppsala University, SE-752 37 Uppsala, Sweden

Abstract

A novel approach to monitoring and control of the coal powder injection in a blast furnace is presented and discussed. Image analysis of video recordings is used as a means to estimate the instantaneous coal flow. Initial experiments at the blast furnace no 3 of SSAB Tunnplåt AB Luleå, Sweden, have been performed and first hand results on modelling and control of a single injection line are given.

1 Introduction

In the blast furnace process, coke is usually used as fuel and reduction agent. Since coal is 40% cheaper than coke, injecting pulverized coal instead of using coke is economically beneficial. According to [2], the share of pulverized coal compared with coke as fuel will rise from 36% to 50% by the year 2015.

A coal injection plant is a highly automated plant, where incoming raw coal is stored, ground, dried and finally injected into the blast furnace. During operation, human interaction is only needed for making set-point adjustments. Fig. 1 shows the structure of the plant, where only the injection vessels, distributor, the blast furnace and the monitoring equipment are depicted. The control of the injection process is complicated due to the two phase nature of the injected flow (gas plus particles). Direct measurement of the coal mass flow is difficult since a flow meter installed on the injection pipe only provides a measurement of the cumulative flow of gas and coal powder where coal content might vary significantly.

The total coal flow leaving the injection plant is distributed into several parallel lines. In [4] it is shown how the total coal flow can be stabilized. The problem at hand is to achieve a desired injection distribution of the flow around the blast furnace. Therefore, estimation and control of the coal flow in each line is required.

The coal mass flow estimation is derived from images of the coal jet entering the raceway of the blast furnace. For each injection line, images are acquired in real time using a video camera monitoring the scene through a peephole in the tuyere (see Fig. 1). With the aid of an image analysis scheme, an estimate of the instantaneous coal mass flow is then obtained.

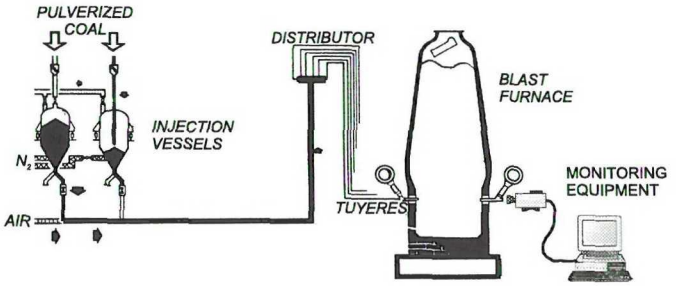

Fig. 1: Setup for video monitoring. Parts of the coal injection plant, distributor, blast furnace and monitoring equipment.

As the coal mass flow to the distributor can be assumed to be constant [3], the flow has to be distributed according to a desired profile between a number of injection lines. Each of these lines is equipped with a flow control valve. Using the estimated coal mass flow as the measurement output and the valve as actuator a mathematical model of the injection process is identified from process data. The obtained model can then be used to design a controller, which stabilizes the coal mass flow in the injection line.

2 Flow estimation

A representative scene of the coal injection process, as recorded with the video camera, is depicted in Fig. 2a. A digitized video frame will below be denoted $F(i, j, \tau)$ where (i, j) represent the pixel coordinates and τ is a discrete time parameter (the shorter notation $F(\tau)$ will henceforth be used).

Initially a binary mask R, representing the actual region of interest, is produced. This is done by forming an image $D = \sum |F(\tau) - F(\tau - 1)|$, $\tau = 2, 3, ...$, *i. e.* an image consisting of accumulated differences (due to motion) between subsequent video frames during a sufficiently long period of time (typically a few minutes).

Since the furnace wall and the tuyere will make up a static scene, no differences will be detected in those regions of the frames. The coal plume as well as the gaseous interior of the furnace, on the other hand, will display a highly dynamic behavior resulting in detectable differences. Masks such as the one depicted in Fig. 3b can thus be straightforwardly produced from a final difference image D by simply selecting the region consisting of values that are high enough (indicating motion).

Once a mask R has been created, the region of interest in all subsequent frames $F(\tau)$

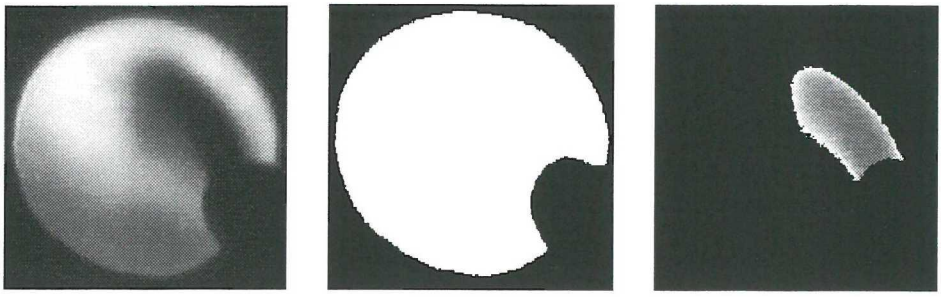

(a) (b) (c)

Fig. 2: (a) Digital image depicting the coal injection process. (b) The binary mask R. (c) The projected plume (segmented from the rest of the image).

can be conveniently detected and the actual measuring procedure (i.e. detecting and analyzing the actual plume inside the region of interest) can be started.

First a grayscale histogram [5] for the set of pixels R_τ, the pixels in a frame $F(\tau)$ that are covered by the mask R, is formed and analyzed. The histograms are typically of a bimodal nature with the darker pixel values (representing the plume) and the brighter pixel values (representing the gaseous background) forming two well separated 'hills'. This enables the detection of an optimal threshold value $T(\tau)$ such that a subset P_τ, representing the coordinates of pixels making up the actual plume, can be determined through the decision rule: $(i,j) \in P_\tau$ if $(i,j) \in R_\tau$ and $F(i,j,\tau) < T(\tau)$.

The resulting set P_τ is then further processed using a chain of binary morphology operations [5] in order to produce a simple connected area inside R representing a 2-D projection of the plume.

The final processed set P_τ of image coordinates (representing the projected plume) is then used to form a relative estimate $m(\tau)$ of the injected coal mass at time τ through the operation

$$m(\tau) = \sum_{(i,j)\in P_\tau} f(R_\tau, i, j, \tau), \tag{1}$$

where the optimal functional form of $f(\cdot)$ is still an open research issue. The most straightforward choice is $f(\cdot) = A$, where A is a constant, *i.e.* a value directly proportional to the total area covered by the pixels in P_τ is used as relative estimate.

A more sophisticated choice is

$$f_\alpha(\cdot) = A_\alpha \left[R(i,j,\tau) + \epsilon\right]^{-\alpha},$$

where A_α, α, and ϵ are constants greater than zero (ϵ is included to prevent division by zero). The rationale behind this choice is to give coordinates in P_τ representing low grayscale values a higher weight (due to the exponent $-\alpha$) based on the assumption that they represents regions with higher coal powder density.

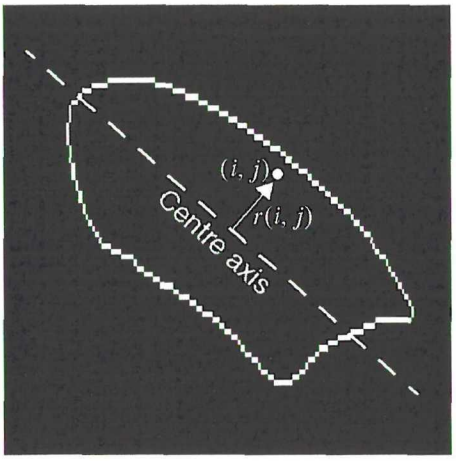

Fig. 3: Elementary volume transform.

As a first attempt for a 3-D model, a rotational symmetric plume has been assumed. The transformation from projected 2-D data to volume data is carried out as follows. First the equation for the center axis of the plume (see Fig. 3) is estimated through principal axis analysis on P_τ, and then the weighted functional

$$f(\cdot) = 2\pi r(i,j) f_\alpha(\cdot),$$

where $r(i,j)$ is the orthogonal distance from the center axis to the position (i,j) (as depicted in Fig. 3), is applied in (1). Using the accumulated flow over a time period of several minutes the estimate $m(\tau)$ can be calibrated (i.e. a suitable value for the contant A_α is determined).

A comparison between one such estimate and a corresponding measurement using a Coriolis flow meter (measuring the cumulative gas/coal flow) is shown in Fig. 4. Obviously the two measurements exhibit a very similar dynamic behavior.

The use of more complex 3-D models, determined by matching parameters (extracted through image analysis of the video feed) with approximate solutions of the governing equations describing two phase flows in systems such as the here discussed, is currently under investigation.

3 Single line flow control

The two-phase flow that is leaving the coal injection plant is usually conveyed over several hundred meters until it reaches the coal distributor. Even if the coal flow is perfectly stabilized directly after the injection plant, fluctuations appear in the flow as the coal particles are conveyed in a so-called dense flow [7].

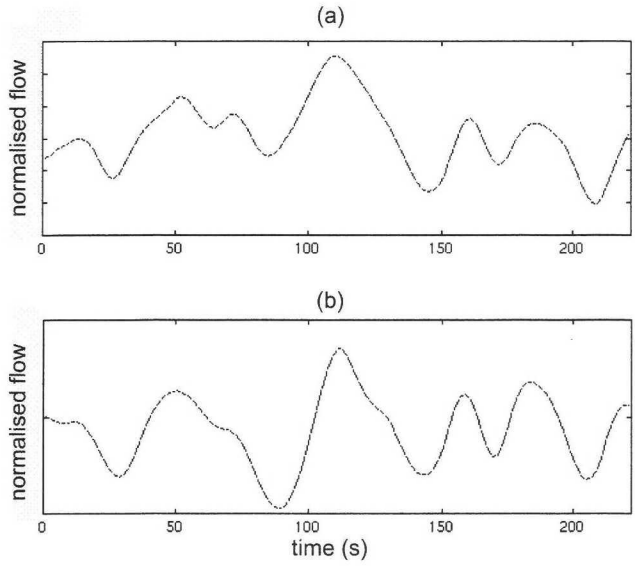

Fig. 4: Comparison of normalised estimated flows. (a) Using an image sequence. (b) Using a Coriolis flow meter.

Distribution of pulverized coal over the blast furnace diameter is provided by the fixed construction of the distributor. No actuators are used to modify the achieved flow distribution profile. Thus, any fluctuations or other disturbances can not the attenuated by this open-loop structure.

Introducing single line flow control, see Fig. 5, where the measured flow in a single line q_{Ci} is fed back to the actuator u_{Ci} via a controller, can remove induced fluctuations and attenuate disturbances. Moreover, set point tracking can be implemented.

Furthermore, it enables the plant operators to achieve desired flow profiles around the blast furnace diameter. Clearly, the energy supply to the blast furnace can be directed to certain regions in the furnace and in turn, temperature control might become possible.

The desired flow distribution profile can be set in two different ways:

1. The sum of the flows in all tuyeres is set and the flow in each tuyere is a fraction of the sum. Consequently, the absolute coal mass flow value in each pipe can vary and the coal flow control of the PCI plant is not affected.

2. The flow in each tuyere is set as an absolute value. Thus, the provided flow from the PCI plant has to be adjusted to the sum of the individual flows and the time delay between the coal injection vessel and the tuyeres has to be considered.

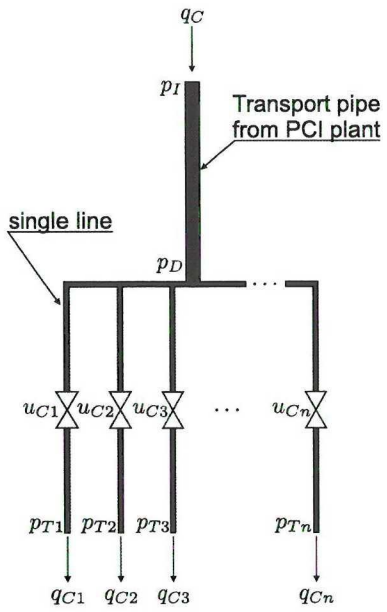

Fig. 5: Physical structure of a single line control setup.

3.1 Implications

Beside the potential of single line flow control, the application has implications for the operation of PCI plants. Mainly the flow control of the plant has to be tightened and the transport delay between the injection vessels and the coal distributor has to be considered.

Variations in the provided coal flow from the PCI plant will directly propagate to each single line and cause counteraction by the controllers. As each control loop is dynamically coupled via the coal distributor it has to be investigated how this multivariable control problem can be successfully solved.

3.2 Video feedback control

There are two ways to measure the coal flow in an injection line, by using a flow meter, *e.g.* a Coriolis flow meter, or by extracting flow information from a video image of the coal jet entering the tuyere.

Considering the uncertainties of the flow measurement and the costs involved with the purchase of the flow meters, video image analysis is an economically attractive alternative. Moreover, the video image is a rich information source, where more than only flow information can be found.

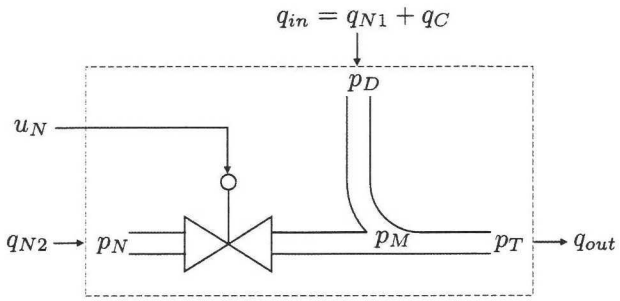

Fig. 6: Schematic drawing of the flow control valve.

From a maintenance point of view, video observation gives the operators another degree of freedom, as maintenance of tuyeres can be based on the evaluation of the video image of the tuyeres.

Here, the flow estimation algorithm is used as a soft-sensor that provides a measurement of q_{Ci}. It is important to note, that the soft-sensor has to be calibrated properly, as the performance of the closed loop system depends on the quality of the measurement.

Since the soft-sensor is part of the dynamic model for the single line, changes in the zoom or position of the scene in the image frame affect model gains or model dynamics.

3.3 Actuator

Using the previously described flow estimation algorithm, a flow measurement is extracted from the video image and fed back. In order to affect the flow in the single line the valve in Fig. 6 is used.

It can be seen that the single line merges with a gas pipe, which can introduce a gas flow into the single line via a valve. Opening the valve causes a flow q_{N2} to the merge. As the total mass flow out of the actuator can not increase, the in-flow q_{in} has to decrease. Thus, the coal flow is reduced. Clearly, the actuator has a negative gain and closing the valve increases the coal flow.

4 Physical model

A physical model for the dynamical behavior of the coal flow in the injection line from the distributor to the observed coal plume in the tuyere consists of three parts.

1. Dynamics of the actuator.

2. Transport delay of from the actuator to the tuyere.

3. Coal plume dynamics.

The dynamics of the actuator is based on the simplification that the flow dynamics in the pipe can be neglected and that the coal particle flow can be governed by fluid flow equations.

Furthermore, it is assumed that the mass flow balance at the actuator output is constant. It can be established that three mass flows are entering the merging point

$$\begin{aligned} \dot{m}_{N1} &= q_{N1}\frac{p_D}{RT_D} \\ \dot{m}_{N2} &= q_{N2}\frac{p_M}{RT_M} \\ \dot{m}_C &= q_C\rho_C, \end{aligned}$$

where $\dot{m}_\bullet$ and $q_\bullet$ denote mass flow and volume flow, respectively. Assuming, distributor and merging point are close to each other, the pressure $p_D \approx p_M$ and the temperature $T_D \approx T_M$.

Thus, the mass balance is obtained

$$\begin{aligned} \dot{m}_{out} &= \dot{m}_C + \dot{m}_{N1} + \dot{m}_{N2} \\ &= q_C\rho_C + q_{N1}\frac{p_M}{T_M} + q_{N2}\frac{p_M}{T_M} \\ &= const \end{aligned} \tag{2}$$

Clearly, an increased flow q_{N2} yields a reduced flow $q_{N1} + q_C$.

In (2) the flow q_{N2} is given as a flow through an 'equal percentage' valve [1]. It is given by

$$q_{N2} = k_{N2} f_{gas}(p_N, p_M) g_{exp}(u_N),$$

where k_{N2} is a factor that maps the opening characteristics g_{exp} to an area. The function f_{gas} describes the flow through a stricture [6].

From the merging point in the actuator to the end of the injection line in the tuyere there is a transport delay t_d. Furthermore, it is assumed that the entering coal flow propagates through the pipe unaltered. Hence, the dynamics can be given in the Laplace domain as

$$G_d(s) = e^{-t_d s} \tag{3}$$

The dynamics of the coal plume are assumed to be fast and reach steady state instantaneously. Moreover, when the two-phase flow enters the tuyere as a jet, the two phases are seen separately due to the optical properties of nitrogen. Assuming, that the coal particles remain visible, which means unburned, for a constant time, the

amount of visible particles characterizes the flow. Therefore, the particle number N_C is directly proportional to the coal flow in the injection line

$$N_C = k_C q_C \tag{4}$$

Combining (2), (3) and (4) a complete physical model is found.

5 Model parameters

Several contiguities in the physical model are unknown and have to be determined from experiments at the blast furnace.

To this end, the actuator has to be affected and the coal flow has to be measured simultaneously by the soft sensor. The setup depicted in Fig. 1 is modified so that the computer is connected to the actuator via a buffer amplifier.

The following experiments are performed:

- Static experiment:
  The valve is opened from closed to fully open in a number of equidistant steps. Each step is held for around 60 seconds. It is assumed that steady state is reached after 30 seconds.
- Dynamic experiments:
  A pseudo random noise signal is generated and send to the actuator. Amplitude, offset and frequency range are varied.

Evaluation of the experiments show that the coal plume in the blast furnace is not only affected by the flow in the injection pipe but also dynamically affected by the blast air flow in the tuyere. During the design of the soft sensor, the effect of this transversal flow is assumed static and thus, it is compensated by a static gain.

Fig. 7 shows logged data of the input signal to the actuator and the output signals from the soft sensor. Correlation analysis shows a weak correlation (less than 20%) between the actuator signal and flow measurement, Fig. 8. Consequently, the dynamic effects of the blast air flow have to be considered in the flow measurement and the soft sensor has to be re-designed.

It can be concluded that more experiments have to be performed in order to get a better understanding of the behavior of the coal particle jet in the blast air flow.

6 Conclusions and further work

A novel method for estimating and controlling the pulverized coal flow in a single injection line to the blast furnace has been presented.

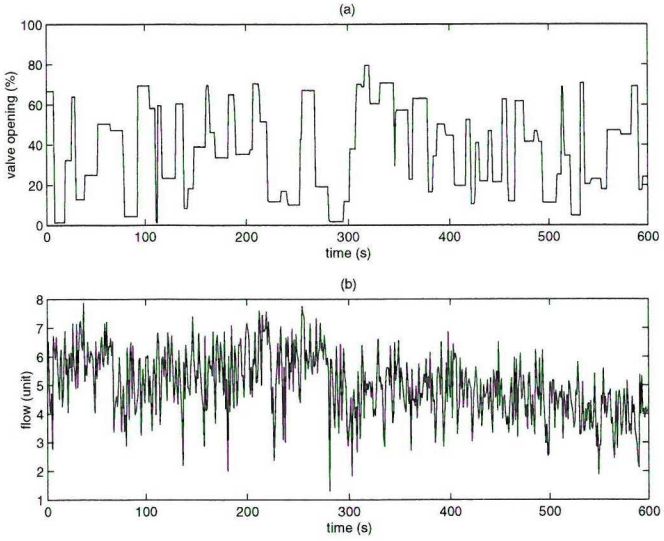

Fig. 7: Process data. (a) Pseudo random noise input signal. (b) Estimated flow from video image.

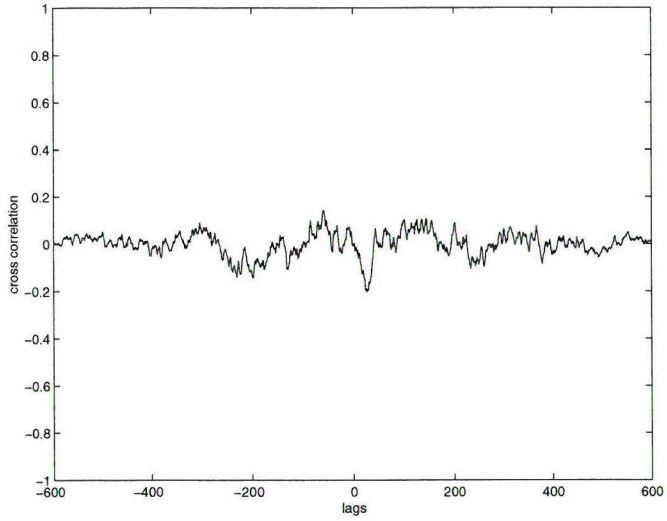

Fig. 8: Normalized correlation function between actuator input and estimated flow.

The design of a soft sensor for coal flow estimation in a blast furnace tuyere is discussed and applied to logged data. The results indicate that reliable coal flow estimation from video images is viable and can be used as a soft sensor for control purposes.

Using the soft sensor output, control of the coal flow in a single injection line becomes applicable. Implications for plant operation are pointed out.

A physical model for the dynamical behavior from the actuator to the observed coal plume has been derived. Initial experiments have shown that the assumption on the blast air flow does not hold. The effect of the blast air on the coal plume dynamics has to be studied more thoroughly.

More experiments have to be performed in order to get a better understanding of the model dynamics. Utilizing experimental data, model parameters have to be derived and the model validation has to be carried out. Subsequently, a model-based controller can be designed for the single line.

7 Acknowledgement

The authors want to thank SSAB Tunnplåt AB in Luleå, Sweden for making the plant and maintenance personnel available. A special thank to Juan Arellano Sanzol who helped with the experiments at the plant. Financial support from the Swedish National Board for Industrial and Technical Development (NUTEK) is also gratefully acknowledged.

References

[1] Control valve handbook. Fischer Controls, 1977.

[2] American Iron and Steel Institute. Steel industry technology roadmap. At *http://www.steel.org/MandT/contents.htm*, February 1998.

[3] Wolfgang Birk, Andreas Johansson, and Alexander Medvedev. Model-based control for a fine coal injection plant. *IEEE Control Systems Magazine*, 19(1):33–43, February 1999.

[4] Wolfgang Birk and Alexander Medvedev. Pressure and flow control of a pulverized coal injection vessel. *IEEE Transactions on Control Systems Technology*, 8(6):919–929, November 2000.

[5] A.K. Jain. *Fundamentals of Digital Image Processing.* Prentice-Hall, Englewood Cliffs, N.J., 1989.

[6] Andreas Johansson and Alexander Medvedev. Model based leakage detection in a pulverized coal injection vessel. *IEEE Transactions on Control Systems Technology*, 7(6):675–682, November 1999.

[7] G.E. Klinzing, R.D. Marcus, F. Rizk, and L.S. Leung. *Pneumatic conveying solids - A theoretical and practical approach.* Chapman and Hall, cop., London, 1997.

LULEÅ TEKNISKA UNIVERSITET

NR: 2002:28
ISSN: 1402-1544
ISRN: LTU-DT--02/28--SE

Utbildning
Doctoral thesis

Institution
Systemteknik

Avdelning
Reglerteknik

Upplaga
200

Datum
2002-08-14

Titel
Industry Applications of Multivariable Control

Författare
Wolfgang Birk

Språk
Engelska

Sammanfattning
In the face of environmental regulations, optimization of industrial processes becomes necessary. This doctoral thesis summarizes the results of three application-driven projects in automatic control that were aimed at process optimization in the steel industry. The objective of the projects was to apply advanced control strategies to two important processes in steel making, namely pulverized coal injection (PCI) in blast furnaces and LD converters. Firstly, an LQ multivariable controller with gas leakage detection system for PCI vessels is designed and analyzed. Secondly, a foam level control system for the LD converter process using an audio signal for measurement is designed. Thirdly, it is attempted to create a single line flow control system for PCI using a video camera. In the latter two cases the conservative approach of inferring unmeasurable physical quantities from the audio and video sources is used.

Moreover, all the designs are tested through implementation or experiments at the industrial plant. The control and gas leakage detection system ended up as a full-scale industrial implementation, whereas the projects comprising audio and video information is still at an experimental stage.

Work with implementation and experiments pays off in experiences.....(cont.)

Granskare/Handledare
Alexander Medvedev

URL: http://epubl.luth.se/1402-1544/2002/28

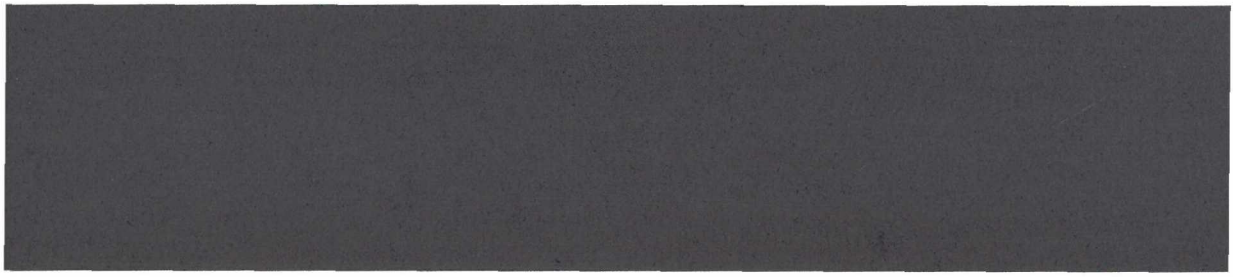

Universitetstryckeriet, Luleå